

Copyright is owned by the Author of the thesis. Permission is given for a copy to be downloaded by an individual for the purpose of research and private study only. The thesis may not be reproduced elsewhere without the permission of the Author.

High Temperature Superconducting Flux pump

A thesis in the partial fulfilment of the requirements for the
degree of

**Masters of Engineering
in
Mechatronics**

at Massey University, Turitea Campus
Palmerston North
New Zealand.

Rowan Martin Walsh

2011

Acknowledgements

Dr Christian Hoffmann, IRL Main supervisor. Christian's advice and guidance throughout the project has been of great value and very much appreciated.

Dr Rod Badcock, IRL supervisor

Dr Liqiong Tang, Massey supervisor

Workshop staff: Shaun Bredenkamp, Robert Jakobsson

Summary

Electromagnets play an important role in everyday life from motors and generators to such devices as Magnetic Resonance Imaging (MRI). The larger a magnetic field needed in such a device the more demand there is in power consumption and space. The development of superconductors (SC) and their ability to dissipate negligible power has made it possible to create larger fields in a more cost effective and space efficient manner. The disadvantage of the SC is that it needs to be operated at cryogenic temperatures (typically below 110 K). Cryogenics is a significant cost factor so the less power needed for cooling a SC magnet the more cost effective the system can become. The main heat load comes from the ohmic dissipation of the current leads necessary to energise the magnet. The current leads provide the electrical connection from the power supply at room temperature to the coils in the cryogenic environment. To circumnavigate this heat load a superconducting device known as a flux pump (FP) can be embedded in the cryogenic environment. The flux pump operation can be generalised as a DC generator, which minimises ohmic heating and makes the power supply needed to energise the magnet superfluous.

HTS 110 is a magnet manufacturer who has assigned the task of implementing a flux pump into a commercial magnet application and developing a complete system capable of controlling a homogenous current level in their magnets. Such a flux pump module was developed and successfully incorporated into an existing SC magnet. This thesis details the mechanical design, control hardware, required software used to create this technology and the benefits it presents.

Compared to the current lead technology, the developed flux pump module reduced the heat load on the cryo-cooler by almost a factor of 5. In addition a produced magnetic field of 750 mT was achieved, which corresponds to a current of 68 A in the magnet coils. Such a high field could not have been obtained in the present setup with conventional technology. The large heat load caused by current leads would increase the overall temperature of the coils and in turn decrease the current capability of the circuit to approximately 20 A, resulting in a field that is more than three times smaller.

A full control system using field strength as feedback to control the rotation of the FP was implemented. This included an iterative hardware design and fabrication process followed by software implementation, that led to a high level system encompassing a PID type control algorithm. The control system achieved a field stability of 30 parts per million (PPM) which puts the system in reach for the needed NMR stability criterion of 1 PPM.

Overall the obtained current magnitude and stability of the FP module in a conduction cooled magnet system makes it the first of its kind worldwide. Potential research into developing the FP system further will see it being incorporated in a NMR / MRI magnet system and other areas of SC magnet applications, where high stability and minimal heat loads are required.

Table of Contents

1	Introduction	8
2	Literature review	11
2.1	Superconductivity.....	11
2.2	Flux Pump Theory.....	13
2.2.1	DC dynamo flux pumps	14
2.2.2	Flux pumping with HTS	16
2.3	Brushless motors	17
2.3.1	Stepper motors	18
2.3.2	Brushless DC motors	21
3	Scope	23
4	Proposed Methodology	24
5	Mechanical Design	25
5.1	Test Apparatus.....	26
5.2	Stage 1 – Stator design	26
5.3	Stage 2 – Rotor design.....	29
5.4	Stage 1 and 2 redesign	31
5.4.1	Stator redesign.....	31
5.4.2	Rotor redesign.....	33
5.4.3	Bearing mount test	35
5.5	Stage 3 – Flux pump module accessories	36
5.6	Cooling system	38
5.6.1	Stirling cooler calibration	38
5.7	FEM analysis	39
5.8	Vacuum chamber	41
5.9	Vacuum feed through.....	44
6	Fabrication	46
7	Assembly.....	54
8	Testing and evaluation.....	61
8.1	Vacuum system.	61
8.2	Cooling of the flux pump unit.....	61
8.2.1	Initial modifications	63
8.3	Full system cool down	64
8.3.1	Degraded coils.....	64
8.4	System evaluation	66
9	Control System.....	69
9.1	Low level hardware selection	69
9.1.1	Magnetic field sensor.....	70
9.1.2	Temperature sensor.....	70
9.1.3	Motor selection.....	71
9.2	Hardware modules	72
9.2.1	Hall sensor hardware module	72
9.2.2	Temperature sensor module	75
9.2.3	Analogue to digital conversion	77
9.2.4	Human interfacing	77
9.2.5	Stepper motor driver	78
9.3	Central processing unit.....	80
9.4	Additional circuits.....	81
9.5	Printed circuit board (PCB) implementation	82
9.6	Embedded software	84
9.6.1	LCD communication.....	84
9.6.2	HPWM signal.....	84
9.6.3	Trim pot	85
9.6.4	Push buttons	85
9.6.5	SPI communication	85

9.7	Control Loop	89
9.7.1	Control algorithm	91
10	Discussion and Conclusion	95
11	References	98
12	Appendix	100
12.1	Hardware schematics	100
12.1.1	Control board	100
12.1.2	Temperature sensing module	100
12.1.3	FT232 RS232 to USB module	100
12.2	PCB layouts	101
12.2.1	Control board	101
12.2.2	Temperature sensing module	101
12.3	Embedded software	102
12.3.1	LCDOUT	102
12.3.2	SPIHall code	103
12.3.3	SPI-EEPROM code	106
12.3.4	Control code	110
12.4	Data sheets	119
12.4.1	RMS- F1/F2 solid shaft - flange mount. metric	120
12.4.2	Allegro A4983 microstepping driver with translator *	121
12.4.3	FT232BL USB UART IC *	123
12.4.4	Arepoc HHP_NP 768 Hall probe	124
12.4.5	AD620 instrumentation amplifier *	125
12.4.6	AD623 instrumentation amplifier *	126
12.4.7	MCP3550 single - channel 22 - bit delta - sigma ADC *	128
12.4.8	25LC1024 1 Mbit SPI Bus Serial EEPROM *	129
12.4.9	M542 Economical microstepping driver *	130
12.4.10	1.8° size 42mm high torque hybrid stepping motor	131
12.4.11	Display tech LCD module *	133
12.4.12	PIC18F87K90 microcontroller *	134

List of figures

Figure 2-1. Levitating Magnet demonstrating the Meissner effect	11
Figure 2-2 - Type I superconductor	12
Figure 2-3 - Type II superconductor	13
Figure 2-4 - Flux pump representation	13
Figure 2-5 - HTS and LTS IV curve showing flux flow regime	14
Figure 2-6 - Flux pumping illustration DC dynamo	16
Figure 2-7 - HTS flux pumping method	17
Figure 2-8 - Variable-reluctance (VR)	18
Figure 2-9 - Permanent-magnet (PM)	18
Figure 2-10 - Hybrid	19
Figure 2-11 - Wiring configuration of unipolar stepper motor	19
Figure 2-12 - Wiring configuration of Bipolar stepper motor	20
Figure 2-13 - BLDC types	21
Figure 2-14 – Schematic of the basic anatomy of a BLDC motor	22
Figure 5-1 - Flux pump Test apparatus	26
Figure 5-2 - Stator SC arrangement	27
Figure 5-3 - Original stator design	27
Figure 5-4 - Thermal conductivity of Copper (Van Sciver, 2010)	28
Figure 5-5 - SC at tangent to copper bus bar	29
Figure 5-6 - rotor assembly & Cross section of rotor assembly	30
Figure 5-7 - G10 Sapphire system	32
Figure 5-8 - The new stator design	33
Figure 5-9 - Redesign of rotor	34
Figure 5-10 - a. Cross section of FP showing Cu mount. b. Cross section of FP showing G10 mount	35
Figure 5-11 - Shows the deformation of a test sample of G10	35
Figure 5-12 - a. G10 centre support. b. Stainless steel centre support	37
Figure 5-13 - Final design of flux pump	37
Figure 5-14 - Two thermal bus bars	38
Figure 5-15 Heat load calibration set up & Cryotel GT measured performance data	39
Figure 5-16 - a. Simplified FP model. b. FP model containing mesh	39
Figure 5-17- Temperature profile	40
Figure 5-18 - Heat flux flow	40
Figure 5-19 - Vacuum chamber	42
Figure 5-20 - Rotary vacuum feed through	45
Figure 6-1 - Sapphire system	46
Figure 6-2 - Stator	48
Figure 6-3 - Flux pump support	48
Figure 6-4 - Rotor	49
Figure 6-5 - Flux pump assembly	50
Figure 6-6 - Thermal bus bar configuration	51
Figure 6-7 - Motor support column	52
Figure 6-8 - Vacuum chamber	52
Figure 6-9 - Full system	53
Figure 7-1 - Stator layout	54
Figure 7-2 - SC solder joints	56
Figure 7-3 - Assembled flux pump	57
Figure 7-4 - SC current lead assembly	59
Figure 7-5 - SC coil pack	59
Figure 7-6 - Mating of the flux pump and coil pack	60
Figure 7-7 - joining SC leads of the flux pump and coils	60
Figure 8-1 - Additional Sapphire and clamp configuration	63
Figure 8-2 - Super Power angular dependence	65

Figure 8-3 - FEMM of HTS- 110 coil system	66
Figure 8-4 - Cool down of the FP and coil	66
Figure 8-5 - Magnetic field temperature dependence	67
Figure 8-6 - Stabilisation plot at a field of 750 mT	68
Figure 9-1 Control system hierarchy.....	69
Figure 9-2 - FL42STH38-1684B bipolar stepper motor	71
Figure 9-3 - Hall sensor current source.....	73
Figure 9-4 – Instrumentation amplifier stage	74
Figure 9-5 - 4pole active Bessel response filter	75
Figure 9-6 Trim potentiometers and push buttons.	78
Figure 9-7 - Display tech LCD	78
Figure 9-8- A4983 stepper motor driver.....	79
Figure 9-9 - M452 microstepping drive	80
Figure 9-10 - PICkit 44-Pin demo board.....	80
Figure 9-11 – Finished PCB boards. The motherboard on the left and temperature module on the right.	83
Figure 9-12 - Complete hardware module.....	83
Figure 9-13 - SPI communication diagram.....	86
Figure 9-14 - Byte write sequence	88
Figure 9-15 - READ sequence.....	89
Figure 9-16 - Current vs voltage for different rotational frequencies	90
Figure 9-17 - Feedback control loop for the FP	91
Figure 9-18 - PI control stability plot	93
Figure 9-19 - PID control stability plot.....	94

1 Introduction

Electro magnets (EM) are used across a wide range of applications including but not limited to motors and generators, transformers, various relays, magnetic recording and data storage, magnetic locks, particle accelerators, the separation of material, crane magnets, electromagnetic suspension (MAGLEV train), scientific and medical instruments including mass spectrometry and Magnetic Resonance Imaging (MRI). The majority of these applications need to be able to have a fixed or varying field that can be turned on and off. A permanent magnet (PM) cannot be used in such instances as it has a fixed field size that is permanently on. It will typically not have a field strength greater than 1 T, where as some of the above applications require a much higher field than this.

The EM obviously is more complex than the PM in terms of design and has problems associated with it. One major problem is ohmic heating. This can be understood from looking at the DC component of power dissipation, $P = I^2 R$ and the magnetic field B from the relationship $B \propto NI$, where N is the number of turns in the EM. Obviously increasing the current I will increase the field magnitude however at the cost of increasing the power dissipation at a factor of the current squared, which can become very large very quickly. So to reduce this dissipation the magnet designer can increase the number of turns N and have a lower current thus producing the same field. This however does increase the size of the magnet accordingly.

This is where the change from conventional wire magnets to superconducting magnets has the benefits of being able produce a field intensity of several times in magnitude for a given size. This is because a superconductor (SC) can carry current with almost zero resistance thus dissipating negligible power (AMS-02 n.d.). The penalty of a SC is that in order for it to be superconducting, it needs to be cooled below a transition temperature known as T_c , which is done using cryogenic liquids or refrigerators. Cryogenic cooling can be expensive depending on the application and the temperature needed.

The benefits of a SC can be further realised if one is to set up a current in a perfect SC circuit without non-superconducting sections or joints, it can be seen that the current will continue to flow without measurable decrease for a year, and an upper bound of some 10^5 years (Tinkham, 2004). This feature of a superconductor is known as persistent mode. Running a superconducting magnet in persistent mode is advantageous for a number of reasons. But in particular once the coil is energised, no external current will need to be introduced into the circuit. Typically current is passed into the circuit in the cryogenic environment from a Power Supply (PS) that is located at room temperature. The metallic leads through which the current flows to the magnet introduces ohmic heating as well as conducting heat from the room

temperature environment. This can place a large demand on the cryogenic cooling system whether it be a cryo cooler or liquid cryogen. An optimally sized current lead will introduce a thermal load of over 40 W per kA in conducting current from room temperature to 77 K

Superconductors can be split into two classes, The Low Temperature Superconductors and the High Temperature Superconductors. A Low Temperature Superconductor (LTS) is typically a pure metal or alloy having a T_c ranging from 23 K to 0K (Nave, 2010). It is possible to make a zero resistance connection and thus create a fully superconducting circuit that will allow a LTS coil to run in persistent mode. Unfortunately the low T_c of LTS materials means they are expensive to refrigerate.

High Temperature Superconductors (HTS) typically have a T_c above 77 K, the boiling point of liquid nitrogen at atmospheric pressure (2G wire (YBCO) 93 K, 1G wire (Bi-2223 110K). This makes them appealing in terms of cooling efficiency. The HTS material is no longer a pure metal or alloy, it is now comprised of a compound and the most common one to date has the structure $YBa_2Cu_3O_7$ (Nave, 2010). Magnets made with HTS are not able to be run in true persistent mode, as there has been no technology achieved to form SC joints in HTS compounds to date (Rohlf, 1994). Therefore a SC circuit with resistive joints will have a current decay that can be modelled by the equation below.

Equation 1-1

$$I = I_0 \cdot e^{-\frac{R}{L}t}$$

Where I is the current at time t , I_0 is current in the SC at $t = 0$, R is the total resistance in the circuit and L the inductance of the coil.

This decay leads to the problem of needing an external power source to maintain a constant current level in the circuit. This arises to having to use a current lead feed through system, which introduces ohmic heating losses as mentioned before and does not maximise the benefits of operating at higher temperatures.

This problem can be circumnavigated by embedding a device known as a flux pump (FP) in the cryogenic environment and thus removing the current lead feed through system altogether (Hoffman, Pooke, & Caplin, 2011). The flux pump works on the basic principle of Faradays law of induction, where a changing magnetic field, for example a PM moving away from a loop of wire causes a voltage to be induced. According to Lenz law in Equation 1-2 the polarity of the induced voltage is such that it tends to produce a current whose magnetic field opposes the

original field change. This results in a net flux change of zero. A current now flows in the circuit, which will be explained in the coming text.

Equation 1-2

$$V_{ind} = -\frac{d\Phi}{dt}$$

Previous work has led to the development of an HTS DC dynamo flux pumping method . This method uses PM magnets which pass over an HTS tape and as a result flux is injected into the circuit. This injection of the flux increments the current for each pass of a PM magnet. More on this method can be found in the references (Van de Klundert & ten Kate, 1981) . This method is to be used as a basis for creating a prototype flux pumping system that can be used in a commercial HTS magnet.

2 Literature review

2.1 Superconductivity

A superconductor will become superconducting and exhibit negligible electrical resistance if all three of the following conditions are satisfied.

1. The SC temperature is below a value known as the critical temperature T_c for that particular material. This is measured in Kelvin (K)

$$T < T_c$$

2. The current flowing in a given cross section of a SC needs to be below the critical current density J_c . The current density is the measure of current per unit area. This is measured in A/cm^2

$$J < J_c$$

3. The applied magnetic field B to the SC needs to be below the critical field of the SC. B is measured in the Tesla (T)

$$B < B_c$$

If all of the above three conditions are met, a current induced in a perfect superconducting ring or circuit will continue to flow without any measurable decay (Rohlf, 1994).



Figure 2-1. Levitating Magnet demonstrating the Meissner effect

When a superconductor is in a superconducting state it will exclude magnetic fields from its interior. This is known as the Meissner effect. Circulating currents will be produced in the SC to

oppose the build-up of magnetic field in the conductor due to Lenz law. Induced currents would meet no resistance, so they would persist in an opposing magnitude to the applied field to exactly cancel this. This phenomenon poses a problem when one wants to introduce magnetic flux into the superconducting circuit.

There are two types of superconductors, namely type I and type II. In a type I superconductor, a certain field known as the critical field (H_c) will cause the superconductor to transition to a normal conducting state.

This can be represented by Figure 2-2 below. Below H_c the field is completely excluded from the material and it is fully superconducting. However at H_c and beyond there is a complete breakdown of the superconducting state, the field fully penetrates and the SC transitions to a normal conductor. H_c typically occurs at around 100mT. This is a very low field and therefore of no or little use for any applications.

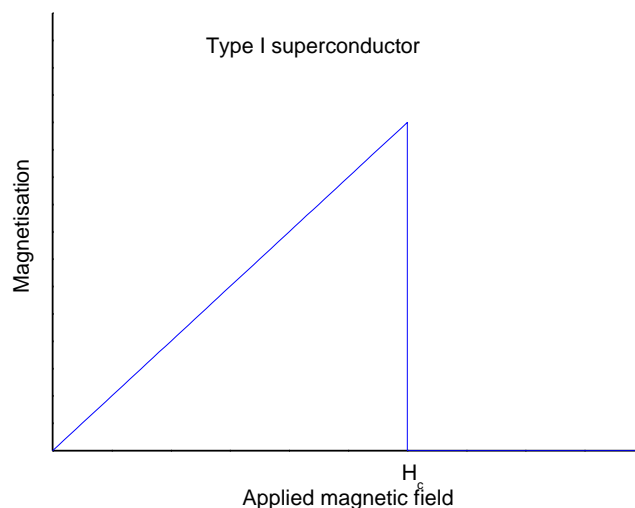


Figure 2-2 - Type I superconductor

The type II SC can exist in two superconducting states as shown in Figure 2-3. Below a magnetic field H_{c1} its properties are the same as a type I SC. Above H_{c1} the applied field is not completely excluded. However the SC is still superconducting at this state as a phenomenon known as the mixed Meissner state occurs. The magnetic field enters in the form of flux lines which are pinned to defects in the SC. These flux lines are normal spots and are surrounded by super currents. As the field is increased this will continue to happen until there is no space for flux lines left and the whole conductor will be in the normal state. This transition is known as H_{c2} and will tend to happen at fields greater than 10T. Most applications use the type II SC.

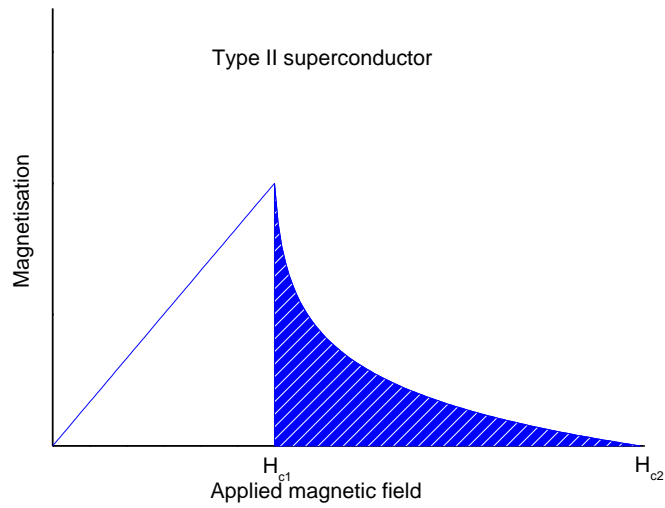


Figure 2-3 - Type II superconductor

2.2 Flux Pump Theory

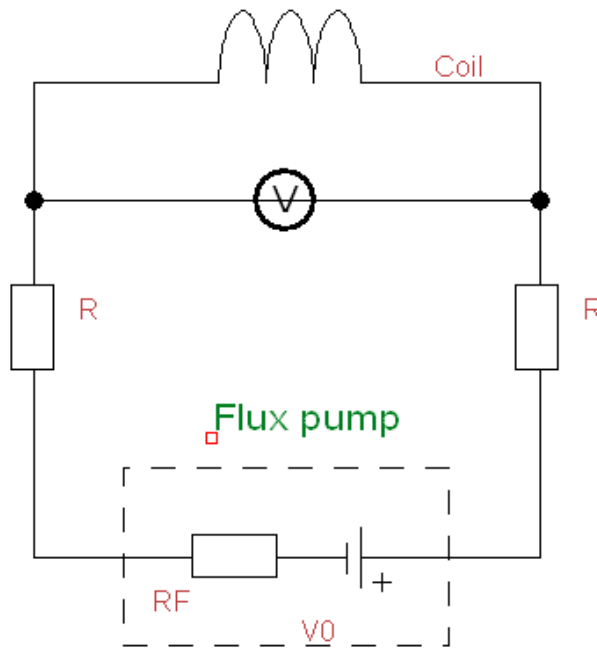


Figure 2-4 - Flux pump representation

The circuit diagram representing the pumping of flux can be realised by Figure 2-4. A coil with a self-inductance L is connected in series with two resistive joins R , a voltage source V_0 and internal resistance of the flux pump R_F . The voltage V_0 represents the induced voltage that

originates from Faradays law of induction. This circuit can be described by Equation 2-1 for the voltage across the coil.

Equation 2-1

$$V = I(2R + R_f) + d\Phi / dt = dLI / dt$$

As $R = 0$ when the loop is superconducting the above equation can be written in an integrated form as shown in Equation 2-2.

Equation 2-2

$$\Phi - LI = \text{constant}$$

Thereby Φ is the externally applied magnetic flux. From Equation 2-2 it can be immediately seen that a change in magnetic flux must always result in a change in current I as the inductance stays constant.

2.2.1 DC dynamo flux pumps

In order to actively increase the current in a LTS superconducting circuit using a flux pumping method, the following procedure was developed (Hoffmann, Personal communication, 2010).

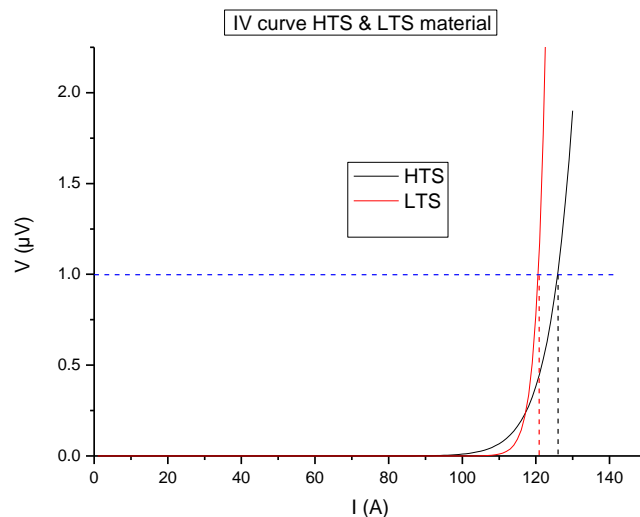


Figure 2-5 - HTS and LTS IV curve showing flux flow regime

As mentioned, applications typically use a type II SC. However the flux pinning in a type II SC is very strong below H_{c2} , therefore it becomes difficult to move flux lines.

Figure 2-5 shows the current-voltage characteristics (IV curves) of a HTS and a LTS and what is known as the flux flow regime. The red curve identifies the LTS IV curve and the black curve the HTS IV curve. Both IV curves follow a power law and are modelled from the equation below, where V is the voltage, I is the actual current, I_c is the critical current of the SC, and n is the exponent. The larger the n value the steeper the curve will be. In this instance the LTS has an n value of 50 and the HTS an n value of 20. These n values are typical for LTS and HTS materials (Tinkham, 2004).

Equation 2-3

$$V \propto \left(\frac{I}{I_c}\right)^n$$

The graph has a blue line at the voltage value of 1 μ V, which can be considered as the criteria for the SC to be in an effective SC state. From the blue line each curve has a corresponding vertical line indicating where their respective I_c is. The graph shows that the voltage of each curve stays at almost zero for a finite amount of current. When significant resistance appears the SC is said to be in the flux flow regime, where flux lines in the SC become mobile. However for the LTS one can see that the flux flow region is very small, according to Figure 2-5 approximately 10 A, compared to the HTS that has an approximately 28 A wide flux flow region in this example. The resistance of the SC curve increases rapidly above I_c , which leads to a rapid increase of power dissipation due to the relationship $P = I^2R$. The SC has to be able to absorb this heat load with a minimal temperature rise in order to remain SC. Since a LTS has an operating temperature of approximately 4 K the specific heat c is extremely low. The mass of the LTS is very small too, so combining these two terms in Equation 2-4 below, a large heat load Q leads to a large increase in temperature (Ekin J. W., 2006). Consequently a thermal runaway occurs, which is known as a 'quench' and the SC state breaks down.

Equation 2-4

$$Q = m \cdot c \cdot \Delta T$$

The HTS has a less rapid increase in resistance meaning a larger flux flow region to operate in, which is mentioned earlier and is approximately a factor of three bigger. The HTS is typically operated at the liquid nitrogen temperature where its specific heat capacity is much larger than at liquid helium temperatures (4.2 K), thus it can absorb the heat produced much better and keep the temperature rise low enough as to ensure a quench does not occur.

It can be concluded that the type II LTS cannot be used to inject magnetic flux into a circuit due to the heat dissipation problems when flux lines are moving (flux flow regime). However the type II LTS can be used in conjunction with a type I LTS to achieve flux injection into a SC circuit. This is explained below.

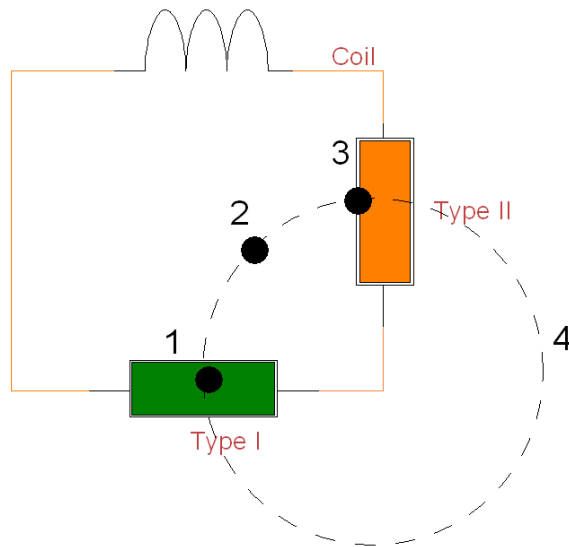


Figure 2-6 - Flux pumping illustration DC dynamo

In Figure 2-6 the circuit has a SC coil, a segment of type I SC, type II SC and a PM which is denoted by black circles. The PM moves in an iterative circular motion along the path of the dashed circle and the numbers denote the different stages of the flux pumping operation. At stage 1 the PM magnet is passing over the type I SC. This causes a normal conducting region or spot to be created, as the level H_c shown in Figure 2-2 can easily be exceeded by a PM. It is to be noted that the PM pole surface area must be smaller than the SC width to ensure that only a normal conducting spot is created. This allows flux lines to fully penetrate the circuit at the region or spot without creating a non-SC path in circuit. Thus when a magnet is moved across the SC, the flux lines follow and at stage 2 they have effectively been 'smuggled' into the SC circuit. At stage 3 the PM is being moved over the type II material. The PM sends the corresponding region into the mixed state. However the flux lines get strongly pinned to defects in the type II SC. So when the PM moves to stage 4 in the diagram the pinning force is too great for the flux lines to follow. The flux that was 'smuggled' into the circuit is now trapped and as result screening currents are generated, following Lenz law to compensate for the removed magnetic field. This iterative process increases the current by one unit for every complete magnet rotation.

2.2.2 Flux pumping with HTS

The type I SC typically has a T_c below 10 K, so the approach described above cannot be used for HTS. HTS material is a type II SC so it is difficult to achieve a normal conducting region or spot. The only ways possible to do so are as follows (Hoffman, Pooke, & Caplin, 2011):

1. Lower the J_c significantly so a coil or PM can overcome H_{c2} as in Figure 2-3.
2. Local heating to exceed T_c

Both options are considered impractical for any real applications. However it is not necessary for a normal conducting region to exist in order to inject flux, if a flux flow regime exists where flux lines can be moved without causing a quench.

Figure 2-7 shows a diagram to illustrate the flux pumping method with HTS. The diagram shows the cross section of a circuit in which a SC coil is connected to a HTS loop. At the opposite end to the coil sits a rotor containing 6 PM. This rotor is free to rotate about its central axis on a stationary axel. It is positioned so that during rotation the magnets cross the tape with very little clearance.

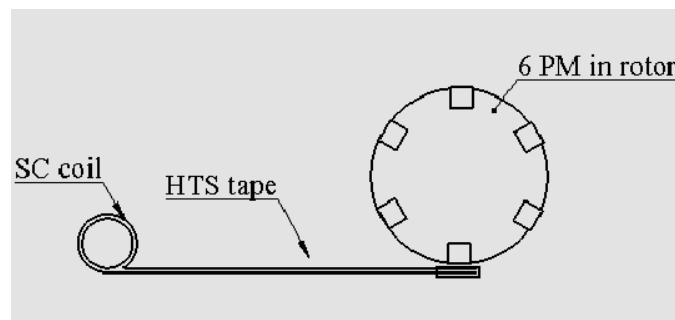


Figure 2-7 - HTS flux pumping method

When a PM approaches the HTS tape it sends a corresponding region into the mixed state allowing flux lines to enter and be pinned to pinning centres. The PM continues to rotate and a counter torque is applied to the rotation of the rotor due to the strong pinning forces acting against the movement of the PM. If a large enough torque is applied to the rotor the pinning force can be overcome and flux lines will be pulled off their pinning centres. The flux lines follow the motion of the magnet and are pushed through the SC. This flux motion causes a resistance and thus a voltage drop. Due to the specific heat of the HTS being larger at liquid nitrogen temperature it can absorb the heat generated from the increase of resistance with little temperature rise. This avoids an immediate quench and magnetic flux enters the circuit. When the magnets upwards trajectory leaves the circuit, the flux lines that entered the circuit cannot follow due to the pinning in the HTS conductor and are trapped. This in turn generates a current due to Lenz's law which is iteratively increased for every magnet passing by.

2.3 Brushless motors

Since the mechanical approach of moving a PM over a superconductor is to be used, a motor will be employed to provide the mechanical rotation. Two types of motors are to be investigated. The DC brushless motor and the DC stepper motor. Both motors do not use brushes, which is important in terms of reliability and robustness. The system could be running for days, weeks, etc so the less wearing parts, the better. AC motors were not considered due to their typical size and the additional hardware needed for the AC voltage source.

2.3.1 Stepper motors

There are three basic types of stepper motors, a variable-reluctance-, PM- and a hybrid-stepper motor.

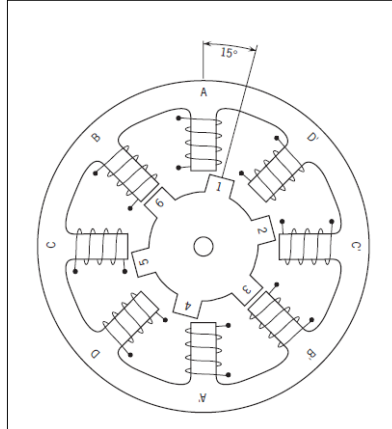


Figure 2-8 - Variable-reluctance (VR)

Figure 2-8 shows a cross sectional view of a typical VR motor (Solarbotics, 2003). The rotor is made of a soft iron toothed core, the stator consists of a series of windings. When these windings are energised with a DC current the poles become magnetised. Rotation is carried out when the attraction of the iron teeth to the energised poles occurs.

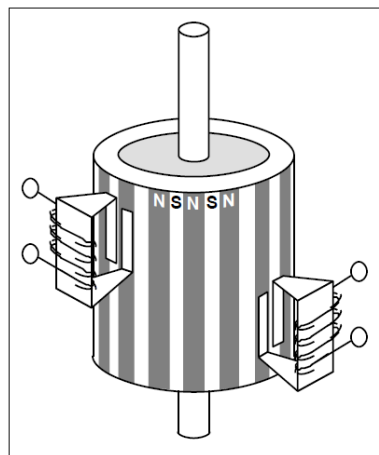


Figure 2-9 - Permanent-magnet (PM)

Figure 2-9 shows the simplified design of a PM stepper motor (Stutz, 2000). They are typically a

low cost and low resolution motor, which have a range between 24-48 steps per revolution. Permanent magnets are used on the rotor in an alternating north south pattern. The coils are energised to create an alternating north south field in order for rotation to occur. The magnetised rotor poles provide an increase in magnetic flux intensity, which compared with the VR stepper gives an increase in torque characteristics.

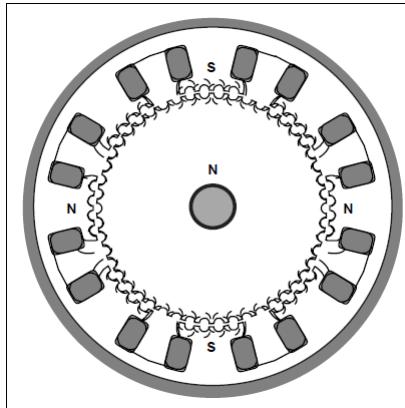


Figure 2-10 - Hybrid

Figure 2-10 - Hybrid shows the cross sectional view of the Hybrid stepper motor. It is more expensive than the PM version, but offers better step resolution, torque and speed. It uses the best features from a PM and a VR stepper. Like in the VR version the rotor is multi toothed and contains an axially magnetised concentric magnet around its shaft. The rotor teeth provide an even better path for guiding magnetic flux to preferred locations in the air gap. This further increases the detent, holding and dynamic torque characteristics when compared to the VM and PM stepper motors.

The three types of stepper motors usually take on two forms of coil configuration, Bipolar and Unipolar.

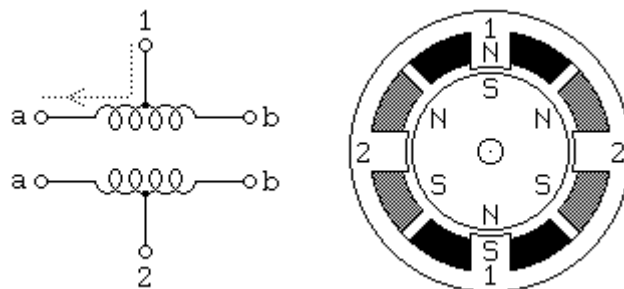


Figure 2-11 - Wiring configuration of unipolar stepper motor

The typical wiring configuration of a unipolar stepper motor is illustrated in Figure 2-11. It usually has 5 or 6 wires. A centre tap is attached to each of the two pole windings and attached to a positive supply. The two ends of each coil are alternately grounded to reverse the direction of the field produced by each winding. The cross section of the motor in Figure 2-11 is set up so it has 30° per step. Motor winding 1 is distributed between the top and bottom motor poles. Motor winding 2 is distributed between the right and left motor poles. The PM rotor has 6 poles, alternating north south, which gives the 30° resolution. In Figure 2-11, current is flowing from terminal 1b to 1a, which causes the top stator pole to be north and the bottom stator pole to be south. If the power from winding 1 is removed and winding 2 is energised the motor will turn 30°. Alternating this procedure will result in continuous rotation (Introduction to Stepper Motors).

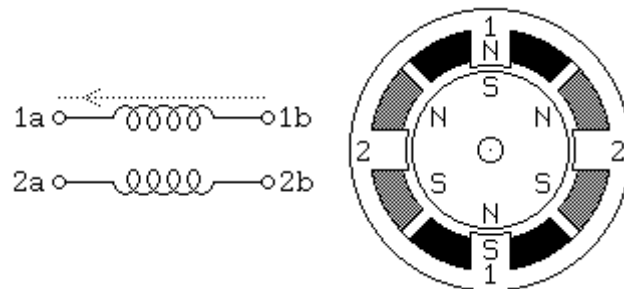


Figure 2-12 - Wiring configuration of Bipolar stepper motor

Bipolar stepper motors are constructed the same as unipolar stepper motors, however the wiring of the windings differs. There are no longer any centre taps which reduces the number of wires to four. However this makes them harder to control and requires a complex driver. An H bridge configuration is used, which allows the polarity of each end of the coil to be controlled independently. The control sequence is the same as a unipolar stepper (Solarbotics, 2003).

Advantages of a stepper motor (Introduction to Stepper Motors) :

1. Rotation angle of the motor is proportional to the input pulse (can be accurately controlled in open loop).
2. In a stationary position the motor has full torque (as long as windings are energised).
3. Precise positioning and repeatability. Good stepper motors have an accuracy of 3-5% of a step and the error is not cumulative from one step to the next.
4. Excellent starting and stopping response.
5. Very reliable. No brushes used, so the lifetime is determined by the bearings.
6. The motor responds to digital input pulses which provide open loop control.
7. Possible to achieve a very low speed synchronous rotation with a load that is directly coupled to the shaft.

8. A wide range of rotational speeds is possible due to the speed being proportional to the frequency of the input pulses

Disadvantages of a stepper motor (Introduction to Stepper Motors)]:

1. Resonances can occur at certain coil switching frequencies.
2. Not easy to operate at extremely high speeds.

2.3.2 Brushless DC motors

There are two types of the brushless DC motors (BLDC), either with the stator positioned on the outside of the rotor or inside of the rotor.

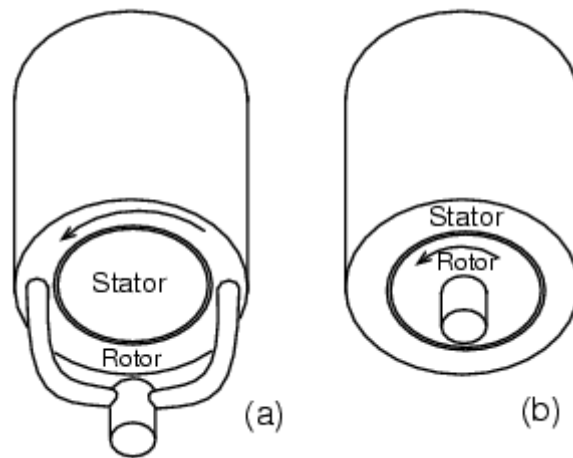


Figure 2-13 - BLDC types

Motor a in Figure 2-13 has the rotor on the outside whereas motor b has the rotor on the inside (Solarbotics, 2003). In the outer rotor design the windings are located in the core of the motor and the opposite is true for the inner rotor design. This means that magnets on the outside act as an insulator and therefore reduce the rate of heat dissipation from inside the motor. The outer design generally runs at a lower duty and a lower rated current for this reason. The primary advantage of the outer rotor design is the relatively low cogging torque. The inner rotor design effectively dissipates heat as the windings are on the outside. A motor's ability to dissipate heat directly impacts on how much torque it can produce. Thus the latter is the most commonly used version (NMB, 2010) (Brown, 2002).

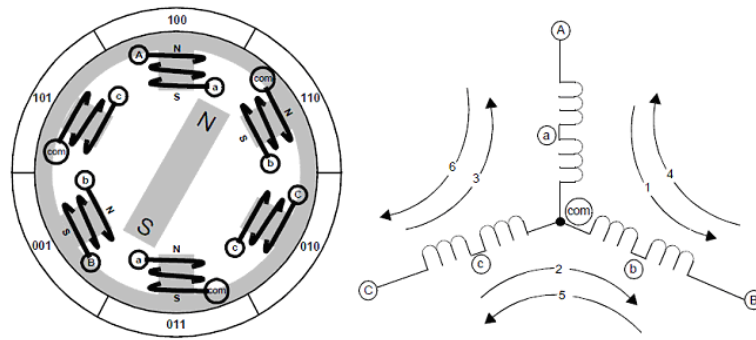


Figure 2-14 – Schematic of the basic anatomy of a BLDC motor

In a BLDC motor electrical energy is converted to mechanical energy by the magnetic attractive forces between the magnetic rotor and the rotating magnetic field induced by the windings. Figure 2-14 above shows electromagnetic circuits connected at a common point (Brown, 2002). Each electromagnetic circuit is split in the middle, thereby allowing the PM rotor to move in the centre of the induced field. Most BLDC motors have a three-phase winding topology with a star connection. In this type of configuration the motor is driven by exciting two phases at a time. The static position of the rotor in Figure 2-14 occurs from a current path flowing from A to B seen as path 1 in the schematic of Figure 2-14. Due to the fields produced by such a current path it can be seen that the rotor is exactly between windings Ab and aB. The rotor can then be made to rotate 60 degrees by changing the current path from C to B seen as path 2 in the schematic of Figure 2-14. The suggested magnetic alignment is only used for visual purposes. In reality the maximum torque is obtained when the magnetic rotor is rotated 90 degrees away from alignment with the stator field. The key to BLDC driving is to sense the rotor position, then energise the phase that will produce the greatest amount of torque. This is usually done using Hall Effect sensors.

Advantages of a BLDC motor (Brown, 2002) :

1. No brushes and therefore maintenance free. Can run for over 10,000 hours.
2. Can operate at speeds above 10,000 rpm under loaded and unloaded conditions.
3. Responsive and quick acceleration due to inner rotor BLDC motor having a low inertia.
4. High power density. BLDC motors have the highest running torque per cubic inch of any DC motor.

Disadvantages of a BLDC motor (Brown, 2002) :

1. Most expensive DC motor.
2. Most complicated DC motor control required.

3 Scope

There exists a dynamo flux pump that was built to test the concept of pumping flux in HTS. It is currently a laboratory experimental rig that is cooled in a bath of liquid nitrogen. HTS-110 requires research to be conducted into realising how the FP would work in an industrial magnet system. In addition to implementing a FP in the system, it is to be investigated if the FP has the potential to produce a homogenous field that fits the one parts per million (PPM) stability criterion needed for NMR imaging. The end result of this project will see a new flux pump being incorporated into a commercial HTS liquid cryogen free magnet to generate a controlled substantial B-field. This will remove the need for a conventional current lead feed through system as well as an external PS to supply current to the coils.

The laboratory version of the FP having proved the concept for pumping flux using HTS, is far from being ready to be put into a commercial magnet system. It has not been designed for technical applications by where it is capable of energising a commercial SC magnet. It is limited in the following ways:

- The existing HTS FP is submerged in liquid nitrogen. So no cryogenic heat considerations have been taken into account in regard to heat conductance. This is very important once it is operated in a cryogenic liquid free environment.
- Rotational control is currently done using a DC brush motor run at a constant speed that is set by the user. Brushes are prone to wear quickly.
- No control system in place for various fields.
- There is minimal monitoring of the system. Currently only the magnetic field is being sensed. It will be important to have a monitoring system for temperature and magnetic field in place when the FP is operated in a commercial system. This will protect the expensive SC components from damage and facilitates a homogenous level of field control to be achieved.
- The magnitude of the total heat load of a FP in comparison to a current lead feed through system has not been demonstrated.

4 Proposed Methodology

The design of the FP system has two core areas. The mechanical aspect, which consists of mechanical and cryogenic elements and goes through the various stages of design, fabrication, assembly and testing. The second is the development of a control system that is used to automate the system. This consists of embedded hardware and software. Both parts need to be concurrently worked on to ensure there is minimal downtime and testing can happen as soon as possible.

The mechanical aspect needs to be designed applying traditional mechanics as well as considering cryogenic elements, namely heat transfer and thermal contraction. Finite Element Modelling (FEM) should be carried out to evaluate certain design aspects as well as miniature experiments being conducted all of which will enforce design decisions.

The majority of the design will be done using the computer aided design (CAD) software package Solidworks. The FEM is carried out using the software Opera.

The Control aspect will consist of becoming familiar with the PIC microcontroller and the associated development environment. This will mean obtaining a development board that can be easily interfaced with a PC and experimented with immediately. Various hardware will need to be developed for the control and monitoring of the system using electrical circuit theory. At the higher level of the system embedded software will be developed to implement a control algorithm, enable sensor readout and synchronise communication between hardware.

5 Mechanical Design

The flux pump prototype is to be interfaced with an existing commercial HTS-110 suitcase magnet. HTS-110 has stated the following design framework:

- The cryogenic cooling is to be carried out using a Cryotel GT6-40 Stirling cooler, which is rated at 240 W and is capable of providing 15 W of cooling power at 77K according to the manufacturer Sunpower Inc.
- The flux pump is to be interfaced with an existing current feed through flange that is part of the HTS-110 suitcase magnet.
- The dimensions of the flux pump module should not exceed 140 mm wide, 140 mm long and 200 mm high.
- A vacuum chamber to be used that is either constructed from Stainless Steel or Aluminium.
- Obtain an equilibrium temperature throughout the new design that is below 77K. A stable temperature needs to be maintained during operation. It is unknown how the flux pump will operate in this temperature range, as increased flux pinning may become an issue.
- Operational heat load of the FP has to be comparably less than the conventional current lead technology.

The mechanical design needs to be carried out with emphasis on the cryogenic temperatures that will be present to ensure a robust, operational and efficient design is achieved. Materials need to be carefully selected based on expansion coefficients to ensure thermal contraction does not prohibit the operation of the flux pump or cause areas of the design to be subjected to large amounts of compression or tension. Minimising the transfer of heat from the outside to cryogenic environment is very important. There are three forms of heat transfer that need to be considered to ensure this is achieved, namely convection, radiation and conduction. To minimise convection it is important to have a high vacuum system in place that is sustained for long periods of time, in the order of days, weeks, months. Radiation from the room temperature vacuum casing will have a large effect on heat transfer. Reducing the radiation using a form of shielding will be required. Thermal conduction has to be minimised in terms of any suspension mounts that are in direct contact with the FP and any areas at room temperature. However, as conduction is the primary way of cooling the flux pump in this system, it also has to be maximised in some instances. Therefore thermal conductivity of materials along with cross section and dimensions will be important in order to meet the desired conduction requirements.

Overall basic mechanical principles need to be applied. This involves ensuring material characteristics and element dimensions are sufficient thus ensuring stress and strain will not affect the robustness of the design.

5.1 Test Apparatus

During the design process a test rig comprised of interchangeable parts was used to carry out various experiments in order to optimise the final design.

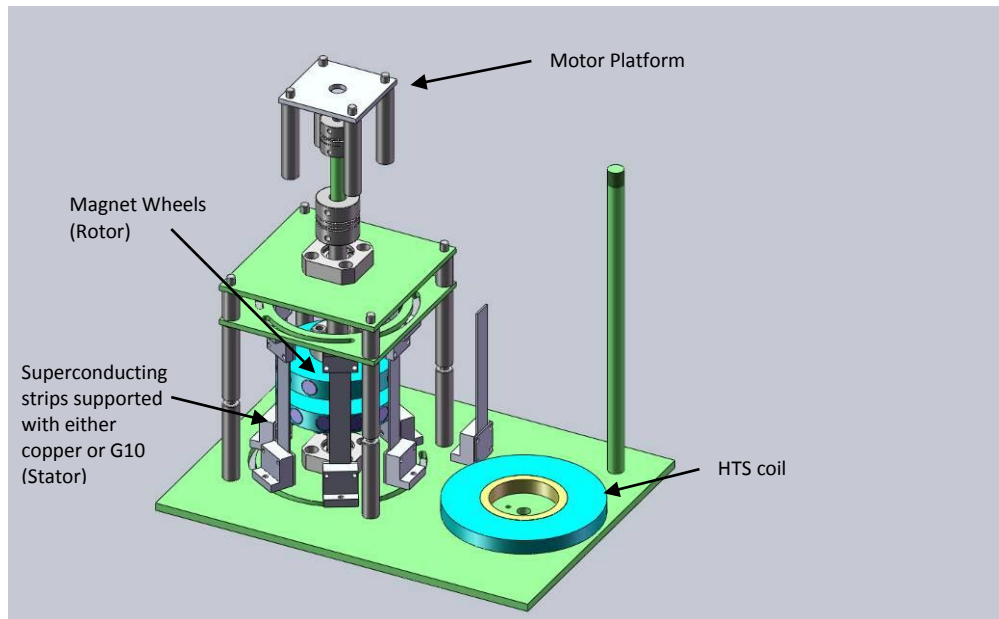


Figure 5-1 - Flux pump Test apparatus

The test apparatus shown in Figure 5-1 consists of a simple stator and rotor system which is used to induce a voltage in the HTS coil. It is capable of taking two types of motors. A low speed geared motor (maximum frequency 4 Hz) and a high speed non geared motor (maximum frequency 40 Hz).

5.2 Stage 1 – Stator design

Stage 1 involved designing the basic superconducting stator. The stator is able to accommodate a maximum of 6 SC strips that are in parallel with each other. The I_c (77K, self-field) of the SC wire is higher than 250 A (manufacturer: Superpower). However the current carrying capacity is restricted to 50 A, which is a result of the wire being operated in the flux flow regime. The current carrying capacity can be increased to 100 A per branch by having two strips soldered face to face. The Superpower tape used in this instance is non-stabilised, meaning that there is no additional copper layer being used to give the SC electrical stability in over-current situations. Figure 5-2 shows the net arrangement of the SC tapes.

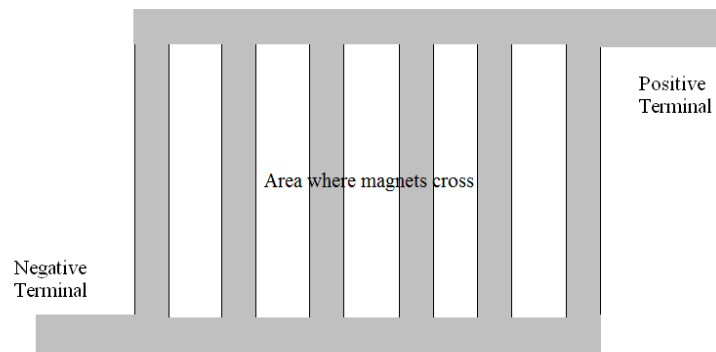


Figure 5-2 - Stator SC arrangement

The SC stator arranges the above net in a circular fashion, which can be seen in Figure 5-3.

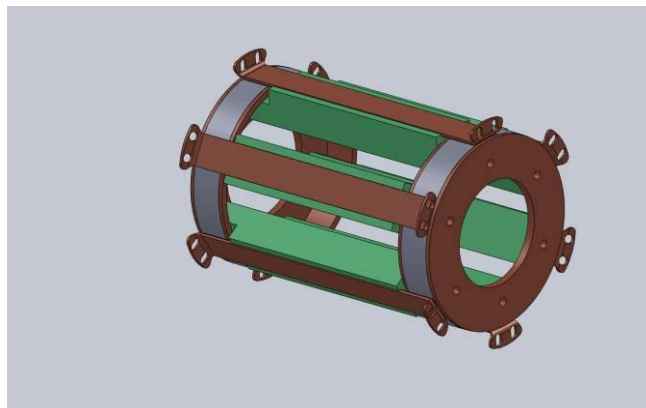


Figure 5-3 - Original stator design

A copper ring is positioned at each end of the stator onto which the positive and negative terminals are soldered. Due to its high conductive properties at low temperatures (Figure 5-4) oxygen free high conductivity (OFHC) copper is the material of choice. The grade of copper to be used here will typically have an RRR value of 100.

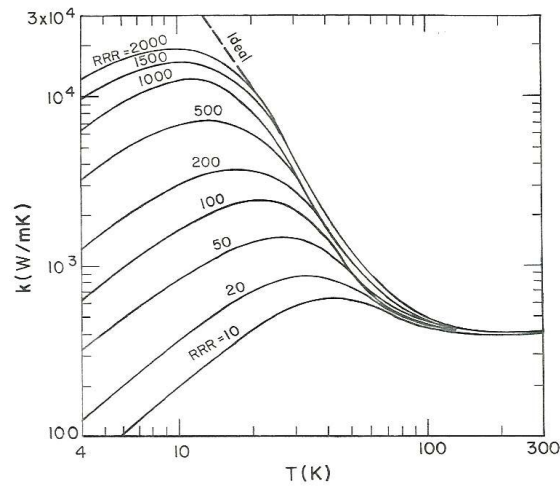


Figure 5-4 - Thermal conductivity of Copper (Van Sciver, 2010)

The SC net shown in Figure 5-2 is to be held in the stator chassis using solder. The positive and negative terminals need to be soldered into the copper rings at the respective ends of the stator. The SC branches are to be soldered to copper strips around the circumference of the stator rings. These copper strips offer structural support to the delicate superconductors as well as acting as a heat sinks to ensure the strips stays at cryogenic temperatures. The green G10 supports shown in Figure 5-3 are there to act as jig when assembling the stator. They are mounted to the copper rings to allow the superconductor to be supported while all the parts are soldered in place. Once the solder has hardened they are removed. This design, although relatively simple to manufacture, has the downside that once assembled the rotor shaft cannot be simply inserted. The magnet rotors will have to be put through the SC strip gaps and then rotated by 90 degrees so the shaft can be slid in. Being neodymium magnets with a strong field, the difficulty arises in ensuring they do not attract towards one another and cause damage. Additionally Figure 5-5 shows the difficulty of mounting the flat copper supports to the round stator ends in this design. The parallel SC strips would need to be bent across their width to match the stator rings circumference to ensure a low resistance join. On the one side this bending has the potential to damage the SC and on the other side the SC strips are not in full contact with the flat thermal bus bar.

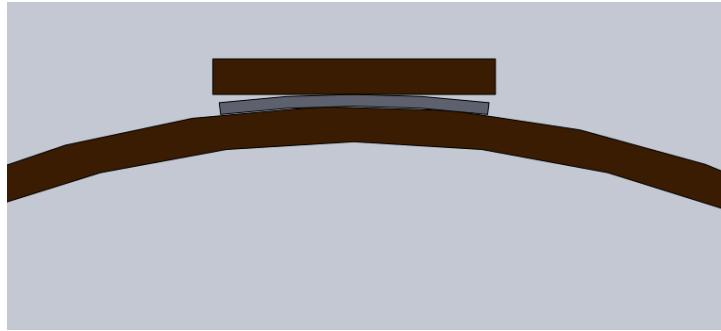


Figure 5-5 - SC at tangent to copper bus bar

5.3 Stage 2 – Rotor design

The rotor houses 36 neodymium PM. 12 PM are placed around the circumference of three aluminium disks, as shown in Figure 5-6. The magnet wheels and main shaft are made of aluminium due to its low density. It is much lighter for a given volume than most other alloys and metals, which is important when one wants to keep the inertia of the rotating system as low as possible. It is also crucial to cool the rotor to cryogenic temperatures so it does not radiate heat and place an additional heat load on the SC strips. Aluminium has a high thermal conductivity of 55 W/(m·K) at 77 K which allows adequate cooling, however it is much lower than the thermal conductivity of copper at 77 K, having 544 W/(m·K). The rotor shaft is connected to the flux pump at one end, which will be at cryogenic temperatures while the other end is connected to the vacuum feed through, which will be at room temperature. In this way a temperature gradient along the length of the shaft will occur. It is important to minimise the heat flow along the shaft, which can be calculated according to Equation 5-1 (Ekin J. W., 2006).

Equation 5-1

$$\dot{q}_{cond} = \lambda(T) \cdot A \cdot dT / dx$$

Where A is the cross sectional area, dT/dx is the temperature gradient along the element, and $\lambda(T)$ is the thermal conductivity of the material at temperature T .

Using tables from Ekin (Ekin J. W., 2006) an approximation can be made along the length of an element using the equation below

Equation 5-2

$$\dot{q}_{cond} = (A/L) \cdot \bar{\lambda} \cdot \Delta T$$

Where L is the length of the element, $\bar{\lambda}$ is the average thermal conductivity between two temperatures and ΔT is the temperature gradient along the element.

By increasing the length L in the above equation, reducing the cross sectional area A and selecting a material with a low thermal conductivity the heat flow can be reduced. Due to the limited room inside the vacuum chamber it is not feasible to make the drive shaft very long. Instead the drive shaft is designed so its first point of contact with the hollow aluminium rotor shaft is at the end of the rotor, furthest from the vacuum feed through. This gives a large L value of 118mm and removes the need to extend the length of the vacuum chamber. The cross sectional area of the drive shaft is manipulated and reduced by making the shaft hollow. These manipulations to geometry and material selection lead to a heat conduction of the G10 shaft to be 9.8 mW. If the drive shaft was directly coupled from the vacuum feed through to opposite end of the FP (right hand side in Figure 5-6) the heat leak would be 54mW.

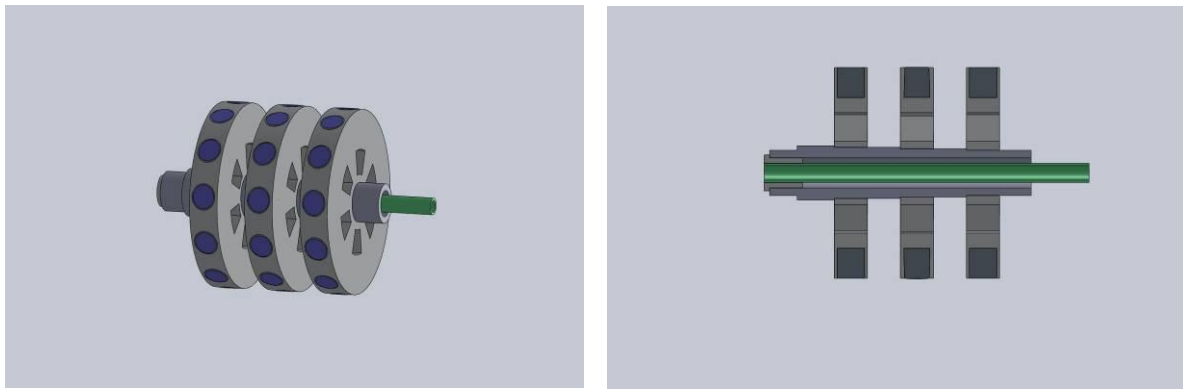


Figure 5-6 - rotor assembly & Cross section of rotor assembly

There are two types of forces that need to be minimised in order to guarantee a rotational system that will run smoothly and not be damaged from vibration. The first force is the axial force, which will typically be caused from components being able to move along the central axis of a shaft. The second is the radial force which can be caused either by a mass imbalance in the rotors, the centre of mass not being positioned correctly on the shaft, or an axle misalignment between the motor and shaft. These forces become an issue during the ramp up stage where the flux pump may reach rotational speeds of up to 1800 rpm. In particular the radial force at these frequencies will cause significant vibrations according to the centripetal force formula $F = mr\omega^2$, as the force F is proportional to ω^2 , the rotational speed.

To reduce the effects of a shaft to motor misalignment, a motor coupling will be used between the vacuum feed through shaft and the flux pump drive shaft, as well as one being used between the stepper motor drive shaft and the vacuum feed through shaft. Tight tolerances on

machining need to be in place in order for the bearing mounts to match one another in terms of alignment.

Ensuring the individual magnet wheels are aligned so they are in balance with each other and cause as less vibration as possible is difficult to guarantee, as the mass and dimensions of the PM are purely determined by the PM manufactures tolerance. To add to this complication, axial alignment of the magnet wheels on the shaft is only ensured in one direction due to the recessed sections for each wheel. However it is not guaranteed in the remaining axial or radial direction. Alignment in these directions is to be maintained by grub screws contacting the shaft. Misalignment can occur if the grub screws are not tightened evenly, they come loose by vibration or contraction due to temperature changes.

5.4 Stage 1 and 2 redesign

The concerns outlined for the stator and rotor design in the previous sections led to a redesign of both assemblies which eliminated these problems.

The stator was modified so that the rotor assembly can be completely assembled before being inserted into the stator. This allows the rotor to be pre-balanced and ensures ease of assembly as well as minimises the risk of the magnets damaging parts of the stator.

Before changes to the stator design were carried out it was decided to check if Eddy currents were going to manifest in the copper bus bars and act like a brake when the PM pass the copper cooling strips. If this was to pose a problem, a non-electrically conducting material would have to be used as the cooling bus over the SC.

5.4.1 Stator redesign

Previous tests carried out had shown that when three superconductors were stacked on top of one another, the third SC tape would not see a magnetic field, thus being magnetically shielded by the inner two strips. However, it was not certain that the intended copper cooling strip performs in similar manner as the third SC strip, thus the following test was carried out.

By using the test rig shown in Figure 5-1 two scenarios were considered. The first consisted of the two superconducting strips being attached to two copper bus bars. The second consisted of the same SC strips while the copper strips were replaced with G10 supports. G10 is obviously not a good thermal conductor, but since the experiment is being carried out in a liquid nitrogen bath thermal conduction will not be a problem. In the instance of a dry cryogen environment the G10 would be used in conjunction with sapphire. Sapphire has a high thermal conductivity

of 1100 W/m·K at 77K (Ekin J. W., 2006) which is even higher than the OFHC copper value. As sapphire is very brittle a G10 reinforcement is necessary to provide rigidity.

Once the rig was cooled to 77 K a simple test involving turning the rotor by hand revealed that with copper strips it was significantly harder to turn than with G10 supports. Obviously significant eddy currents were produced when using the copper cooling strips, which would lead to a large heat generation in a dry cryogenic environment and therefore considered as not being suitable.

This led to removing the copper strips and replacing them with the above mentioned sapphire and G10 configuration in the stator as shown in Figure 5-7. The thermal contraction of G10 (0.213 %) and sapphire (0.079 %) (Ekin J. W., 2006) differ significantly. Calculations indicated that the sapphire strip should be 0.5mm shorter than its G10 equivalent to ensure that the sapphire will not be placed in compression and break during cool down.

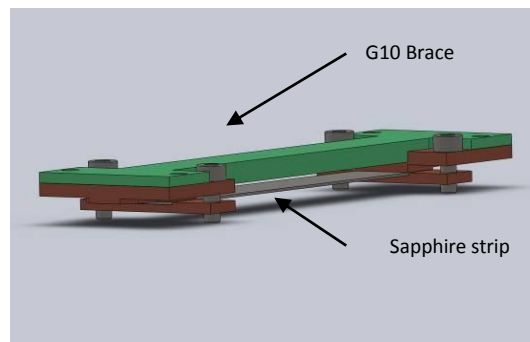


Figure 5-7 - G10 Sapphire system

The new stator shown in Figure 5-8 was designed so the rotor can be pre-assembled, balanced and inserted into the stator without any obstruction. In terms of the SC tape contact area, the stator was designed to have hexagonal ends. This allows a flat surface of contact for each joint and will ensure no bending along the width of the SC strips will take place. The corners of the hexagon in the inside face have radiuses to ensure the two SC current lead strips can be carefully laid over the surface without the risk of being creased and damaged when soldered to the stator. The stator has been designed so it has as little thermal mass as possible. This is important when soldering the SC tapes to the copper as one needs to minimise the exposure time of heat on the SC to ensure it is not damaged. In addition a low thermal mass gives the advantage of requiring less time to cool the rig to an equilibrium temperature. The reverse is true in the case of reheating.

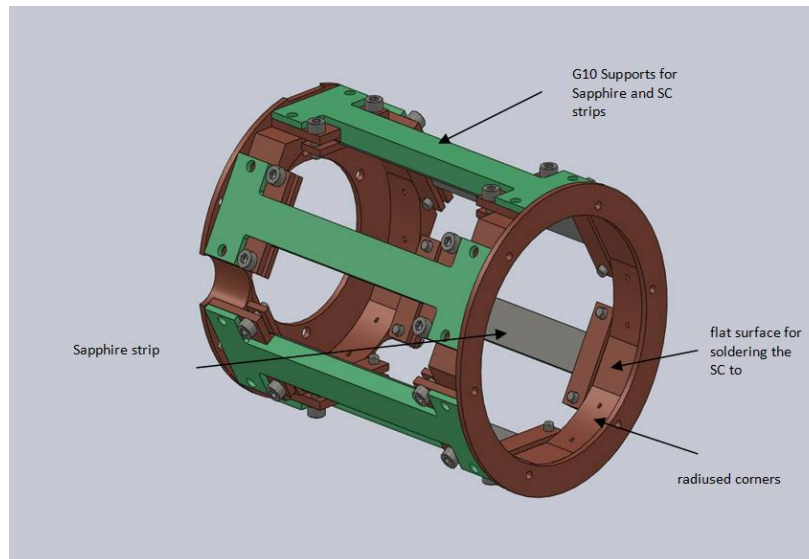


Figure 5-8 - The new stator design

5.4.2 Rotor redesign

The redesign of the rotor shown in Figure 5-9 reduced the amount of parts needed for assembly. The wheels and the aluminium shaft can now be machined from one piece. This removes the problem of aligning the wheels axially and minimises any differences in the radial direction thus minimising radial imbalances. Magnet pockets in the rotor are drilled 3mm deeper than the height of the magnet. This allows steel magnet shoes to be placed on top of the magnets so that the outer circumference can be machined to give a smooth round finish and reduce any radial imbalances. The rotor will be supported at each end of the aluminium shaft by a deep groove stainless steel bearing.

It is important to consider the contraction of the aluminium and the G10 at cryogenic temperatures. Thus it is important to calculate how much the inner diameter of the aluminium shaft and outer diameter of the G10 shaft will shrink in order to size them appropriately and ensure large compressive forces are not present. It is also important to make sure the Aluminium shaft will have the correct fit with the stainless steel bearings at cryogenic temperatures. In (Ekin J. W., 2006) tables for the thermal contraction $\Delta L/L$ with a datum of 293K to a specified temperature can be found for various materials. Aluminium contracts by 0.393%. G10 is not a homogenous material, therefore it contracts differently depending on what plane is considered. The tubes used in this design will be of the pultruded type, so the glass fibres will run around the circumference of the tube. Thus the value of contraction in parallel with the glass fibres should be considered when the radial contraction is to be calculated. (Ekin J. W., 2006) Also shows a table for calculating the change in radius, which uses a wall thickness to radius ratio as the parameter for identifying this change ($\Delta R/R$) in a percentage. Using this table and identifying a wall thickness to radius of 15% the ($\Delta R/R$) of

the G10 shaft can be found to be 0.24%. The Aluminium contracts more than the G10 so it is important to allow a tolerance in diameter to ensure the G10 does not experience a too larger compressive force and fail. The stainless steel bearings will contract by 0.279% at 77K which is less than the Aluminium so in this case one would be more concerned with the aluminium shaft coming lose in the bearing at cryogenic temperatures. The aluminium contracts 0.002mm more than the stainless at 77K thus a fit of bearing inner diameter minus 0.03mm should be sufficient.

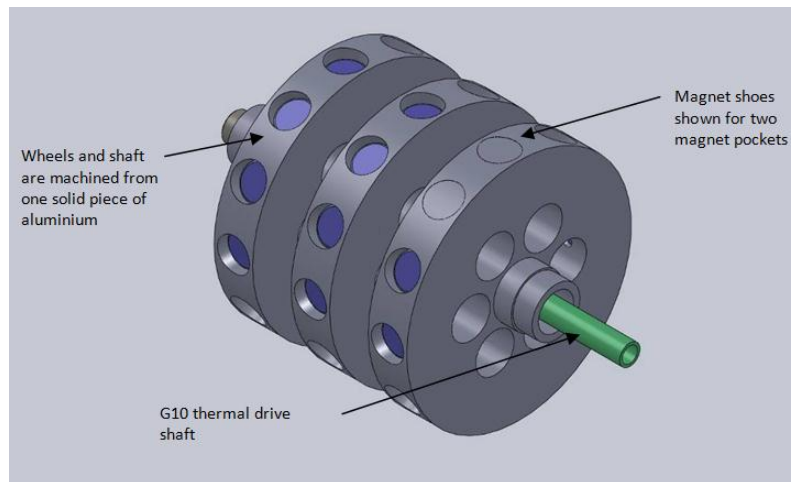


Figure 5-9 - Redesign of rotor

The bearing system to hold the rotor in place will need to be carefully designed. It consists of three different materials which all have different thermal contraction values. If this is not accounted for the material surrounding the bearings contracting could place the bearing in compression and it would seize to function. The bearing itself should be made of one material to ensure that parts will contract homogenously and not seize. A stainless steel bearing was chosen as they are readily available to obtain and consist of all stainless steel parts. The bearing will also not corrode, which is important when running such a part with no lubricant in a dry cryogenic environment with continual thermal cycling. No lubricant exists that will work at cryogenic temperatures.

From the two images in Figure 5-10 below it can be seen that one bearing mount is made of copper and one is made of G10. This is purely for thermal conduction. The copper mount is closest to the cold head and is vital for transferring cooling to the rotor. The G10 bearing mount is used to minimise any heat produced by the rotor from being transferred into the lower section of the stator. The G10 mount is raised from the stator plate by three G10 shafts. This reduces the conduction surface area and retards the heat flow further according to Equation 5-2 mentioned earlier.

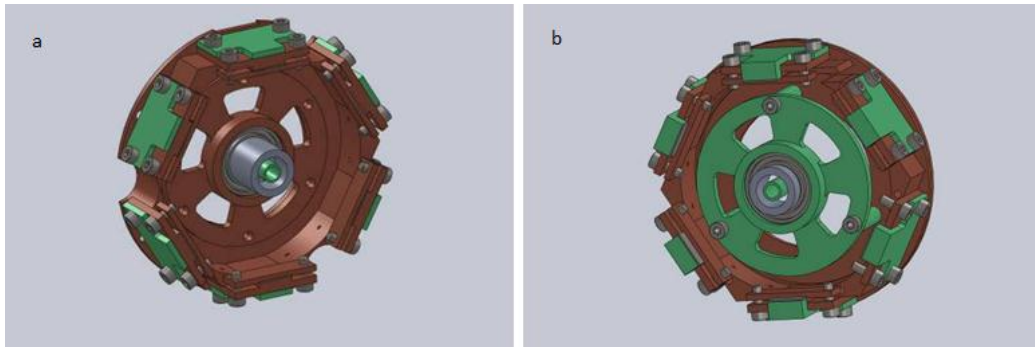


Figure 5-10 - a. Cross section of FP showing Cu mount. b. Cross section of FP showing G10 mount

5.4.3 Bearing mount test

Although calculations were carried out for sizing the various parts needed in the bearing system, it was decided to carry out a test to ensure the parts will not contract in a way that would jam the bearing once in cryogenic temperatures. Especially with a composite such as G10 literature values are not always exact. They can vary depending on the manufacturing process, so experimentation for validation is useful. Due to the G10 bearing mount being made from multiple layers of fibre matting and the thermal contraction being anisotropic, one could expect a circular hole to deform. So it is important to ascertain whether this would be a significant problem. Four test pieces of G10 were machined in the way they would be for the design, except each one had a slightly different diameter to see how it would affect the bearing. The four sizes were 0.03 mm (standard bearing fit), 0.08 mm, 0.13mm, and 0.18mm larger than the bearing. When the bearing mount was tested in liquid nitrogen it was found that regardless of the size of the G10 it would deform too much in the normal direction to the fibres. This would cause misalignment concerns for the rotor and would compromise the usability of the bearing. This deflection is noticeable to the eye without a large magnification and can be seen in Figure 5-11 below.



Figure 5-11 - Shows the deformation of a test sample of G10

As the G10 was found not suitable for a bearing mount, stainless steel was selected as a replacement. Stainless steel has a much higher thermal conductivity than G10 at cryogenic temperatures (7.9 W/m·K) but the value is still much lower than for copper (544 W/m·K). Therefore stainless steel can be used to still effectively minimise the heat flow from the rotor to the back of the stator. Also concerns of compression on the stainless steel bearing will vanish as the same material is being used.

A similar test was carried out to ensure the copper bearing mount would not cause the bearing to seize. Calculations showed that the copper bearing inner diameter would only contract 0.0014mm more than the stainless steel bearings outer diameter. Thus a normal bearing fit plus 0.02mm safety clearance should ensure the bearing still functions correctly. The test confirmed that the sizes are appropriate and the bearing did not jam.

5.5 Stage 3 – Flux pump module accessories

The next stage to the design is the mounts to hold the flux pump in place. The supports are designed in the same way as the drive shaft system to minimise heat conduction by having a large length, small cross section in a confined space. There is a total of three supports in the system. Originally the support was to be made entirely of G10 and it was decided to model the system using a cantilever to see how much one support would deflect when subjected to the weight of the flux pump. The flux pump weighs just over one kg so a load of 15 N was applied in the model with an allowance of 50% as a factor of safety. The inner tube was modelled, as it has a smaller diameter than the outer one and if inner tube will not fail, neither will the outer one. The tube has the following dimensions: O.D. = 8mm, I.D. = 3.5mm and length = 100mm. Equation 5-3 below shows the deflection of a cantilever beam (Young, Budynas, & Roark, 1975).

Equation 5-3

$$y = -WL^3 / (3EI_m)$$

Where y is the total deflection, W is the load applied, L is the length of the beam, E is Young's modulus of the beams material and I_m is the area moment of inertia about the centroidal axis of the beam.

This gives a total deflection of 1.7mm, which can be divided by three as there are two additional supports. Thus a deflection of 0.5mm is expected on each support, a value that is acceptable.

Assuming the outer tube was at 40 K, it was calculated with this configuration the heat conduction through the inner G10 tube from 40K to 293K would be 19 mW

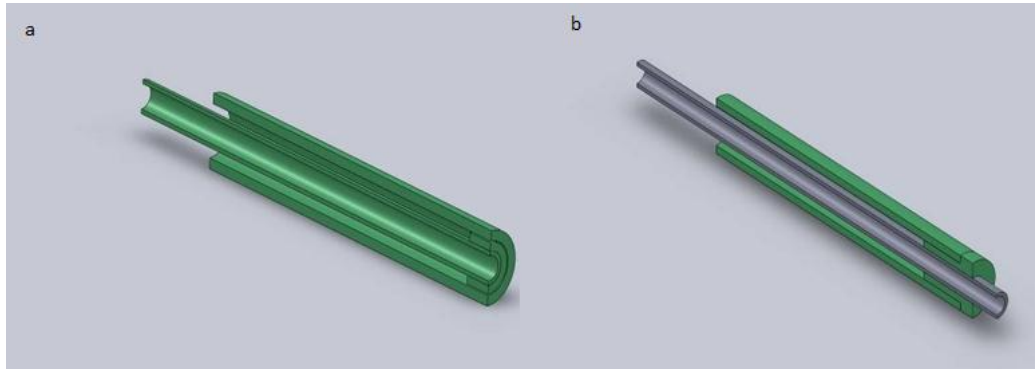


Figure 5-12 - a. G10 centre support. b. Stainless steel centre support

Although such a design (version a in Figure 5-12) has a low heat leak it would be difficult to assemble and the inner G10 rod needs to be at least 8mm in diameter in order to provide adequate support for the FP weight. So it was decided to investigate using a 6.0 mm O.D. stainless rod instead, which has an I.D of 3.0 mm. This was found to deflect 0.5mm for just one support and have a total deflection of 0.17 mm with all 3 supports. The heat load due to the stainless rod under the same conditions as the G10 rod was found to be 500mW which is much larger. Still the G10 outer section will reduce this significantly as a finite element model shows further in the text.

Figure 5-13 below shows the assembled flux pump with the supports incorporated. The three supports will be anchored at one end of the vacuum chamber which is shown further on in the thesis.

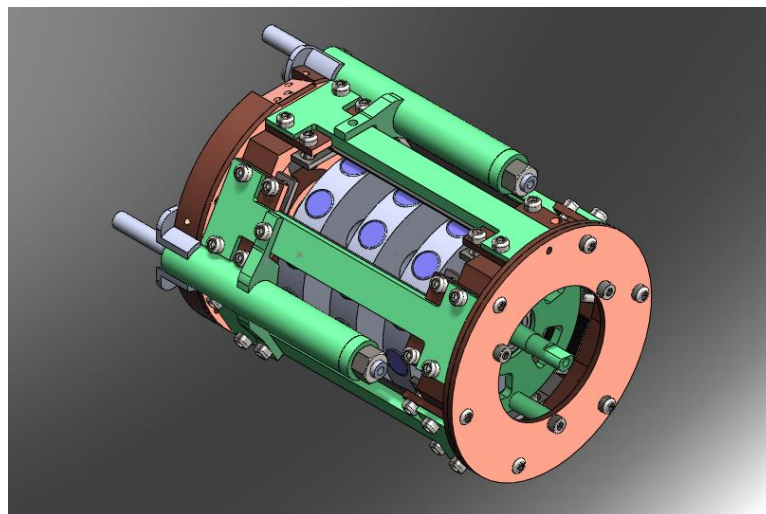


Figure 5-13 - Final design of flux pump.

5.6 Cooling system

The thermal bus from the cryo-cooler to the flux pump is along two semi flexible bus bars. These can be seen in Figure 5-14 below. They consist of a rigid outer bus bar with a inner flexible bus bar. The rigid outer bus bar is made from a solid copper strip, whereas the inner flexible bus bar is made from copper shim stacked in layers. The multiple layers means that the bus bar thickness can be easily adjusted if need be. This allows simple manufacturing in terms of material and fabrication, but will still ensure adequate cooling in comparison to the case that the bars were made from a single piece of solid copper instead.

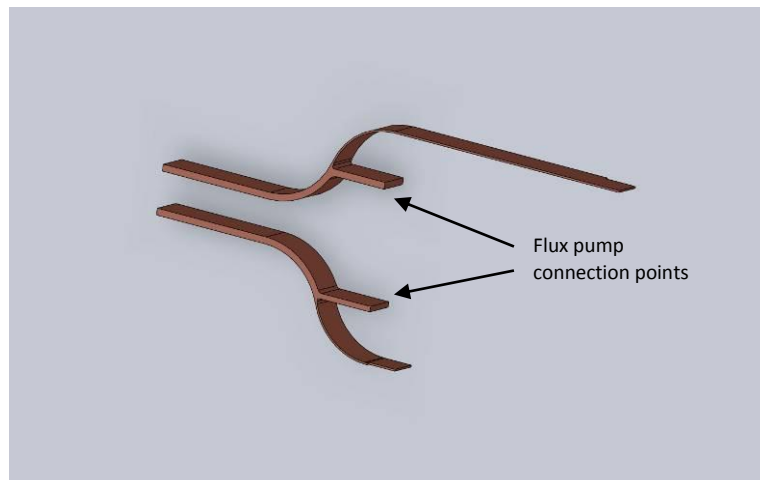


Figure 5-14 - Two thermal bus bars

The thicker portions of the bus bars represent the solid copper thin strips as well as the flexible multi-layer bus bars. These are then anchored at the cryo cooler cold head.

5.6.1 Stirling cooler calibration

It was decided to carry out a calibration test on the Stirling cooler to evaluate its true performance. This involved identifying the lowest temperature possible that the Stirling cooler could achieve in no load conditions. Then a known power could be applied with a resistor element to determine the heat load performance. The setup of the test is presented in Figure 5-15 on the left, and the applied heat load versus temperature in Figure 5-15 on the right. It was found that the minimum temperature achieved under no load conditions was 40 K. At 77K the total heat load capacity of the cryo cooler was 10 W, which is five watts less than in the manufactures data sheet.

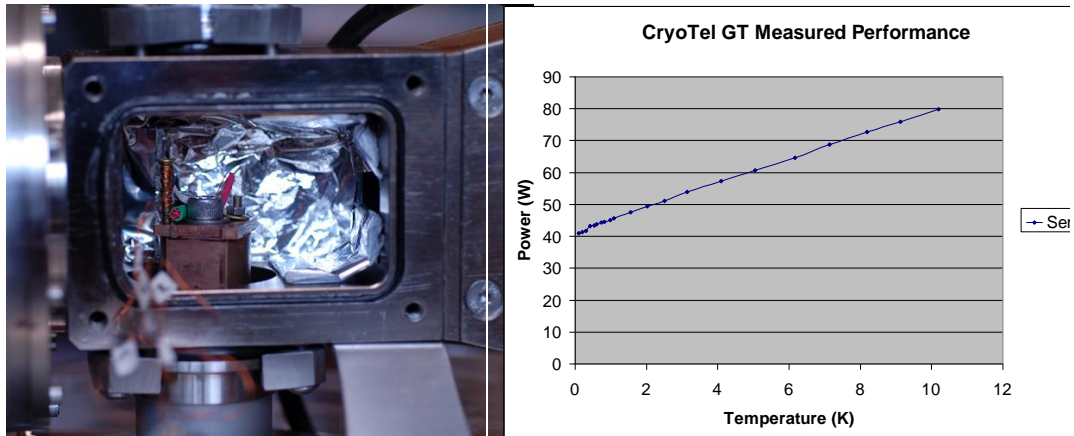


Figure 5-15 Heat load calibration set up & Cryotel GT measured performance data

5.7 FEM analysis

Finite element modelling (FEM) was carried out to validate the calculations and estimations done so far and therefore enforce the design. FEM can give an indication of the actual heat flows in the model and gives a visual representation of the heat and temperature distribution. Thus it is a great aid in trouble shooting. The modelling package used was Opera.

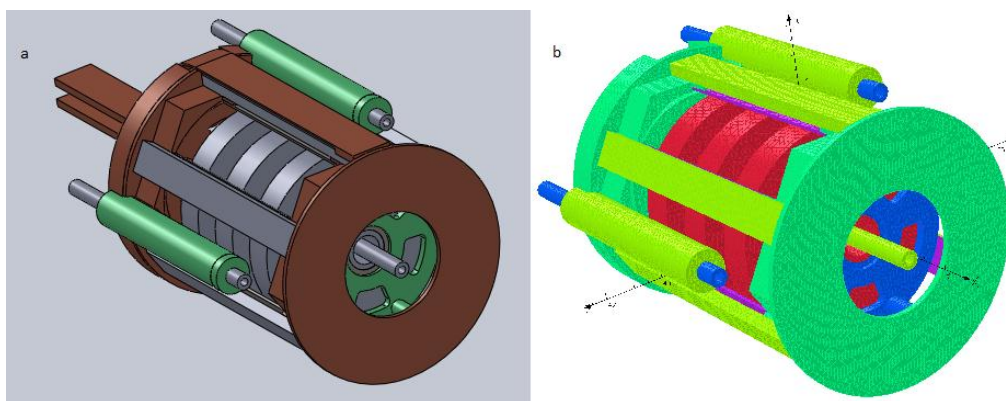


Figure 5-16 - a. Simplified FP model. b. FP model containing mesh

The five materials under evaluation in the FEM are Oxygen free copper, aluminium, G10, 304 stainless steel and sapphire. There are two boundary conditions which are set at 40 K and 293 K respectively. 40 K was the lowest temperature achieved by the Stirling cooler and 293 K is representative of room temperature which the supports and drive shaft are in direct contact

with. The temperature boundary locations for the model were chosen to be the end of the bus bars where they are attached to the cryo cooler, at the end of the 3 supports and the end of the drive shaft. The goal of this arrangement is to identify the total heat load on the cryo cooler that the FP would introduce due to conduction. Various parts of the FP can be investigated and the heat load determined along a particular section, most importantly the value of the heat load due to conduction along the supports. These results can be compared to the original assumptions and calculations to enforce the design.

The FEM package uses a triangle mesh to represent a model body. This mesh can be seen in Figure 5-16 b. The finer the mesh the more accurate the model becomes, however it increases the complexity and computation time. The mesh size used in this analysis was 0.2 cm, which gave a good compromise between computation time and model resolution. When analysing the model after it had been solved, it was found that the total heat load due to conduction was found to be 270 mW. This would indicate that each support would have a heat load of 90 mW. This is a factor of four smaller than the estimate of the stainless steel centre rod considered by itself. But that is to be expected as the G10 outer support length was not factored into the equation earlier. According to the calibration data in Figure 5-15, the FP with a static heat load of 270 mW would place the cold head temperature at approximately 42 K. This does not take the value of radiation heat load into account

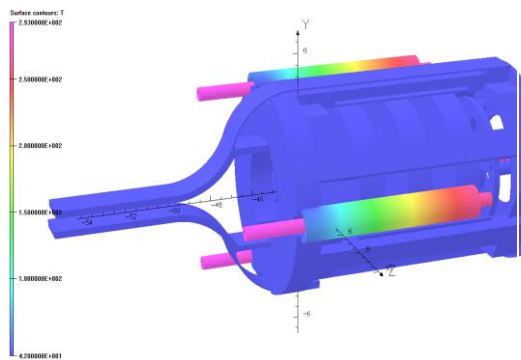


Figure 5-17- Temperature profile

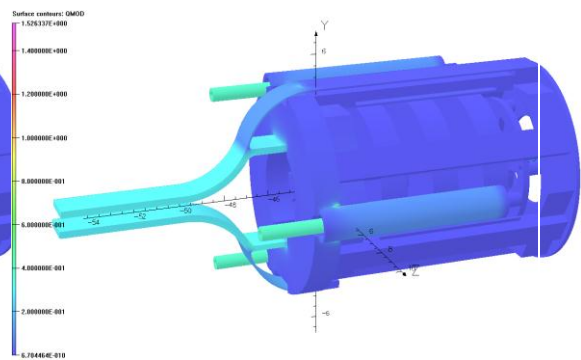


Figure 5-18 - Heat flux flow

Figure 5-17 shows the temperature profile and Figure 5-18 the heat flux flow profile. The temperature profile shows that the supports have a temperature gradient from 293 K to 40 K and the flux pump body is at a uniform temperature of 40K. This indicates that the supports are working correctly in terms of minimising the heat conduction. The heat flow shows a large concentration of heat flux on the cooling bus bars and the supports. This is to be expected as these heat flux concentration areas are close to the boundary locations. The heat flux in the FP

body appears to be uniform. These results validate the FP design in terms of the heat conduction.

The flux pump unit has been designed to the stage where it fits the scope mechanically and cryogenically. The model shows if in perfect conditions, implying being shielded ideally from radiation and in a adequate vacuum to eliminate convection, the system will have a static heat load of 270 mW. The design has taken into account the expansion coefficients of materials and appropriate tests have been done to ensure parts will not be detrimental to one another in terms of compression and tension. There is a high degree of confidence that the rotational system will not seize and will run appropriately. A design is needed to interface the flux pump unit with the existing HTS-110 commercial magnet. This primarily will mean designing a suitable vacuum chamber.

5.8 Vacuum chamber

When designing the vacuum chamber it is important to ensure it is sized appropriately for the application. This will mean that it is not too small and will not interfere with the flux pump unit but also not too big, which will require more material as well as longer evacuation times. Material and joint selection is important for achieving a high vacuum (typically smaller than 10^{-5} mbar). The material of the vacuum chamber, that will typically be at room temperature, needs to have a high degasification rate as degassing limits the pumping speed as well as the ultimate pressure achievable. Degassing occurs when an extremely thin layer of water vapour or gas molecules adhere to the surface of a solid. The degassing rate has the units of $(\text{Pa}\cdot\text{m}^3/\text{s})/\text{m}^2$. Degassing is usually negligible for metals, however is not for organic materials like epoxy due to its significant vapour pressure. Water vapour on the surface of any material is independent to the material type, as degassing in this case is proportional to the surface area of the material. The water vapour can only be removed by baking out the vacuum vessel and the higher the temperature the more effective this method becomes (Ekin J. W., 2006). Any dirt, oils and even finger prints will affect the degassing rate so it is imperative to have a thoroughly clean surface. In addition the less joints the system has the better, as there is less area for leaks to appear. Typically for the targeted high vacuum condition, an accessible joint can be achieved using a viton o-ring system. When designing the vacuum chamber it is desirable to have it mounted external to the FP, thus allowing easy access to the FP whilst still attached to the HTS-110 magnet casing. The geometry of the vacuum chamber should be simple. This will reduce manufacturing costs and allow some standard parts to be used. Figure 5-19 below shows the design of the vacuum chamber.

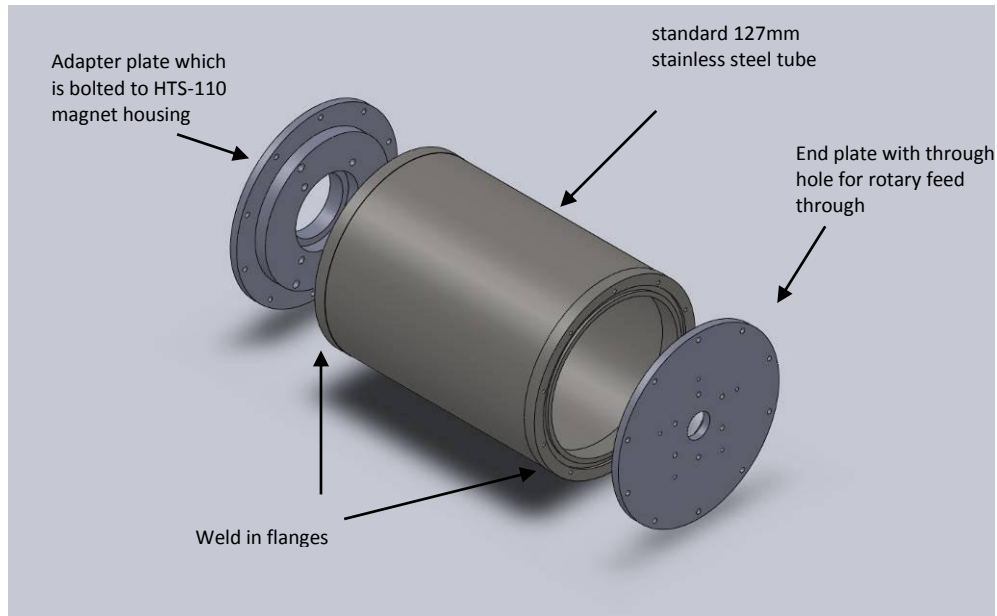


Figure 5-19 - Vacuum chamber

A cylinder geometry was chosen for the vacuum chamber as a standard tube size could be utilised. A model could then be quickly developed to determine the appropriate size of the wall thickness needed to ensure the chamber would not implode under vacuum.

There are two main stresses that need to be considered when developing a cylindrical pressure vessel, the hoop stress and the axial stress. These stresses need to be 50% lower than the yield stress of the material to ensure it does not fail (Young, Budynas, & Roark, 1975). For a thin wall cylindrical pressure vessel with radius r and wall thickness d , the hoop stress it will experience around its circumference from an internal gas pressure P is given by

Equation 5-4

$$\sigma_{hoop} = Pr/d$$

The axial stress it will experience along its length is

Equation 5-5

$$\sigma_{axial} = Pr/(2d)$$

These formulae were taken from (Young, Budynas, & Roark, 1975). It can be seen from the above equation that the hoop stress around the cylinder is twice the axial stress along the axis of the cylinder. Thus a longitudinal joint running the length of the cylinder needs to be twice as strong as a transverse joint.

The largest dimension of the FP from the central axis is 104mm and choosing a standard stainless steel tube with outer diameter 127mm and wall thickness of 1.6mm provides adequate room for the FP unit plus the necessary multi-layer insulation.

Taking the yield stress of 240 MPa of 304 stainless steel at room temperature and halving this to 120 MPa for a safety factor of two, one can determine the minimum thickness needed.

Rearranging the hoop stress equation and setting P to 101324.9 Pa (largest pressure difference possible), r the tube radius to 0.0635m (standard 5 inch) and using a stress of 120 MPa one obtains a minimum wall thickness of 50 μ m. A standard 127 mm diameter tube with a wall thickness of 1.6mm exceeds this value by far.

The flanges shown in Figure 5-19 can be machined from a stainless steel rod and welded in at each end of the stainless steel tube. The flanges bolt to the adapter plate and the end plate, both of which are O-ring sealed. The plates are clamped using M3 bolts to ensure an initial seal before the vacuum takes hold. M3 was used so the flange size could be minimised. Due to the stainless steel bolts screwing into stainless steel and only being M3, it is desirable to not have them too tight in case of the thread being stripped. Thus 10 bolts were used around the outside to ensure a large enough clamping pressure. The adapter plate is attached to the HTS-110 magnet housing via four M5 bolts and a sealing O-ring.

When using O-rings in a vacuum system it is important to have a large initial clamping force on faces where the O-ring is seated between. Therefore when choosing an O-ring the cross sectional area of the O-ring should be maximised, so the applied compressive force can be maximised. It is also important to design the groove correctly for the particular O-ring. Standardised tables containing the groove dimensions are available for standard O-rings. This ensures that the O-ring can be compressed by the correct amount and that a sufficient seal is achieved. The finish of the machined groove should have a tight tolerance and be free of oils, dirt and burs. This will prolong the life of the o-ring and minimise the chance of a leak occurring.

Radiation is a large contributor of the heat load on a system and the large surface area of the vacuum chamber will be the major contributor of radiation on the FP. This amount of radiation can be modelled by the equation below (Ekin J. W., 2006).

Equation 5-6

$$q = \sigma E A T^4$$

Here σ is the Stefan-Boltzmann constant, E the emissivity of the material, A the surface area and T the temperature of the surface. Using the surface area of the flux pump subjected to room temperature in the above equation, the heat load due to radiation was found to be

2.6 W. In order to reduce this heat load layers of aluminium coated plastic foil (also known as multi-layer insulation MLI) are wrapped around the FP, which reduces the heat load through reflection. The heat transfer through the MLI scales inversely with the thickness of the MLI stack. Each layer of the MLI is usually separated by a nylon or silk layer, which greatly reduces contact conduction. For this reason it is important that the MLI is not tightly packed else contact conduction will dominate the heat transfer.

According to the manufacturer of the MLI material used in this project (RUAG), the equation below represents the reduction of heat load due to radiation when using MLI. This particular MLI consists of 10 aluminised plastic layers separated by nylon cloth.

Equation 5-7

$$q_{radiation} = (A_{total}) \cdot 1.5 \frac{W}{m^2}$$

The MLI reduces the radiation heat load to a value of 130mW, 20 times smaller than the 2.6 W seen with no radiation shielding. With the FEM and the radiation heat load it could be concluded that a total static heat load of 500 mW was present.

5.9 Vacuum feed through

A rotary vacuum feed through is used to transfer mechanical rotation from the room temperature environment to the cryogenic vacuum environment. There are various types of a rotary feed through that can be used in vacuum applications. Some include the typical O-ring sealed solid shaft feed through, a magnetically coupled feed through, and in this instance a ferromagnetic fluid solid shaft feed through is being used. It uses a magnetic fluid to seal the shaft whilst still allowing rotation to occur. The main advantage is that it can transmit large torque without the issue of O-ring fatigue.

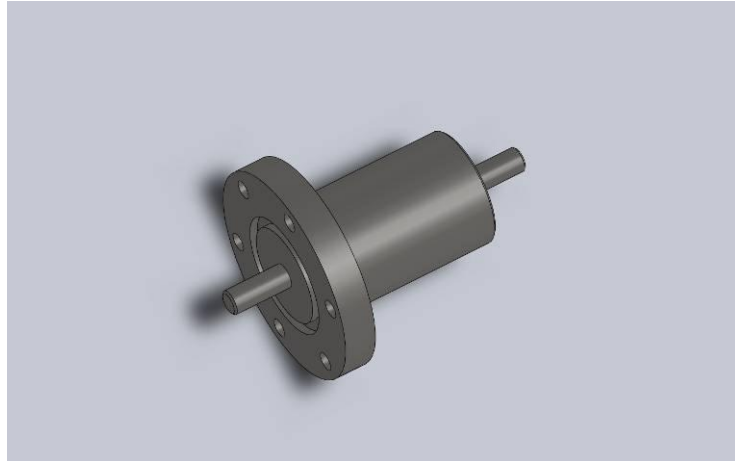


Figure 5-20 - Rotary vacuum feed through

Figure 5-20 shows the feed through, which is supplied by the company Rigaku vacuum products, situated in the USA. It is bolted to the stainless steel vacuum chamber via six M4 bolts and sealing between the stainless plate and feed through is provided by using a standard O-ring. The data sheet of the feed through can be found in Appendix 12.4.1.

6 Fabrication

Having completed the design it is necessary to carry out a design check. This will ensure that it is possible to assemble the FP and all of its components can be physically made. The design check will also identify the parts require a particular fabrication process. Using standard parts will reduce the manufacturing time and reduce the cost of fabricating custom parts. For repetition of symmetrical parts, machining time can be reduced by using a water jet cutting machine. Further machining of parts can take place either by traditional machining methods or a computer numerically controlled (CNC) machine.

The design check involved creating an assembly in Solidworks mimicking the process of one putting the system together in a physical form. Indication of whether or not parts would collide or issues with inserting a fastener could be easily avoided. This allowed one to discover minor problems, such as inserting a fastener and having very little space to tighten it. Identified problems could be remedied before the fabrication process begun and prevent frustration and re-work in the future.

Fabrication of the flux pump was seen to take place in three stages depending on the urgency of particular assemblies. The first stage involved the fabrication necessary for the stator.

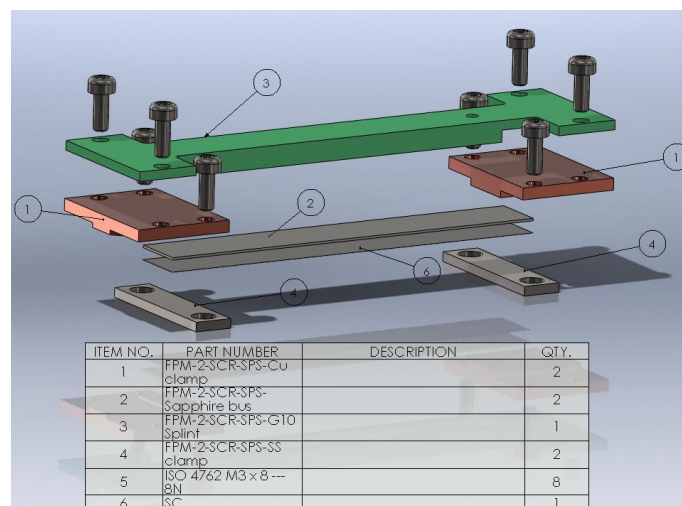


Figure 6-1 - Sapphire system

Figure 6-1 shows the assembly named 'sapphire system'. No standard parts could be used for this assembly, a series of water jet cutting and traditional machining operations were carried out to produce the required parts. The sapphire system consisted of the following parts:

- Item 1

Two of item 1 is to be machined from OFHC Copper per assembly. A tolerance of ± 0.05 mm is required to ensure symmetrical alignment around the stator and sufficient heat transfer takes place.

- Item 2

Item 2 is to be cut out of a four inch diameter sapphire wafer. This is achieved using a CNC wafer cutting machine. One wafer will typically yield four strips and one strip is to be used per assembly.

- Item 3

G10 is known to blunt cutting tools quickly so contact machining should be minimised where possible. Item 3 is G10 so the basic 2d shape should be water jet cut and the three dimensional aspects of the part machined using a milling machine. This will save on time and work shop consumables such as milling tools. A machining tolerance that matches item 1 needs need to be maintained to ensure adequate alignment.

- Item 4

There are two of item 4 in each 'sapphire assembly' and in total 12 pieces. Due to the large amount of item 4 the basic shape will be water jet cut to save time. The face that is in direct contact with the SC and sapphire will then have the face surfaced using a milling machine. This is to ensure a uniform pressure will be applied to the SC and sapphire when clamped in place.

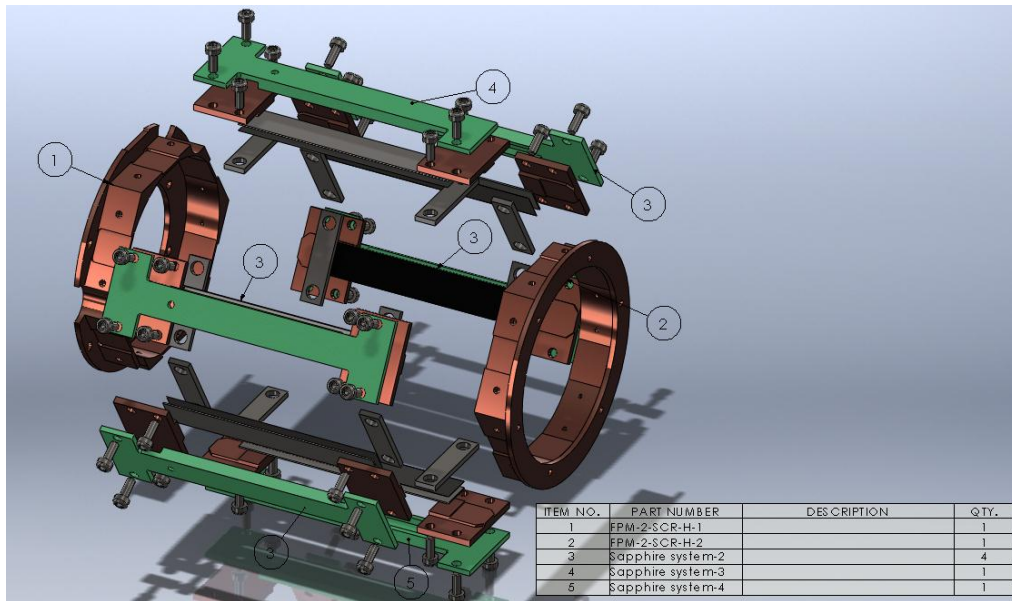


Figure 6-2 - Stator

Figure 6-2 shows the six 'sapphire system' assemblies which form the skeleton of the stator and houses the six SC branches. However two of the G10 (item three in Figure 6-1) pieces have a section cut away as clearance for the SC positive and negative current leads, they are numbered 4 and 5 respectively. The two OHFC copper Hexagonal ends of the stator, items 1 and 2 are to be machined using a CNC machine A tolerance ± 0.05 needs to be achieved to match the other critically aligning parts mentioned earlier.

Stage 2 consists of fabricating the remaining items of the flux pump unit. This includes the suspension mounts to support the FP inside the vacuum chamber, the PM rotor and the thermal bus bars.

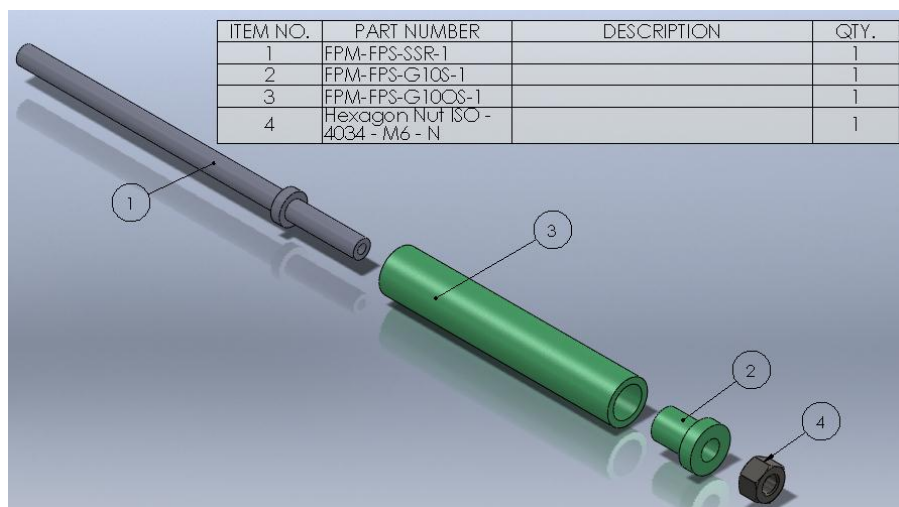


Figure 6-3 - Flux pump support

Figure 6-3 shows the three FP support assemblies need to be fabricated.

- Item 1

Item 1 is turned down to the required dimensions from a solid stainless steel rod using a lathe.

- Item 2

Item two utilises a standard size G10 pultruded tube. This particular tubing had a high manufactures tolerance of $\pm 0.2\text{mm}$ so to ensure the tube is concentric, further machining to the inside and outside diameters was carried out to give a tolerance of $\pm 0.05\text{mm}$

- Item 3

Item 3 was turned down to the required shape form a solid piece of G10 composite using a lathe.

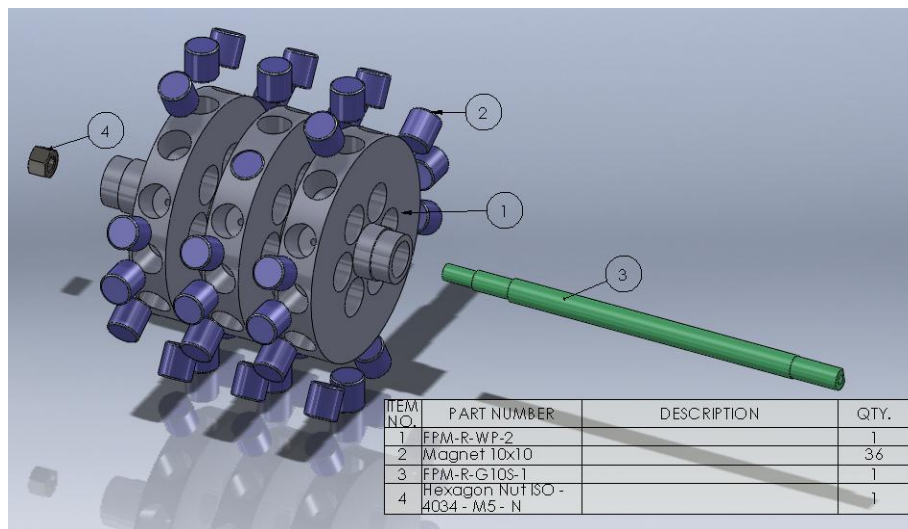


Figure 6-4 - Rotor

Figure 6-4 shows the single PM rotor assembly required and fortunately 36 of the items could be purchased as standard parts. This left two items to be custom fabricated

- Item 1

Item 1 was machined on a CNC lathe from a solid piece of Aluminium. Due to a shortage of staff in the workshop at IRL the piece was out sourced to Sanpro industries in Lower hutt in order to maintain the fabrication schedule.

- Item 2

Item 2 consisted of a standard N42 grade neodymium rear earth magnet which could be sourced from a company known as Super magnet man, Located in the USA for a very reasonable price.

- Item 3

Item 3 was a standard size G10 pultruded tubing that had a similar issue with the manufactures tolerance as item 2 in Figure 6-3. So additional machining was carried out to achieve the required dimensions tolerance as well as cut the right and left hand threads necessary for the locking nut system.

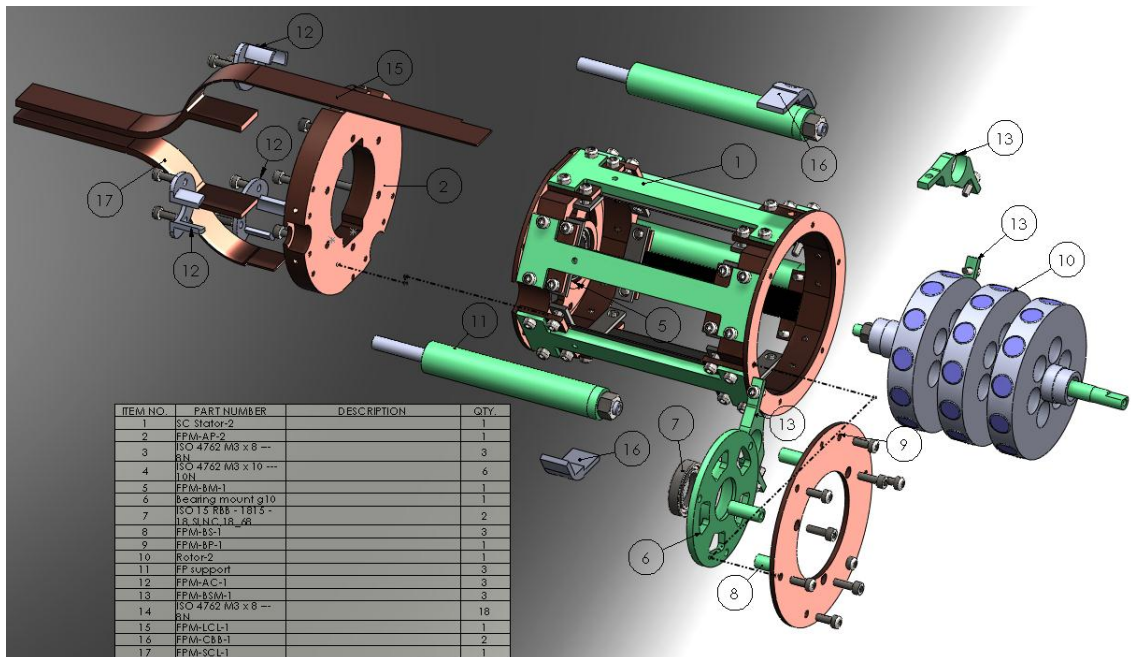


Figure 6-5 - Flux pump assembly

Figure 6-5 shows the assembly of the remaining parts needed to complete the flux pump unit.

- Item 2, 5, 9 and 16

Item 2 is an adapter plate, item 5 houses one of the stainless steel bearings, item 9 is the back plate of the FP and item 16 is a guide for the positive and negative current leads. All four items are machined from a solid round piece of OFHC copper using a CNC machine.

- Item 6

Item 6 is the stainless steel bearing mount at the opposing end to item 5 and was machined from a plate of stainless steel using a CNC machine.

- Item 8

There is three of item 8 which were turned down from a solid piece of stainless steel using a lathe. All three pieces had a M5 tap threaded running all the way through.

- Item 12

There is three of Item 12, which holds the three FP supports in place (item 11). They are machined from solid pieces of aluminium using a CNC machine

- Item 13

There is three of item 13 which is an additional mount for the FP supports (item 11). Item 13 is water jet cut from a piece of G10 composite and the mounting holes drilled post the water jet cutting operation.

- Item 15 and item 17

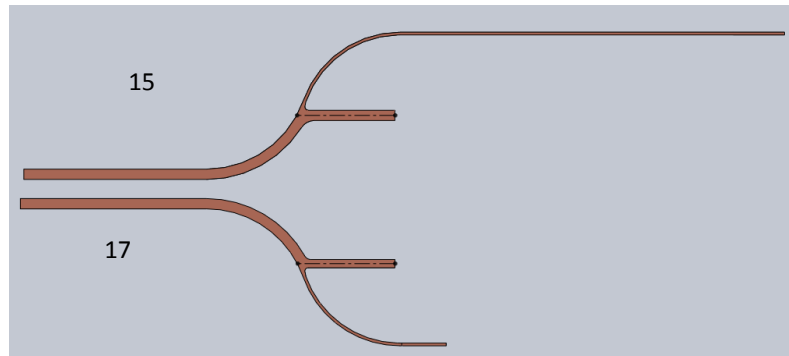


Figure 6-6 - Thermal bus bar configuration

Figure 6-6 shows the two thermal bus bars, item 15 and item 17. Each thermal bus bar is made of two solid OFHC copper strips and then multiple layers of OFHC copper shim. The two solid strips for each bus bar make it possible to achieve the above shapes. Where the black dotted line is on each bus bar is where the two pieces meet in union and are soldered together. The thicker portion of each bus bar represents the multiple layers of OFH copper shim stacked on top of each other. A one to one scale of the image above is to be used as a jig for bending the four solid strips into the correct shapes to form the two solid bus bars.

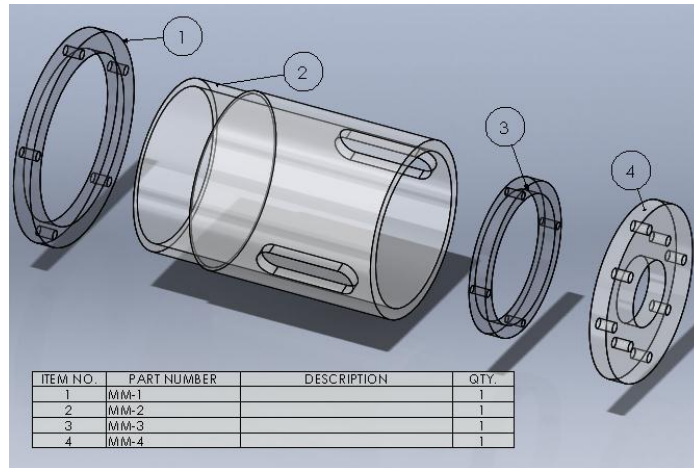


Figure 6-7 - Motor support column

Figure 6-7 shows the motor mount, which is attached to the outside of the vacuum chamber and will hold the stepper motor.

- Item 1, item 3 and item 4

These pieces are made from a Perspex sheet. They were cut out using a CNC machine.

- Item 2

Item 2 was a standard piece of Perspex tubing. It was then turned down at one end using a lathe and the sections cut out using a milling machine.

Items one, two and three were glued together by injecting chloroform through a hypodermic needle and syringe into the joints.

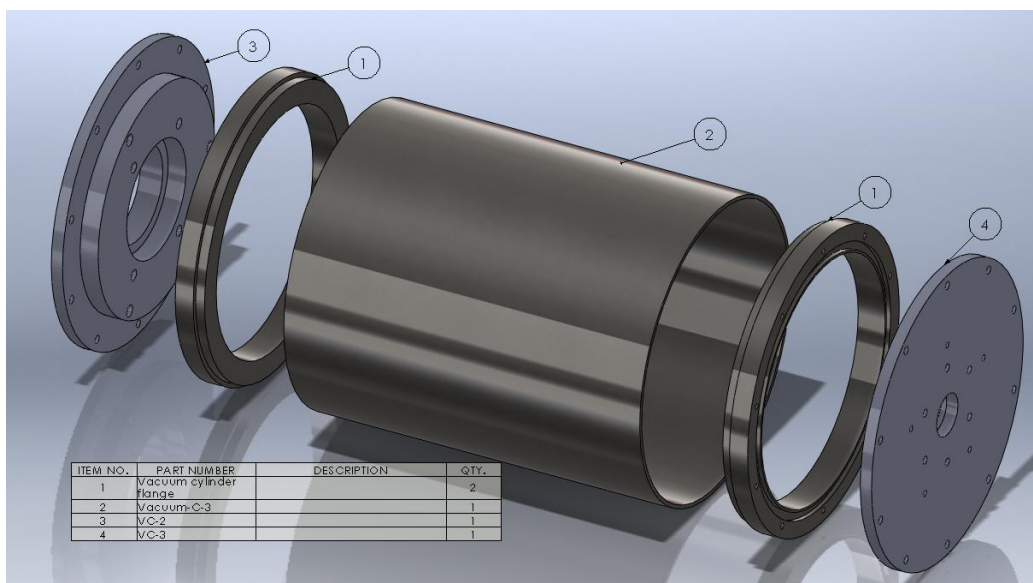


Figure 6-8 - Vacuum chamber

Figure 6-8 shows the vacuum chamber which will serve as the mounting interface to the current feed through flange on the HTS-110 magnet as well as housing the flux pump

- Item 1

There is two of item1, one for each end of the vacuum chamber, which serves as the sealing flange. Items 3 and 4 bolt to these flanges. They encompass an o-ring groove and are designed so they can be welded into each end of the stainless steel tube. They were turned by SanPro industries.

- item 2

Item 2 is standard five inch 316L stainless steel tube cut to length ‘

- Item 3 & 4

Item 3 is the adapter plate as well as the front of the vacuum chamber. Item 4 is the back plate of the vacuum chamber. Both were made from a 316L solid stainless steel rod and turned on a lathe. The fastening holes have then been post drilled using a milling machine, all of which was out-sourced to SanPro industries.

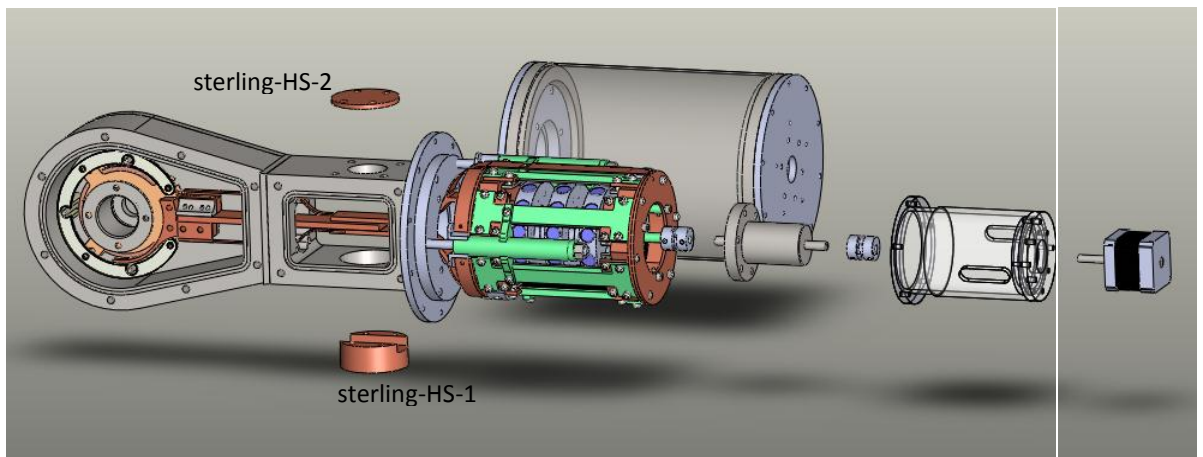


Figure 6-9 - Full system

Items Sterling-HS-1 and Sterling HS-2 were the only additional pieces that were fabricated for the final assembly. They were machined from OFHC copper in a CNC machine. Other parts such as the vacuum fittings, motor couplings and motor were ordered as standard parts.

7 Assembly

Assembly of the FP was concurrently carried out with the fabrication phase. As mentioned earlier the flux pump is to be built over three stages. The first stage of assembling the stator is expected to take the longest, as this involves the handling of a number of delicate and expensive materials namely the SC strips and the sapphire. Before such materials are used in the assembling process, the stator chassis should be assembled. One can check that machined surfaces match up with one another and that adequate mounting surfaces are present for the sapphire and SC.

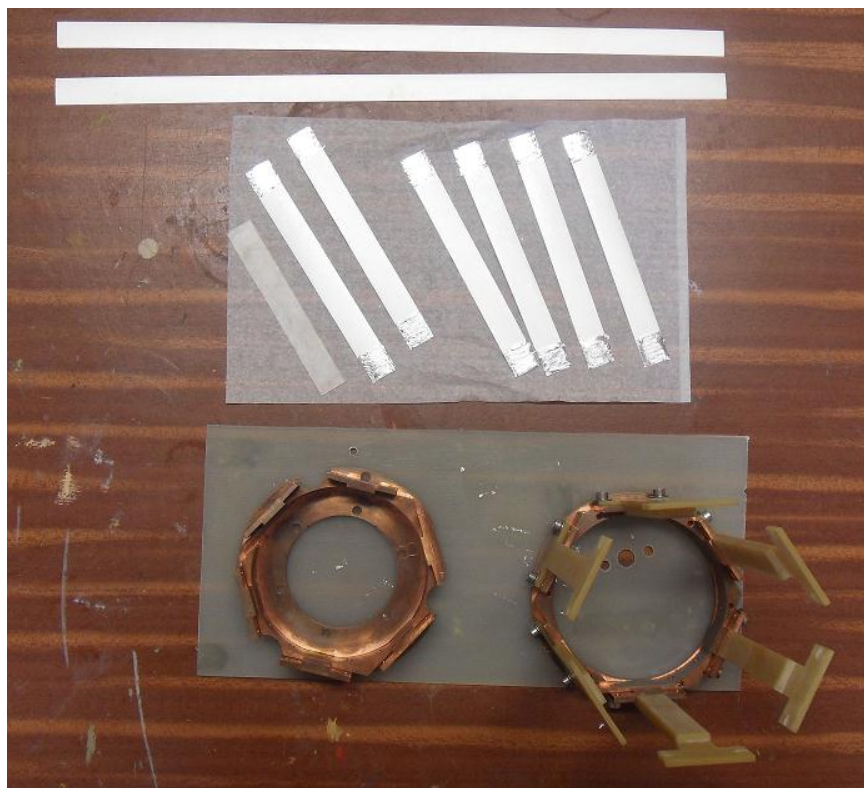


Figure 7-1 - Stator layout

Figure 7-1 shows the stator during the assembly stage. It is ready to have the six paired strips (face to face soldered strips) soldered into the stator chassis. Below each branch of SC strips will sit a sapphire strip which can be seen in the Figure 7-1 above. Throughout the assembly process it is important to wear gloves to ensure the oil from one's hands does not get on the SC or copper as this oxidises the copper and can damage the SC. Since each strip pair carries 100A and it is expected that the coil will need below 200A to reach its I_c , only two SC segments are needed. It is unknown how well the conduction cooling system will absorb the heat from the SC branches, so for this reason if problems are encountered it will be a far simpler process to

debug two strips opposed to the original six, thus a decision was made to solder in only two branches at this stage.

It is necessary to pre tin the SC strips in the areas where the solder joint is to take place. Pre tinning allows one to control the soldered area when using a heating element and ensures a low resistance joint. The solder to be used in this instance is indium silver. Indium silver has a melting temperature of 143 °C. It is important to use a solder that has a low melting point and imperative to minimise the amount of heat exposure time, due to the fragile nature of the SC. One must note that there is a SC side and a non-SC side. When joining a SC, it is imperative that the joint contains two SC sides.

A practice run is essential to successfully solder the strips in place. The SC can be replaced with thin strips of card, allowing one to achieve the correct procedure of laying down the strips and identifying how they should be soldered. The card is inexpensive and the process can be repeated as many times as the assembler feels is necessary, until they are ready to solder the expensive and fragile strips.

It was found that the best way to solder these strips in place was as follows:

- Using masking tape, gently tape the positive and negative current lead SC strips into each of the ends of the stator. This needs to be done with the SC side facing inwards. Tape should be placed in between the points where the SC is going to be soldered to the stator to ensure it does not move.
- Lay in place a sapphire strip on the respective copper faces, as seen in Figure 6-2.
- Insert a SC branch with the SC side facing to toward the central axis of the stator. This will involve gently lifting the SC strips at each end of the stator and sliding the branch in. It is important not to bend this particular tape with less than a radius of 15mm.
- The slight pressure of the tape at each end of the stator is enough to keep the branch in place. This process can be repeated for the remaining five branches or in this case the remaining one
- Once the SC branches have been laid out correctly, it is necessary to remove the sapphire strips, as they have a high thermal conductivity. This property will hinder one from localising the heat to create a sufficient solder joint.
- The securing clamps are put in place, shown in Figure 7-2 to ensure the SC does not move during the soldering operation.
- One end of the stator should be heated up at a time. It needs to be heated up as uniformly as possible to ensure certain points are not exposed to more heat than others.

- Clamps and pegs should be used as shown as in Figure 7-2 below, to provide pressure and ensure a low resistive joint is achieved.
- The same procedure should be carried out for the other end of the stator.

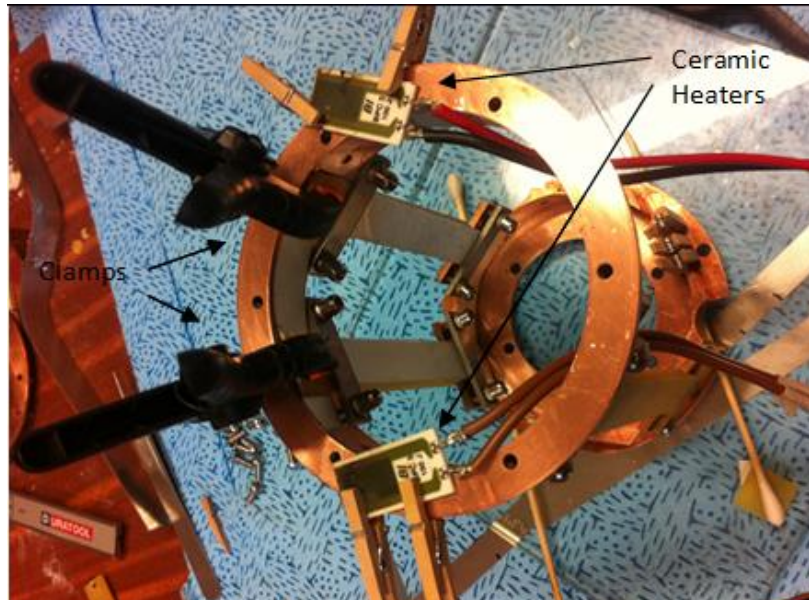


Figure 7-2 - SC solder joints

The assembly of the rotor was the next stage in the assembly. Involved was preparing the rotor for gluing in the magnets. The rotor had to be free of all dirt and grime and any burs that may be present. Glue was then applied to the N50 permanent magnets which were pressed into the machined rotor. On top of the magnets, mild steel pole shoes were pressed in. No glue was needed as it was an interference fit as well as the ferrous mild steel being attracted to the magnet. The glue was then left to cure overnight. The assembled rotor was then placed in a lathe and the pole shoes skimmed down to match the diameter of the rotor. The G10 shaft was screwed into one end of the rotor using a right and left hand thread nut locking system, this is best illustrated by Figure 6-4. This would ensure rotation in both directions would not cause the shaft to come loose.

The next stage involved attaching the copper pieces, items 5 and 2 from Figure 6-5. The items are secured in place by M3 screws that pass through both items. This needs to be aligned within 0.5mm to ensure that the system is symmetrical and the rotor is not offset.

Before the rotor could be inserted into the stator the back end clamps, item 4 in Figure 6-1 securing the sapphire and SC in place had to be removed. This was necessary as their position created a space that was smaller than the diameter of the rotor. This does not affect the position of the SC or sapphire, as the SC is soldered and the sapphire is still clamped at the opposite end. The rotor could then be inserted into the bearing mount

along with the stainless steel bearing. It should be noted that the stainless steel bearing had all the grease removed, as at cryogenic temperatures the grease will freeze and the bearing will seize to operate. This is best done using acetone in an ultrasonic bath. Frictional wear at cryogenic temperatures does not become an issue as the heat is absorbed by the cryo cooler, however this will impose an additional heat load.

The stainless steel bearing mount situated at the opposing end of the stator can be assembled. This involves attaching the three support poles (item 8 from Figure 6-5) to the stainless bearing mount (item 6 from Figure 6-5) and then attaching the other end of the supports to the copper back plate (item 9 from Figure 6-5). A total of 6 M5 stainless steel screws were used for this. This sub assembly containing the stainless steel bearing can be attached to the rotor and secured to the stator. An alignment of 0.5mm needs to be achieved. The finished solution of this stage can be seen in Figure 7-3.

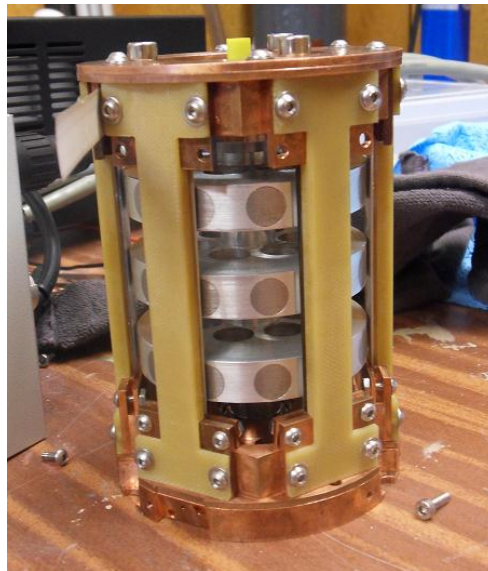


Figure 7-3 - Assembled flux pump

The three supports that are used to mount the flux pump in the vacuum chamber can be assembled. Each support contains a stainless steel rod, three G10 pieces and a securing nut. The inner G10 tube can be glued into the outer G10 tube (items 2 and 3 respectively from Figure 6-3). The support bracket can then be glued on at the opposite end. This is best done by mounting the G10 outer support to the allocated recess in the flux pump and screwing down the securing clamp first. The stainless steel rod (item 1 from Figure 6-3) can then be inserted.

The next stage consists of fitting the thermal bus bars and can be completed with the rotor in or out, however in this case for simplicity it is done with the rotor removed. The Stirling cooler is to be mounted to its mating vacuum flange and the main heat sink attached (Item Stirling-

HS-2 from Figure 6-9). The four segments of the thermal bus bars, seen in Figure 6-6, are to be bent into shape using the method described in the fabrication section. The sections on each of the four pieces where they are to be soldered (dashed black line in Figure 6-6) are to be tinned with high temperature solder. With the FP secured into its designated mating points the smaller portions of each thermal bus bar can be attached to the FP. The two longer sections can then be clamped to the two smaller sections, as well as being seated in the recess in item Stirling-HS-2. Adjustments can be made as necessary and when the correct alignment is achieved the bus bars can be removed from the FP with the clamps still attached. A heating element can be attached to each bus bar and the solder joint completed. A high temperature solder that has a melting point of 290 °C is to be used. This ensures that when the SC current leads are soldered in place with low temperature solder, the high temperature solder will not melt and break the joint. The OFHC copper shim can be cut accordingly and bolted to each bus bar at the same point where the bus bars bolts to the FP.

The vacuum chamber consists of three main components (items 3, 2 and 4 from Figure 6-8) item 2 can be treated as one part when the two end flanges are welded in place. The two ends are sealed using a nitrile o-ring and is initially held in place by a clamping force until the vacuum takes over. 10 M3 bolts are evenly spaced around the outer diameter of each end to supply a uniform clamping pressure. Testing of the vacuum chamber for leaks needs to be done, which will be discussed in the next section.

The SC current leads now need to be soldered to the two thermal bus bars. This is best left to one is ready to put the coil in, due to the delicate nature of the SC. Both bus bars need to be tinned with the indium silver solder as well as the SC current leads. It is important that the SC side is tinned. The SC current leads that connect the FP to the coil can be soldered to their respective thermal bus bars one at a time. This involves clamping the SC to the bus bar in the correct orientation and then applying heat using a ceramic resistor. The heating should cease as soon as there is signs of the solder to be molten. Due to the delicate nature of the SC and the larger thermal mass of the bus bar, it is desirable to heat from the bus bar, thus minimising the exposure of heat to the SC.

The resistance of OFHC copper decreases significantly with temperature, so it is important to electrically insulate the two copper bus bars from one another so that voltage generated by the flux pump does not flow across these relatively low resistance interfaces. A electrical connection across here would lower the voltage seen across the coil. Insulation is done by inserting a non-electrically conductive cell of nomex paper between where one of the bus bars connects to the front of the stator.

A join between the thermal bus bar SC lead and the stator SC lead needs to take place for both the positive and negative current leads. There is large thermal mass around where the joints are to occur (the copper stator ends) and heating the entire stator to complete the join could be detrimental to the health of the SC. So to accommodate for this a piece of thin card is placed between the large thermal mass and the SC current leads. A ceramic heater is then clamped on top of the SC and the heating procedure carried out. This is shown at one end of the stator in Figure 7-4 below



Figure 7-4 - SC current lead assembly

There are two double pan cake coils that will be in the magnet system. The coils fit in the existing coil chassis for the suit case magnet. The coils were wound by HTS - 110 and assembled as shown in Figure 7-5 below. The current leads for the coils have been soldered to two 12mm pieces of SC, which places them into a parallel configuration and will reduce the complexity of joining the flux pump current leads to the coil leads.



Figure 7-5 - SC coil pack

The coil pack can be secured in place in the magnet housing and then joining of the flux pump and coil can take place. This needs to be carefully carried out, as any damage to either components current leads would lead to a lot of rework.



Figure 7-6 - Mating of the flux pump and coil pack

Figure 7-6 shows the two magnet housings in union with one another and the current leads from the FP overlapping the current leads from the coil. It is necessary to join the current leads again trying to limit the amount of heat transferred into the SC. The same method as mentioned earlier is used, by where pieces of thin card are inserted between the SC and highly conductive parts, thus reducing the amount of heating time.

Figure 7-7 shows the soldering technique used. The thin piece of card is placed between the thermal bus bar and the SC leads. The ceramic resistor is then clamped on top of the SC leads. This is a similar joining method as mentioned earlier, which allows concentration of heat and minimises the overall heat exposure time on the SC.

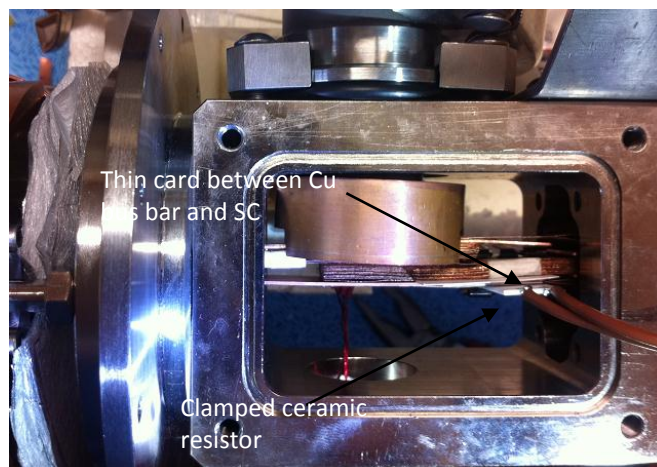


Figure 7-7 - joining SC leads of the flux pump and coils

8 Testing and evaluation.

Labview is used as the software for monitoring and recording data in the testing phase. This allows developing a simple program quickly that interfaces with various hardware in a laboratory environment. The program uses a combination of other data logging programs made in the past at IRL. The field magnitude of the coil is measured using a hall sensor, the voltage across the coil and the various PT100 signals. The data is logged to a .txt file for later use and a real time display of the information is implemented.

8.1 Vacuum system.

Before testing the function of the flux pump it is imperative to ensure that the vacuum system is adequate in order to provide sufficient insulation. According to Ekin (Ekin J. W., 2006) a vacuum that is to be used for insulation usually is at a level located in the high vacuum region, which is lower than 10^{-5} mbar. To achieve a high vacuum it is important to have the vacuum space as clean as possible and free of containments, as this will minimise out gassing. Cleaning every part in the vacuum space with acetone works well to remove dirt and oils.

The first test involved assembling the vacuum system without the flux pump and evacuating in two steps. First with a roughing pump, which will achieve a pressure of no lower than 10^{-3} mbar, followed by the second stage employing a turbo pump which would be expected to get the system below 10^{-5} mbar.

Results showed that the vacuum could not get below 10^{-1} mbar. As there are multiple joints in the system it was probable that the leak was occurring from one of these joints. A helium leak detector was used to inspect each and every joint of the system. A source of Helium was sprayed around the various joints from top to bottom (as helium rises) and if a leak was present the helium would diffuse through the leak space and be signalled by the leak detector from its on-board mass spectrometer. It was found that the primary leak source was due to little fibres on one of the vacuum chamber O-rings, something so small was enough to cause a large leak. The O-ring was cleaned and the vacuum system put back together.

The vacuum procedure was then carried out again and a pressure of 5.6×10^{-6} mbar was achieved, which fits the criteria of the vacuum needed.

8.2 Cooling of the flux pump unit

Cooling with the FP connected to the cooling bus was carried out to verify the thermal model including the temperature distribution and to identify the static heat load the FP presents. The

current leads from the flux pump were soldered together to create a short circuit and voltage taps were placed across this solder joint to identify if a voltage was being produced during the operation of the flux pump.

The system had a temperature sensor mounted at approximately 3/4 the length of one of the SC strips (S1) and one on the back of the flux pump (S2). Since the design was symmetrical through the central axis of the flux pump and wire feed throughs were limited, it was decided that the one sensor on the SC would be adequate. The sensor on the back of the FP was at the furthest point away from the cooling source.

It was found there were a few problems in terms of the cooling of the SC. These included a large temperature gradient as well as localised heating of the SC when the magnets were rotating over the SC.

While sensor S1 reached a temperature of 56 K, S2 was found to reach a minimum temperature of only 86K. The two sensors are within 40mm to each other and are directly connected via a sapphire piece. The cause for a large temperature gradient could be due to two main reasons. One being a large heat leak via a direct short to the room temperature or the second reason being a break in the conduction path. Looking at the temperature of the cold head, it was found to be 45 K which indicates a heat load of approximately 800 mW, according to Figure 5-15. This eliminates a large heat leak as one would expect a large heat load to be present on the cryo-cooler. Thus one can have a high degree in confidence in saying that there is a break in the conduction circuit.

Rotation of the rotor was checked during the cool down process as well as when the temperatures reached a steady state. It was found at 86K the rotor would move freely with a slight torque required, however due to the temperature of S2 not getting close to the value of S1, it was presumed that the rotor would not be below 77 K.

When the flux pump was rotated at 86 K, it could be seen that there was a voltage being produced, which changed as the rotational speed was varied. This indicated that the flux pump was in fact operating. The heat was not sufficiently being extracted from the SC during rotation, as the frequency of rotation increased a temperature rise could be seen in both sensors. This could be a combination of the issue stated above as well as the SC not being thermally anchored to the sapphire correctly.

8.2.1 Initial modifications

Upon inspection of the flux pump, once warmed up, it was found that the sapphire strips were indeed broken and thus the cause of the large temperature gradient. The cause of the strip breaking was due to burs on the copper face in which the sapphire mounted to. With such a brittle material like sapphire it is imperative to have a smooth surface as it will not deform but will shatter. It was suspected that the localised heating during rotation was due to the poor contact of the SC on the sapphire. Therefore an additional sapphire piece was placed on top of the SC with two additional clamps placed evenly along the length of the sapphire-SC sandwich to provide better thermal contact. The additional clamps can be seen in Figure 8-1.

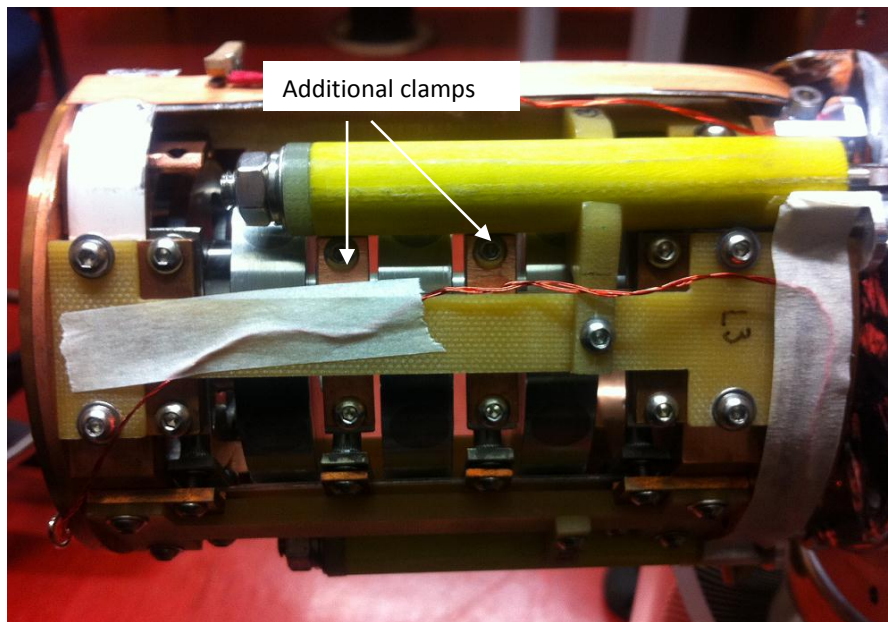


Figure 8-1 - Additional Sapphire and clamp configuration

The system was cooled down and the temperatures of S1 and S2 were found to be within 1K of each other, 56K and 57K respectively. The heat load was measured to be approximately 600mW. This is in excellent agreement with the FEM analysis and radiation approximation.

Below 77 K it was found the rotor did not seize, however needed a significant torque to be applied in order for the rotor to begin rotating. This is due to the SC largely being below its T_c and thus being superconducting. The force experienced to rotate the rotor is largely an effect of the flux lines being pinned at defects in the superconductor.

8.3 Full system cool down

With the coil in place the entire system was cooled down. Voltage taps were placed across the coils current leads to determine the voltage the flux pump was generating and a temperature sensor (S3) was placed on the coil pack.

It was found that the voltage across the coils was very low which indicates a large loss in the system or a possible flux injection problem. It was suspected that the pole shoes on the rotor could be the source of reduced voltage. This could be easily confirmed by measuring the field at the pole shoe and comparing it to the measured field on top of a identical PM used. The permanent magnet had a field of approximately 350 mT at its surface compared to the pole shoe having approximately 90 mT at its surface. The pole shoe was in fact degrading the field rather than the intended purpose of projecting it.

A new rotor was made by where the pole shoes were omitted and the PM were positioned so their faces were at the circumference of the rotor. With this new rotor the voltage across the coil was significantly larger, similar to the values produced by the experimental rig used in liquid nitrogen.

8.3.1 Degraded coils

Still, when trying to energise the coil it was found that we could not achieve a field greater than 160mT (at 74K) in the coil. A large temperature rise could be seen on the coil, indicating I_c of the coil itself had been reached. This was confirmed in a liquid nitrogen bath experiment, where energising the coils with a power supply revealed a critical current of approximately 12 A only. Obviously the windings of the coils were damaged in the production process. The 2G wire used in the coils is notorious for having issues when the coils are potted. The resin used for potting contracts at a different rate to the SC, which can cause the SC to become damaged and as a result significantly degrade the performance of the coil. In this instance this is suspected to be the problem.

Due to limited human resources in HTS-110 at the time a coil wound by researchers, Dr Hoffmann and myself, was used as a temporary solution to avoid a large amount of down time. The coil was to be dry wound, meaning that it would not be potted. This would reduce the risk of degrading the coils I_c .

It was expected that the I_c of the coils would be above 40 A at 77 K, however when tested in liquid nitrogen the critical current was found to be 24A only. As damage to the windings could be excluded, this result must be related to the angular field dependence of the critical current. The characterisation of a short sample of the Superpower tape uncovered an angular

dependence of I_c as shown in Figure 8-2 below. At a field of 150 mT with a field angle of approximately 120° , the I_c was degraded to 24A which is in agreement of the result seen in tests carried out.

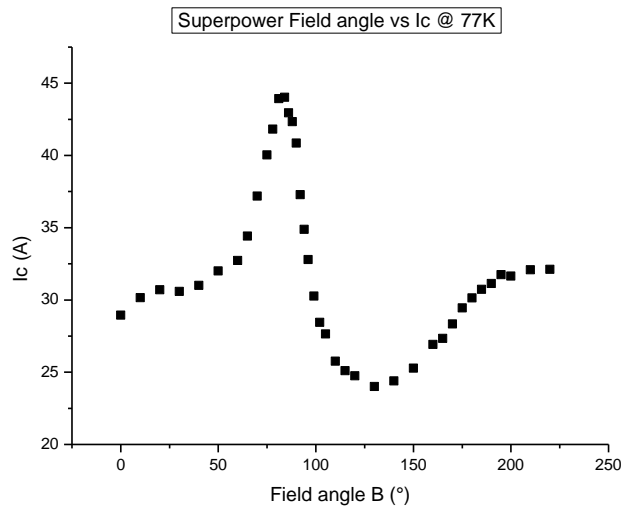


Figure 8-2 - Super Power angular dependence

The I_c degradation can be further explained by the below FEM magnetic model. As I_c is temperature dependent it is expected that the I_c of the coils at 55K will be much higher than in the liquid nitrogen. However the I_c can be degraded depending on the angular field dependence. This is can be understood by looking at the cross sectional FEMM model below and the angular field dependence data. One can see four rectangular sections named 'SC tape layers', which represent the SC tape cross section when wrapped around the former. Field lines are crossing over the tapes at various angles which has the effect shown in Figure 8-3. The I_c is degraded at certain points according to this. This information can be used to calculate the expected I_c however this is outside the scope of this thesis.

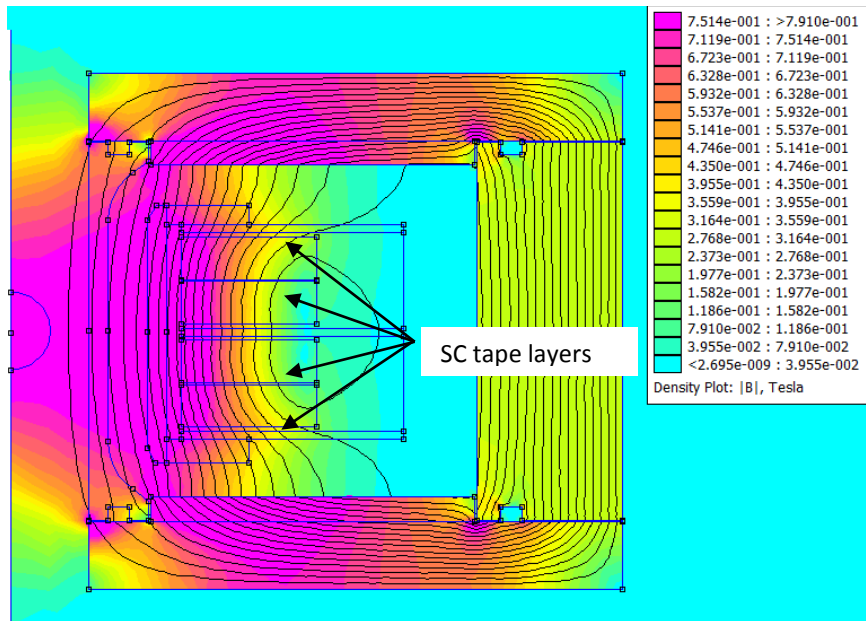


Figure 8-3 - FEMM of HTS- 110 coil system

8.4 System evaluation

The entire system was assembled with all the necessary changes listed previously. Figure 8-4 shows the cool down rate of the system at the various temperature sensor locations. The temperatures of the three sensors when the system reached steady state was 55.6 K (S1), 56.5 K (S2), and 54.1 K (S3).

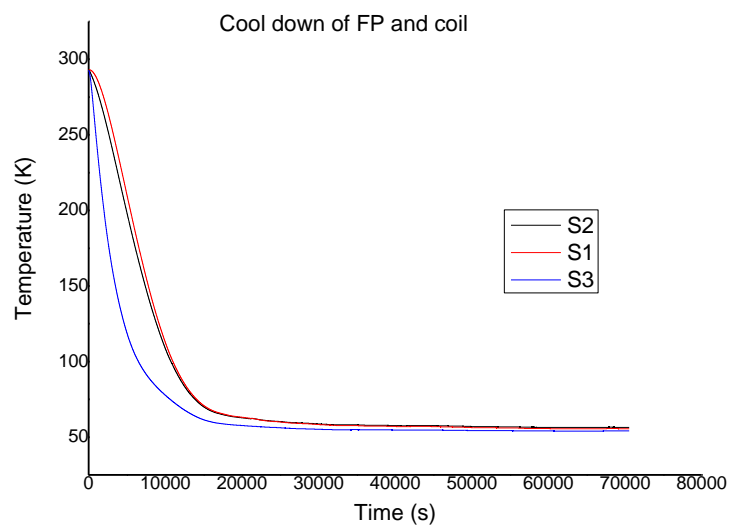


Figure 8-4 - Cool down of the FP and coil

These improvements in the cooling architecture as well as the new set of coils led to a higher current, and therefore higher magnetic fields generated. A maximum field of 860 mT has been achieved to date (Hoffmann, Walsh, Karrer-Mueller, & Pooke).

However limitations are imposed as at this field the temperature of the coil does not stabilise. Obviously the coils are driven in the resistive state and heat is dissipated. As the I_c of the coil is a function of temperature, this in turn continues to lower the field magnitude over time and can be seen in Figure 8-5 below.

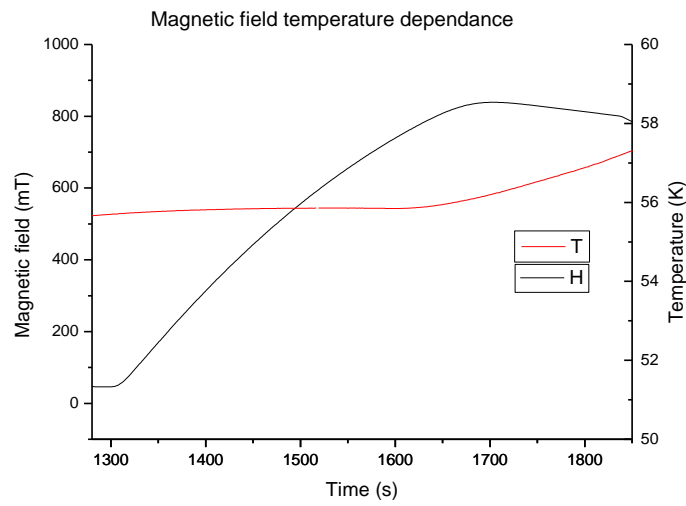


Figure 8-5 - Magnetic field temperature dependence

Figure 8-5 is a plot of magnetic field and temperature versus time. The magnetic field is shown with a black line and the temperature with a red line. Observing the plot it can be seen at approximately 760 mT that the rate of change of the temperature increases rapidly. This is presumed to be where the coil is approaching I_c . At the maximum of 860 mT the voltage generated by the FP balances the voltage drop due to the resistance present in the coil. Beyond this point the current, and therefore the field is decreasing which indicates that the I_c of the coil is decreasing and the balance condition mentioned above is shifting to lower currents. Below 760 mT in Figure 8-5, it can be seen that the temperature appears to be stable which could indicate the upper limits of stability for this particular configuration. For this reason all further characterisation was done at fields no larger than 750 mT.

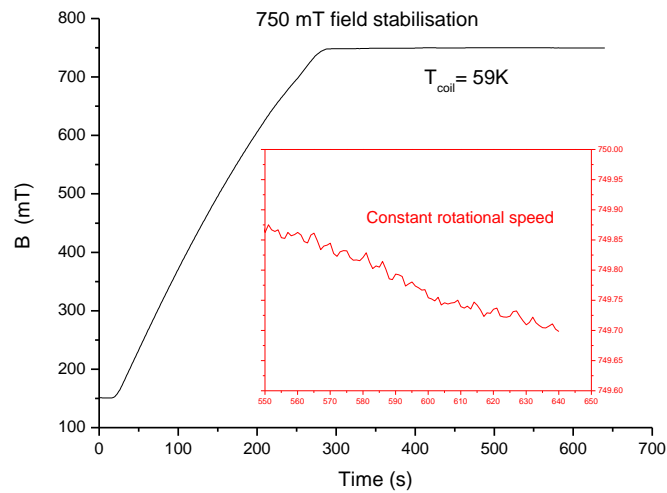


Figure 8-6 - Stabilisation plot at a field of 750 mT

Figure 8-6 shows the stability plot of the coils field at 750 mT achieved by manually manipulating the speed of the stepper motor. The black line shows the full scale range of the field produced by the coils. The red insert shows a scaled range of the coils for the time period between 550 and 650 seconds. This is after the field had been stabilised and the stepper motor set at a constant rotation speed of 0.75 Hz. Although at a constant rotation speed the voltage produced from the flux pump should also remain constant, an equilibrium state cannot be achieved. A field drift occurs which would be indicative of a temperature change in the system. A change of temperature seen at the coil can increase or decrease the field size that the coil can produce. The same can be said about the FP in terms of the amount of voltage it can produce, as the flux pinning has a temperature dependence. In depth experiments would be required to determine the effects of such temperature changes, which is currently outside the scope of the project. The total heat load at this temperature was no larger than 1.2 W and a total current of 68 A was flowing in the SC circuit. This is still a factor of 4.5 times smaller than the current lead feed through system at a comparable current.

It can be concluded that the temperature drift does pose a complication for the control system, as the temperature needs to be controlled along with the motor frequency. Future work will see the implementation of temperature control to further the stability of the system. However, the heat load generated by the flux pump is comparably small when compared to the current lead feed throughs. If a current lead feed through set up was to be used and the same current of 68 A is supplied, the T_c of the SC would be possibly reached causing a quench. In order to avoid a quench, the current in the circuit would need to be significantly reduced and thus would significantly reduce the field size.

9 Control System

In order for a stable field to be present in a coil that is energised using the HTS dynamo FP method, a feedback element needs to be incorporated that relates rotational speed of the FP to the current magnetic field in the coil and adjusts the rotation accordingly. This assumes that all other variables that effect the field are kept constant. However when considering the HTS - 110 commercial magnet system there is another element that needs to be controlled, which is the temperature, as mentioned in section 8.4. In order for a near perfect control the temperature needs to be incorporated into the feedback loop. Temperature will not be included in the control loop at present, due to the investigation that needs to be carried out to identify what is causing the temperature rise and the extent of this. Due to time restrictions this will be investigated in future work and then be incorporated into the control loop.

The control loop is to be implemented at the highest level of the system, which is to be in the form of software. This will typically take place in a processing unit, however there needs to be a series of other levels or sub systems in order for this to happen. This is summarised and illustrated by the hierarchy diagram in Figure 9-1 below.

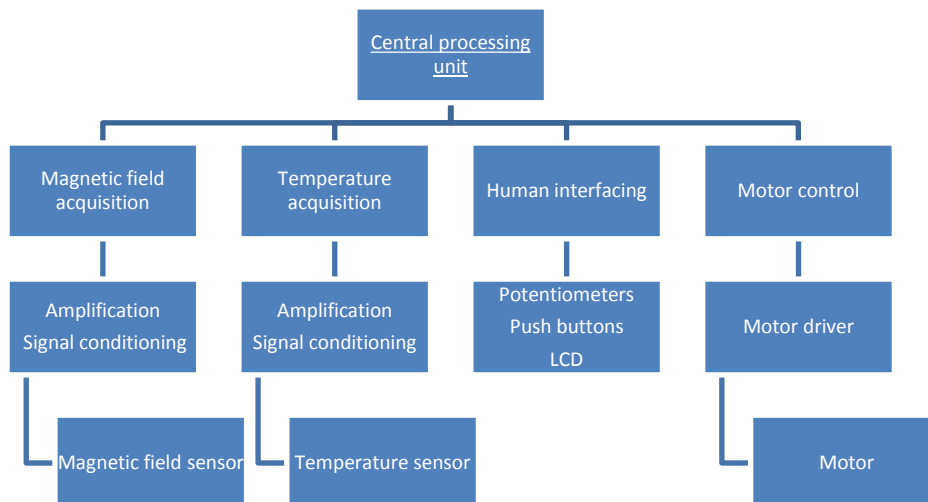


Figure 9-1 Control system hierarchy

9.1 Low level hardware selection

Figure 9-1 clearly shows at the lowest level of the control system that sensors and a motor need to be selected. These elements must be picked based on the requirements of the system.

9.1.1 Magnetic field sensor

The magnetic field sensor needs to meet the following requirements:

- Supply a signal that represents a field of positive one Tesla and negative one Tesla
- Operate at cryogenic temperatures
- Fit in the bore of the HTS 110 commercial magnet

Typically when measuring field at cryogenic temperatures IRL have used Arepoc hall sensors. They can operate at a temperature ranging from 1.5 K to 350 K and in fields of ± 5 T. This was recommended by IRL specialists as a good sensor for obtaining the magnetic field in cryogenic conditions. The particular hall sensor used was a Arepoc HHP-NP hall probe, the data sheet can be found in Appendix 12.4.4. The physical dimensions of this hall probe are such that its largest dimension is over a factor of two smaller than the magnets bore.

9.1.2 Temperature sensor

The use of the temperature sensor was initially intended just for monitoring temperature as opposed to a feedback signal, as the additional temperature dependence was not discovered until after the hardware modules had been designed. So a high degree of accuracy was not needed. However the following conditions should be met.

- Operate between 40 K – 300 K.
- Have an accuracy of greater than or equal to 0.25 K.
- A size that allows it to be placed in small areas such as the width of the SC.

Two common types of resistance temperature element sensors exist for cryogenic temperatures. Metallic resistance thermometers and semiconductor-like resistance thermometers. Both of which change resistance with temperature

A PT100 (Platinum metal, 100 Ω at 0°C) element sensor is the most common metallic resistance temperature sensor. The sensor has a resolution at best of up to ± 20 mK over a temperature range from 20 K to 300K if the correct calibration technique is achieved. The resistance of a PT100 element increases with temperature so the higher the temperature the stronger the signal becomes. The semiconductor based temperature sensor has the opposite effect in resistance with temperature, so the lower the temperature the stronger the signal. They can achieve a resolution at best of ± 1 mK depending on the semiconductor material (Ekin J. , 2006) . The semiconductor based temperature sensor is typically more expensive and not as readily available as the less expensive PT100 sensor. Since the resolution of the PT100 was higher than needed, less expensive and readily available, it was chosen as the temperature sensor.

9.1.3 Motor selection

Reliability has to be a key feature in the FP so it is an obvious choice in selecting a motor with no brushes. Brushless AC motors were not investigated due their usually large size and that the hardware of the FP will be running from a DC power source. This left BLDC motors and stepper motors. Due to the advantages and disadvantages of each outlined in section 2.3, a stepper motor was selected over the BLDC motor. This was primarily due to the complexity and cost in developing the driver hardware of a BLDC motor. The stepper motor was also the less expensive of the two.

A stepper motor that was small in size when compared to the FP and consumed low power (less than 5 W) was desired to carry out rotation in the FP. It was known that the torque needed to move the flux pump was below 0.1 NM. This was verified using a torque wrench that had the lowest setting of 0.1 NM. It was applied to the FP and rotated. The torque did not register on the torque wrench indicating it was below 0.1 NM. The FL42STH38-1684B bipolar stepper motor was chosen as the motor to drive the FP. This had a maximum coil rating of 1.68 A. It was comparably small when compared to the FP, having a maximum dimension of 42mm . It was unknown of the upper limits of speed needed in the operation of the FP. However there was a large torque of approximately 0.38 NM at the lower pulses per second range (PPS) and a torque of 0.08 NM at the higher PPS range according to the data sheet, which can be seen in Appendix 12.4.10, this equates to a rotational frequency of up to 50 Hz. This makes this particular stepper motor suitable for the rotation of the FP. The stepper motor can be seen in Figure 9-2 below.



Figure 9-2 - FL42STH38-1684B bipolar stepper motor

9.2 Hardware modules

The baseline components have been selected so it is important to develop hardware modules to interface with these, as well as mediums to allow for human interaction with the system.

This section is concerned with the second level in the control system hierarchy diagram in Figure 9-1

The first stage in each hardware module is identifying the inputs and outputs, the range of a measurement or control signal, the resolution, and any other relevant information related to the module. Based on these requirements schematics can be designed using various monolithic chips and components. The designs will be drawn using the freeware package design spark supplied by RS components. The designs can be validated by building prototype circuits on vero board. Testing and if needed modification can then happen. Once the various modules have been proven to work, they can be transferred onto a final or series of final printed circuit boards (PCB) ready for the next stage in the system design.

9.2.1 Hall sensor hardware module

It was decided to position the hall sensor in the magnets bore which should have the largest magnitude in field. This portion of the system is situated at room temperature. Future work will see the sensor being incorporated inside the magnet, however for debugging reasons it is kept outside at this time. The hall sensor has the following input and output requirements according to the data sheet in Appendix 12.4.4.

- A nominal control current of 20 mA
- Output of the linear hall probe is 180.9 mV/T

These specifications identify that the hardware module for obtaining this signal is going to require the following.

- Constant current source.
- Difference amplifier for amplifying the signal.
- Signal conditioning to remove any components that are not DC.

This sets guidelines in order for a hardware design to take place. A stable current source that can supply a continuous value of 20 mA is needed to energise the hall sensor. This can be achieved in a number of ways. One of which is shown in Figure 9-3. This was a modification of a circuit obtained from a microchip application note, this can be found in the references (Baker, 2008).

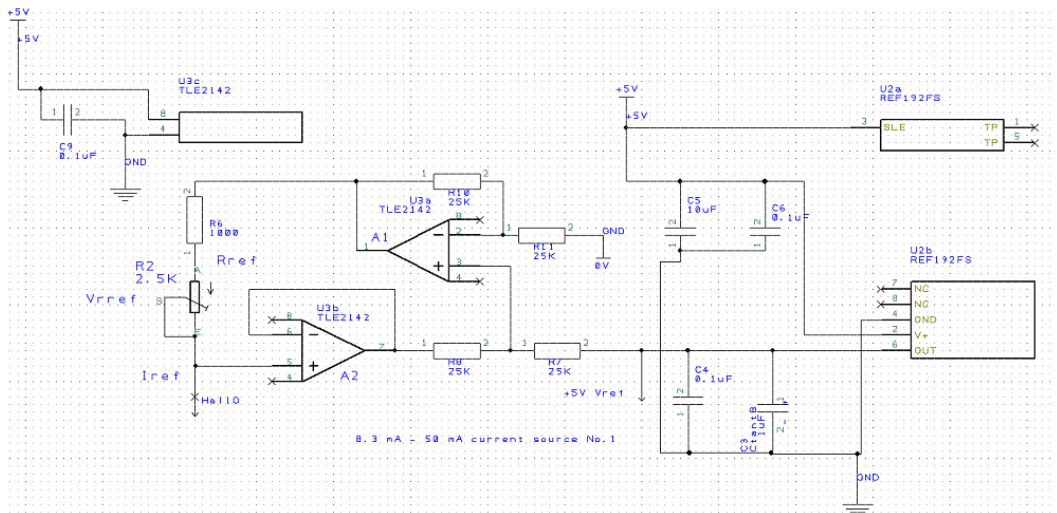


Figure 9-3 - Hall sensor current source

Amplifier A1 in Figure 9-3 along with the four resistors labelled R10 – R13 form a difference amplifier that has a differential gain of one, due to the four resistors being equal. A precision voltage reference of 5 V (V_{REF}) is applied to the non-inverting input of the amplifier. The output of A2 is the voltage seen at the point labelled HallO. This leads to the expression in Equation 9-1 below for the voltage output of A1. G is the gain of A1

Equation 9-1

$$V_{OUTA1} = V_{OUTA2} + GV_{REF}$$

Therefore the voltage seen across the combined resistance of R5 and R6 is equal to $V_{OUTA1} - HallO$ and can be denoted V_{RREF} , which is equal to $V_{REF} (+5 V)$. R5 is a fixed resistor and R6 is a trim pot, this allows an adjustable resistance from 100Ω to 600Ω, this can be denoted R_{REF} . From Ohms law one can see that this would give a current denoted I_{REF} in the range of 8.3 mA to 50 mA. The current I_{REF} is independent to the voltage of HallO therefore the hall sensor will be supplied with a constant current of 20 mA if the resistor network R_{REF} is tuned accordingly. Having an adjustable current source gives the flexibility of fine tuning the circuit as well as using the circuit for other applications that require a current source.

A positive and negative field measurement of one Tesla is desired, this equates to a measurement range of ± 180.9 mV. The signal from the hall sensor will eventually be inputted into a single supply analogue to digital converter (ADC), so the signal needs to be offset and amplified to match a reference value. A +5 V precision reference was decided upon as a reference value. It is a readily available component and can be used in other parts of the circuit such as the current source. The lower 2.5 V of the reference is to represent the negative field and the upper 2.5 V, the positive field. The signal being ± 180.9 mV needs to be amplified so it

will be $\pm 2.5V$. This will be the first step, amplifying the incoming signal by 13.8, followed by offsetting the amplified signal by 2.5V. The signal is relatively small so a differential amplifier setup with a high common mode rejection ratio (CMRR) and high input impedance should be used. This will minimise noise and reduce the load on the sensor signal. The obvious choice is an Instrumentation amplifier. Being a monolithic chip it removes the need to have the traditional three OA and a network of external resistors, making the system less prone to component tolerances and thus improving the overall accuracy and precision. For more information see (Kitchin & Counts, 2006). The particular instrumentation amplifier (IA) that was used was an Analog Devices AD620, see Appendix 12.4.5 for data sheet. As for creating the offset a standard operational amplifier (OA) was used in conjunction with a trimming potentiometer to create a 2.5V fixed voltage that was feed into the reference pin of the IA. The manufacture stated that the reference voltage must have a low input impedance, which the output of a OA has. Figure 9-4 shows the instrumentation amplifier circuit with the 2.5 V offset.

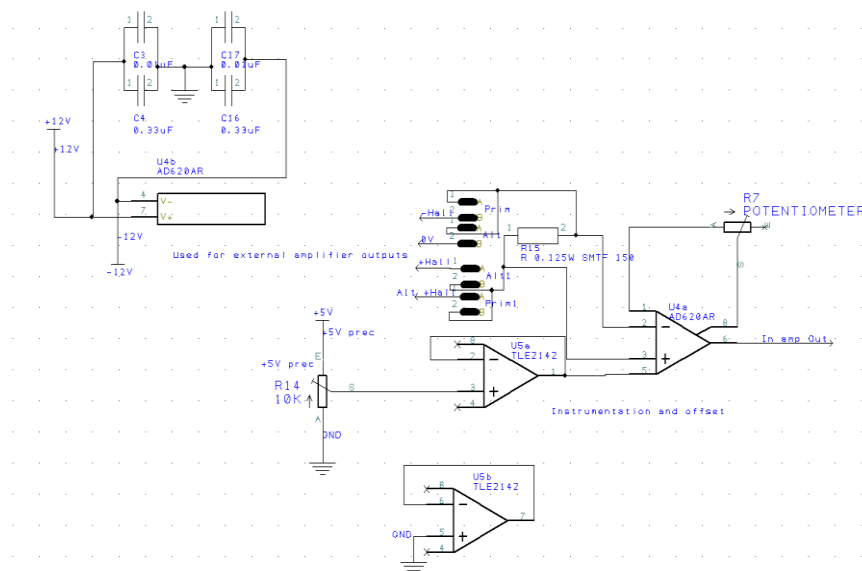


Figure 9-4 – Instrumentation amplifier stage

The signal out of the IA is DC so to shield against any stray frequencies interfering with this output signal, a 1 Hz 4pole active Bessel response filter was applied. It is an effective low cost filter recommended by Analogue devices, (Kitchin & Counts, 2006) for data acquisition. The circuit contains two OA and a network of capacitors and resistors.

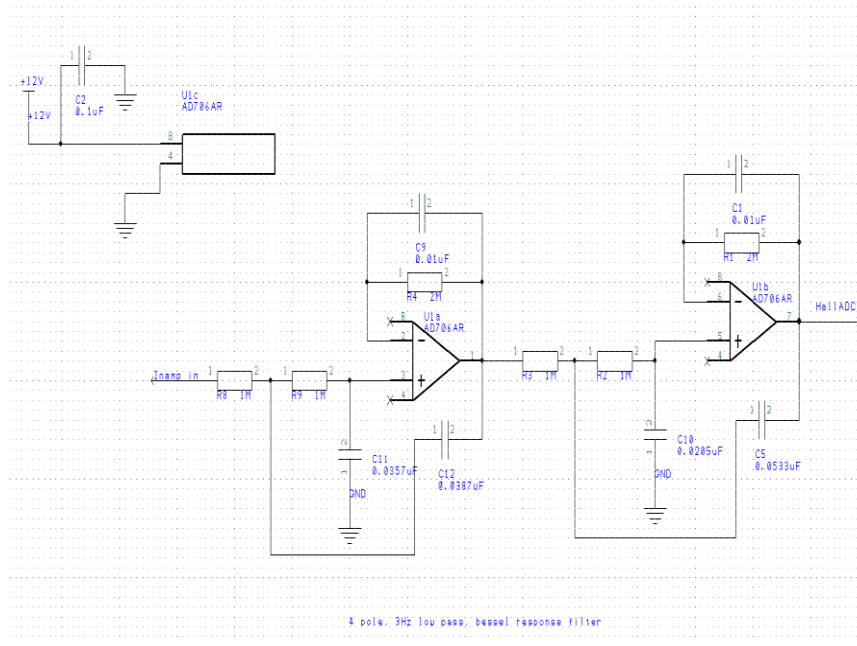


Figure 9-5 - 4pole active Bessel response filter

The output from the filter is sent to a ADC which will be discussed later in the text.

9.2.2 Temperature sensor module

The system is to have three temperature sensors that are placed according to Section 8.2. As mentioned in Section 9.1.2 the PT100 sensor is to be used for measuring temperature. A PT100 sensor consists of the metal Platinum, when supplied with a fixed current the resistance of the material can be measured. Platinum metal has a resistance of 100 Ω at the triple point of water (0 $^{\circ}\text{C}$), this is why it is called a PT100. The PT100 should be supplied with a constant current of no larger than 1 mA, as any larger has the potential to cause ohmic heating, thus giving a temperature reading that is not a true representation of the part being monitored. The resistance of a PT100 sensor changes with temperature according to the Callendar-Van Dusen equation below (Instruments, 1996)

Equation 9-2

$$R_t = R_0 [1 + At + Bt^2 + C(t-100)^3]$$

where R_t is the resistance of the RTD at temperature t , R_0 is the resistance of the RTD at 0 $^{\circ}\text{C}$, A , B and C are the Callendar-Van Dusen co-efficients and can be seen in the table below. The unit of temperature is degrees Celsius ($^{\circ}\text{C}$). For temperatures above 0 $^{\circ}\text{C}$, C is zero

A	B	C
3.9080×10^{-3}	-5.8019×10^{-7}	-4.2735×10^{-12}

Due to the characteristics of the PT100 it can be realised that it has the following input and output.

- 1 mA constant current source
- Voltage range of 0.85 mV to 110.47 mV (40 K to 300 K)

To acquire the PT100 signal the following hardware needs to be developed.

- Constant current source.
- Difference amplifier for amplifying the signal.
- Signal conditioning to remove any components that are not DC.

The requirements of the hardware are very similar to what was needed for the hall sensor. Thus the same basic schematics can be used with some modifications to match the characteristics needed for a PT100 sensor.

The same current source used for the hall sensor is to be used for the PT100 with minor changes to supply a lower current. This includes the R_{REF} value and the voltage reference V_{REF} in Figure 9-3 changing. The PT100 outputs the same polarity voltage as the input current. As a result V_{REF} is changed to 2.5V as there is no offset needed and this reduces the power dissipation in the amplifier chip. R_{REF} is changed to give a constant current in the range of 0.7mA to 2.5 mA. The schematic of this can be seen in Appendix Temperature sensing module12.1.2.

Due to the sensitivity of the PT100 sensor it is imperative that lead resistance of the current leads is not taken into the measurement system. To eliminate this the voltage across the PT100 can be measured using two additional wires and therefore removing the resistance error. This is a common practice known as a four point measurement. The output from the four point measurement is to go into an acquisition system that is very similar to the hall sensor module, however there is not offset required so a single supply IA is used instead. The AD623 IA was the chosen amplifier. It was from the same family of IA amplifiers as the one used in the hall sensor module and had very similar characteristics. The data sheet can be seen in Appendix 12.4.6.

The exact signal conditioning circuit applied in the hall sensor hardware module in Figure 9-5 was replicated and applied to the PT00 hardware module.

Due to the fourth order polynomial used for determining the temperature of the PT100, it is not practical to implement such an equation in a microcontroller. It will require multiple lines of code and significantly increase computation time. To accommodate for this, look up tables are used to store a series of predetermined values corresponding to the input values from the

temperature measurement system. To avoid overfilling the RAM of the microcontroller, the look up values can be written to the EEPROM. The microcontroller generally has a small internal EEPROM. So to circumnavigate this problem, an external based EEPROM is used which will use the SPI protocol. To achieve a resolution of 0.01 K a total of 29001 data points are needed and a 16bit representation is to be used for each data point. This would require an EEPROM that is greater than 464016 bits. The 25LC1024 1 Mbit SPI Bus Serial EEPROM will have twice the capacity needed which will meet the needs of the data storage and leaves room to store extra data in the near future if needed. The data sheet for this can be found in the Appendix 12.4.8.

9.2.3 Analogue to digital conversion

In order for the signals from the hall sensor and the PT100 hardware modules to be processed in a central processing unit, they have to be converted to a digital format. This requires an ADC. A microchip branded serial port interface (SPI) analogue to digital converter ADC was used as this could be easily interfaced with most microcontroller units that have inbuilt SPI hardware. The SPI protocol is a standardised method of data transfer. The higher the resolution of the ADC the more accurate the measurement will be, however precision is just as important. So it was decided to use a 22 bit Delta-Sigma ADC. See datasheet in the Appendix 12.4.7. This had a 2ppm typical full scale error and a low output noise of 2.5 μ V.

9.2.4 Human interfacing

Human interfacing is the medium by which the human user interacts with the control system or more specifically the central processing unit. The control system is going to need the following inputs and outputs.

- Buttons to switch between modes and adjust values
- Trim potentiometers for adjusting values
- LCD screen to display any relevant information.

It was decided to have four push buttons and two potentiometers which gives an adequate amount of input controls and if all are not needed they can be unimplemented. The schematic for this can be seen in Figure 9-6 below.

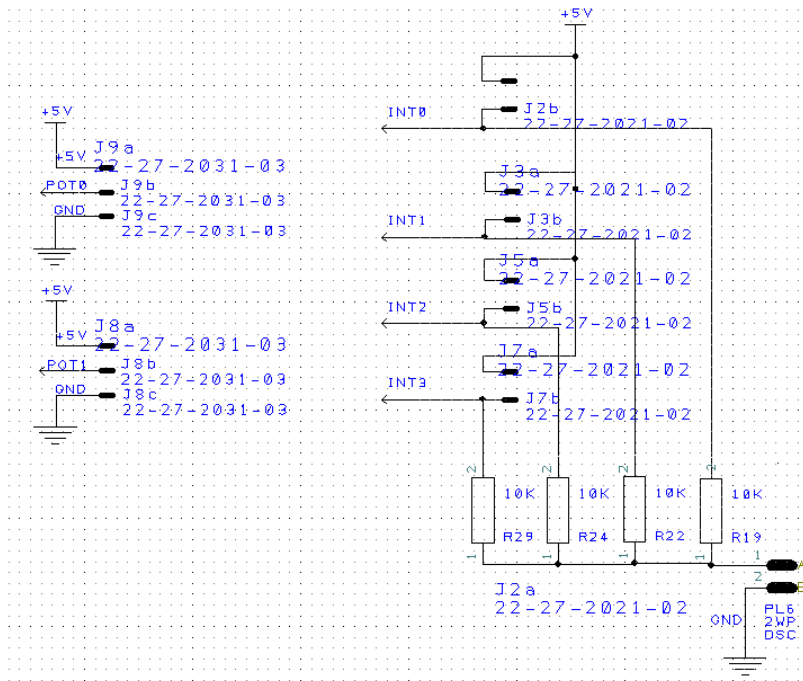


Figure 9-6 Trim potentiometers and push buttons.

Figure 9-6 shows the potentiometer plugs on the left and the four push buttons on the right. The push buttons are configured so they are active low.

The LCD module is a 4-line, 20-character alphanumeric display. It has a Hitachi 44780 like driver built in, which allows standardised commands to be sent to it in order to display information. The data sheet is shown in Appendix 12.4.11 and can be seen in Figure 9-7 below.



Figure 9-7 - Display tech LCD

9.2.5 Stepper motor driver

According to Section 2.3.1 the bipolar stepper motor coils need a series of pulses to create a changing magnetic field that will cause the rotation of the stepper motors rotor. The design of such a driver would require a large amount of development which is not going to be effective

in terms of time and money. There are many drivers available that simply require an input pulse that will be translated into the signals required to drive the stepper motor coils. Other inputs in the drivers allow one to change the drive direction, the steps per revolution and enable/disable the current to the coils.

According to the data sheet the stepper motor requires a driver that can output a current of up to 1.68 A.

An Allegro based stepper motor drive on a breakout board was found at IRL . It has the capability of supplying 2 A which is more than the required 1.68 A. Figure 9-8 shows the breakout board The break outboard had no heat sink and relies on the thermal layout of the PCB that it was attached to. It was found after a finite amount of time, over 10 minutes the motor would start to skip steps and run very poorly. This was suspected to be a result of the driver suffering from ohmic heating. The data sheet in Appendix 12.4.2 has a plot of temperature versus power dissipation of the chip. One can use Equation 9-3 (Thermal Design) to calculate the junction temperature of the driver and then compare this to the value shown on the temperature versus power dissipation plot to obtain the maximum allowable power dissipation. Where T_{Jmax} is the maximum allowable junction temperature of the device, P_{Dmax} the maximum power dissipated by the device, θ_{JM} the junction to ambient temperature resistance and T_{amb} the ambient temperature around the device

Equation 9-3

$$T_{Jmax} = (P_{Dmax} \cdot \theta_{JM}) + T_{amb}$$

According to the specifications of the stepper motor and a current limit set at 70 % of the maximum current, 1.2 A, it will be dissipating 3.24 W. setting $P_{Dmax} = 3.24 \text{ W}$, $\theta_{JM} = 32 \text{ }^\circ\text{C/W}$ (which is applicable to the PCB layout used in this circuit), and $T_{amb} = 25 \text{ }^\circ\text{C}$ in Equation 9-3. A max temperature of 175.4 $^\circ\text{C}$ is occurring, this temperature equates to under 1 W of allowable power dissipation according to the plot in the data sheet thus indicates why the stepper motor is not performing correctly. To decrease T_{Jmax} one needs to decrease the θ_{JM} , which can only be done by implementing a large heat sink. Due to the small size of the chip it seems impractical to simply attach a large heat sink.



Figure 9-8- A4983 stepper motor driver

It was decided to use a commercial stepper driver that had sufficient heat sinking and could be simply interfaced to the control board using many of the same signals as used on the previous stepper drive. The replacement stepper motor drive was an M542 microstepping driver from leadshine technology co. It was capable of supplying 4.2A of current. This can be seen in Figure 9-9 and the datasheet in Appendix 12.4.9. It is a standalone unit so it has been designed accordingly to dissipate the heat correctly.



Figure 9-9 - M452 microstepping drive

9.3 Central processing unit

Now that the hardware for sending and obtaining signals has been developed a central processing unit is needed to collate the various signals and process them. This will also contain the algorithms necessary for control of the system. There are many types of microcontrollers that could be used as the central processing unit. PIC microcontrollers from Microchip is one of the available brands and is used by HTS-110, they have a wide range of functionality which makes them easily compatible with the hardware designed so far. For that reason a PIC microcontroller will be used.



Figure 9-10 - PICkit 44-Pin demo board

As The PIC microcontroller was to be used in the project as the central processing unit, It was decided to acquire a low cost development board so learning of the PIC development environment could be learned immediately.

To utilise time effectively a software known as PICbasic Pro (PPB) was used as the programming environment. This uses the BASIC type programming language and has many single line commands that replace lines of assembly language. Thus allowing quick development of software. PBP has the added advantage of being able to insert segments of assembly language in the programming environment. This may be desired when a more efficient routine is needed, making PBP a very powerful tool for embedded software applications.

The Development board gave a good indication of what extra features were needed for the final control system and gave the ability to test the hardware modules. This lead to the choice of a PIC 18F87K90 chip. This particular chip has 80 pins, 60 of which can be dedicated to I/O. It has two SPI ports which makes it appealing in the fact that one can have a SPI port dedicated to the hall sensor and one for the temperature measurement. The Hall sensor measurement is the primary feedback for the magnetic field control loop, so it is important to read that as frequently as possible. For that reason it makes sense to have the less frequent temperature measurement on a separate SPI port. It can have a maximum oscillator speed of up to 60 Mhz thus maximise the run time of code implemented. For a full list of specifications see the data sheet in Appendix 12.4.12.

9.4 Additional circuits

It was decided to include an additional circuit to control temperature. This will not be used in this thesis but allows the ability for it to be integrated in the future once the temperature drift issue has been further investigated. This circuit consists of two MOSFET devices that can be switched on and off to create a varying voltage using a pulse width modulated (PWM) signal from a microcontroller. This allows control of two heater units. The schematic of this can be seen in the control board schematic in Appendix 12.1.1

The microcontroller has built in RS232 hardware so it was decided to include a Future technologies FT232 RS232 to USB chip on the motherboard so one could send information in or out of the microcontroller in future applications. This would be useful for data logging to a PC. The datasheet for the chip can be seen in Appendix 12.4.3 . The schematic used to incorporate the chip was found here (FTDI) and is shown In Appendix 12.1.3.

9.5 Printed circuit board (PCB) implementation

The various prototype circuits that were designed and implemented on vero board, were tested and appeared to work as desired. However due to the nature of the vero board, circuits populated on it are susceptible to noise, can get very untidy and complicated to debug. It was decided to design two new boards, one with all the previous hardware modules except the temperature sensing one and the second containing three temperature sensor modules. This was to save space on the main mother board and allow for additional temperature sensors if needed. One could simply stack the SPI interfaced temperature boards on top of each other to increase the total amount of temperature sensors.

The PCB's were laid out so the components were spread about evenly and human interaction component plugs were in places so they were easily accessible. The PCB's had the following characteristics.

- 1.2mm thick FR4 composite boards
- Each board was a two layer PCB
- The power and ground traces were set at 1.3mm thick where possible and the signal traces were set at 0.38mm for the microcontroller signal traces and 0.8mm for the other signals.
- Red solder mask to provide insulation to the copper traces and a white silk screen for component labelling.

The fast changing of current levels in a digital circuit can cause current spikes to occur in the ground plane which directly affects the analogue circuits. To reduce this once the board had been laid out a copper pour was done on both sides around all the traces. One side was made to be the positive supply and the other the ground. This acts as a capacitor to dampen the noisy currents from the digital circuitry. Having a ground plane also increases the overall ground impedance, thus reducing high frequency ground bounce.

The PCBs were routed using the software design spark which the schematics were designed in. The PCB's were fabricated by PCB core in china. PCB core could fabricate the board in a timely fashion with a competitive price to match what places in New Zealand could offer .The PCB layouts of the boards can be found in Appendix 12.2.1 and Appendix 12.2.2 respectively. The ground and positive voltage planes have been removed so one can see the wire traces.

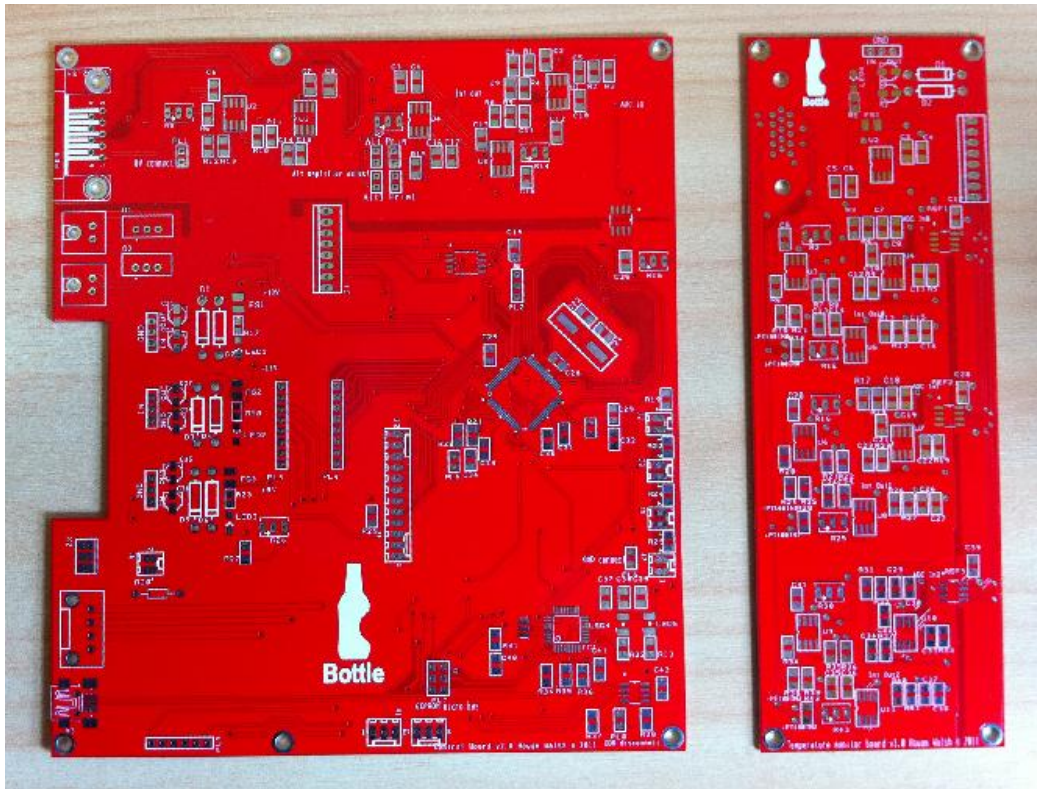


Figure 9-11 – Finished PCB boards. The motherboard on the left and temperature module on the right.



Figure 9-12 - Complete hardware module

Figure 9-12 shows the full hardware module. The two PCB boards and the motor driver are mounted inside.

9.6 Embedded software

The highest level in the control system is the software, which can now be implemented on the working hardware modules. The first step of creating the software is to develop test cases for each hardware system. This tests the functionality of each hardware module at a end user level and allows a software units to be developed and used later in the control algorithm.

9.6.1 LCD communication.

PBP has a built in command for communicating with Hitachi 44780 controllers or the equivalent. This makes interfacing with an LCD a quick and easy process. The LCD is essential for displaying useful information to the human user, and also a very useful tool for debugging software. Thus it is the first module to be implemented in software.

The developer needs to add defines in order to customise various commands used in the PBP language. This can be done using the following lines of code. Words after the ' are comments.

```
' Define LCD registers and bits
DEFINE LCD_DREG PORTD 'Set LCD data port
DEFINE LCD_DBIT 0 'Set starting data bit
DEFINE LCD_RSREG PORTH ' Set LCD Register Select port
DEFINE LCD_RSBIT 1 'Set LCD Register Select bit
DEFINE LCD_EREG PORTE 'Set LCD Enable Port
DEFINE LCD_EBIT 2 'Set LCD Enable bit
DEFINE LCD_BITS 4 'Set LCD Bus size (4 or 8 Bits)
DEFINE LCD_LINES 4 'Set number of lines on LCD
DEFINE LCD_COMMANDUS 1500 'Set command delay in us
DEFINE LCD_DATUS 44 'Set data delay time in us
```

The following sends characters to the LCD

```
LCDOUT $FE,1, "Hello" 'Clear display and show "Hello"
```

The full LCDOut function coding can be found in Appendix 12.3.1.

9.6.2 HPWM signal

PBP has a built in function for the onboard hardware pulse width modulation (HPWM) signal. Again defines are put in the code to identify which ports and configurations are to be used. An example is shown below.

```
;PWM defines
```

```
DEFINE CCP4_REG PORTG 'Hpwm 1 pin port
```

```
DEFINE CCP4_BIT 3 'Hpwm 1 pin bit
```

```
DEFINE HPWM1_TIMER 2 'Hpwm 1 timer 2 select
```

```
HPWM 1, 127, 1000 'channel 1 HPWM, 50% duty cycle, at 1KHz frequency
```

9.6.3 Trim pot

When using a trim pot to adjust a parameter in a microcontroller the varying voltage from the trim pot has to be converted to a digital signal and is done via the ADC on-board the microcontroller. PBP has a function for the accessing the on-board ADC. Again defines are set at the beginning of the programme.

```
;ADC defines
```

```
DEFINE ADC_BITS 12 'ADC set at 10 bits
```

```
DEFINE ADC_CLOCK 5 ' Set clock source to Frc/3
```

```
ADCIN 0, adcVar 'ADC channel, store in variable advVar
```

9.6.4 Push buttons

The push buttons are interfaced with I/O that have a hardware interrupt multiplexed to their respective pin. PBP has an Interrupt handler that can be used to handle any of the interrupts used on a PIC microcontroller. Configurations for the interrupts must be set according to the PIC datasheet.

```
ON INTERRUPT GOTO intHandler 'When an Interrupt occurs jump to the sub routine int Handler
```

9.6.5 SPI communication

There are two hardware modules that run via the SPI communication protocol on the PIC18F87K90 microcontroller. One is the external 22 bit ADC and the other is the external EEPROM. The ADC is only sending information to the microcontroller whereas the EEPROM is

sending and receiving information. There is no SPI function in PBP, and as each device is different a function has to be developed to suit the function of each individual device.

The 22 bit ADC requires 3 pins for the SPI control, CS, SDO/RDY, and SCK.

CS - clock select. Pulling CS low will begin a conversion on the ADC. Enables one or more SPI devices.

SDO/RDY - Serial data out/ ready. This is the output data pin. Once a conversion is complete, the pin will go active low, acting as a ready flag.

SCK - Serial clock - synchronises data communication with the device.

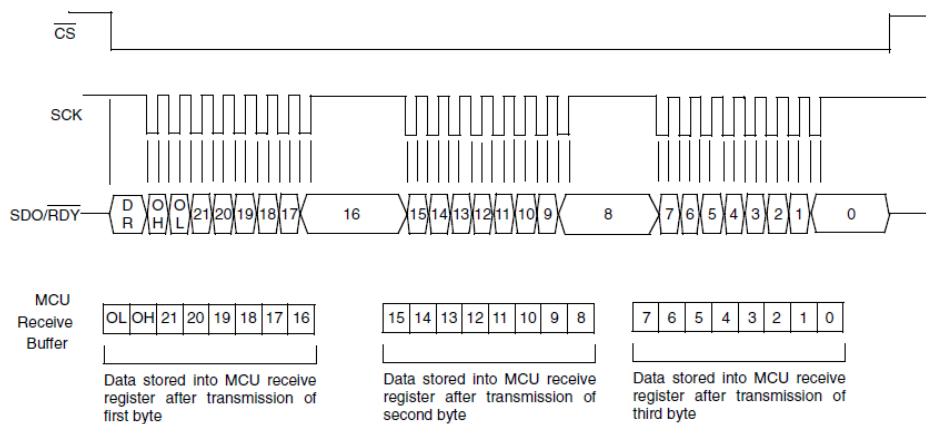


Figure 9-13 - SPI communication diagram

Two functions were made to obtain the necessary information from the ADC. The 22bit value is read in 3 blocks, each a byte big. The routine 'getdata' saves the 3 byte sized blocks into an array. The function 'letclear' is called from 'getdata' which simply checks if SSPBUF buffer is full and then resets the raised flag if this is true. The commented code can be seen below.

```

getdata:
    low cs2
    pause 120
    For i = 0 to 2 ' loop for 3 characters
        SSPBUF = 0 ' write to SSPBUF to start clock
        gosub letclear
        a[i] = SSPBUF ' store received character in array
    
```

Due to having 16 bit variables available in PBP the 16 most significant bits were used from the ADC output. That meant that 32767 bits were allocated each to the positive and negative

fields. This gives a resolution of 0.03mT. So this will be a limiting factor in how accurate the control of the field can be. The full code can be seen in Appendix 12.3.2.

```
Next i          ' get next character

high CS2
Return

letclear:
  IF SSPSTAT.0 = 0 Then letclear ' wait for SPI Buffer full status
  pauseus 50
  SSPSTAT.0 = 0      ' reset flag
  Return
```

The SPI for the EEPROM requires the following pins:

CS - clock select. Pulling CS low will enable the EEPROM for data transfer.

SO - Serial out. Data is transferred out of the device. During a read cycle, data is shifted out on this pin after the falling edge of the serial clock occurs.

WP - write protect. A low level signal protects the chip from write access

HOLD - Used to suspend transmission to the device while in the middle of a serial sequence without having to retransmit the entire sequence again.

SCK - Serial clock. Used to synchronise the communication between the device and the master.

SI - Serial in. Data is transferred into the device. Data is latched in on the rising edge of the serial clock.

A brief description of the write and read process are listed below. For a detailed explanation refer to the data sheet in Appendix 12.4.8.

The following requirements are for a write sequence to occur.

1. The write enable latch must be set by issuing the WREN instruction. CS needs to be pulled low then the eight bit 'WREN' instruction sent. Once CS has gone high again the write enable latch is set.
2. 'CS' needs to go low. A 'WRITE' instruction can be sent
3. The 24 bit address needs to be sent. This is done in three bytes.
4. The data byte(s) are sent. Up to 256 bytes can be sent before another write cycle is necessary. 'CS' needs to be pulled low for the 'WRITE' sequence to be completed.

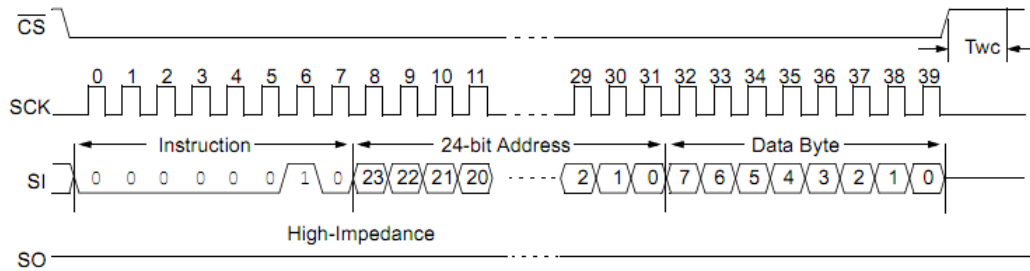


Figure 9-14 - Byte write sequence

WriteData:

```
'Send the write enable sequence (WREN)
CS3 = 0      ' Enable serial EEPROM
out = 6      ' load write enable sequence
gosub Outputdata
CS3 = 1      ' Disable serial EEPROM
;Send the write sequence (WRITE)
CS3 = 0      ' Enable serial EEPROM
out = 2      ' load write sequence
gosub Outputdata
out = 0      'Load high address byte
gosub outputData
out = 0      'Load middle address byte
gosub outputData
Out = 55     'Load address location (low byte)
gosub outputData
Out = 29     'Load actual storage variable
gosub outputData
CS3 = 1      ' Disable serial EEPROM
```

OutputData:

```
SSP2BUF = out      'Write value to SSPBUF register
Gosub letclear
rxData = SSP2BUF  'Write value of SSPBUF register to rxData variable
Return
```

For a read sequence to occur the following procedure has to be implemented.

1. CS needs to be pulled low . The 8-bit 'READ' instruction is sent
2. The 24 bit address needs to be sent. This is done in three bytes.

- The data at that address can then be moved onto the 'SO' pin. The next address can be read providing 'CS' is still low and clock pulses are present. The read process can carry on indefinitely and will rollover from address 1FFFFh to 00000h . To terminate 'CS' must be pulled high.

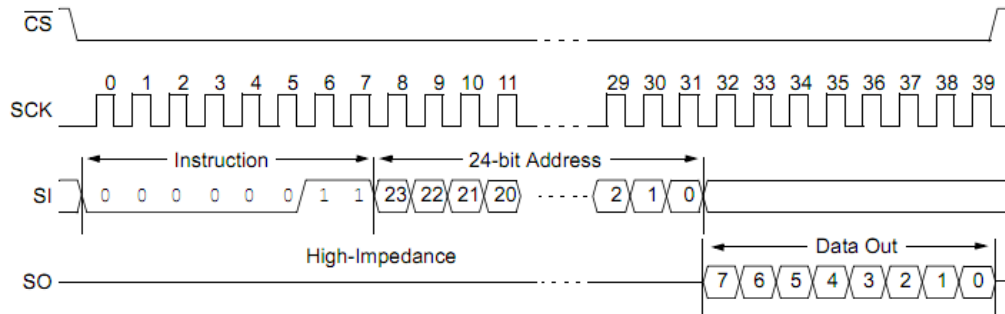


Figure 9-15 - READ sequence

Send read sequence (READ), read address 0x55

```

Cs3=0
out = 3      'load read sequence
gosub outputdata
out = 0      'load high address part
gosub outputdata
out = 0      'load middle address part
gosub outputdata
out = 55     'load low address part
gosub outputdata
out = 0      'call output to read 1 byte
gosub outputdata
cs3=1

```

A full listing of the code for the EEPROM module can be seen in Appendix 12.3.3.

9.7 Control Loop

It has been shown that with manual control the field can be stabilised, however there is a drift in the field over time. For a near perfect control it is imperative to find the source of the drift and manage this in the control loop, however this is out of the scope of the current work and will be worked on in the near future. The focus is to implement a control loop on the system as

it stands and evaluate the effectiveness of this control loop . It is expected that there will still be a drift, but minimising the field deviation within this drift is important.

The frequency of rotation is proportional to the voltage generation, however this is dependent on what current is present in the circuit. From Figure 9-16 one can see that as the current in the circuit is increased the voltage generation decreases. This relationship will need to be factored into a model in the near future.

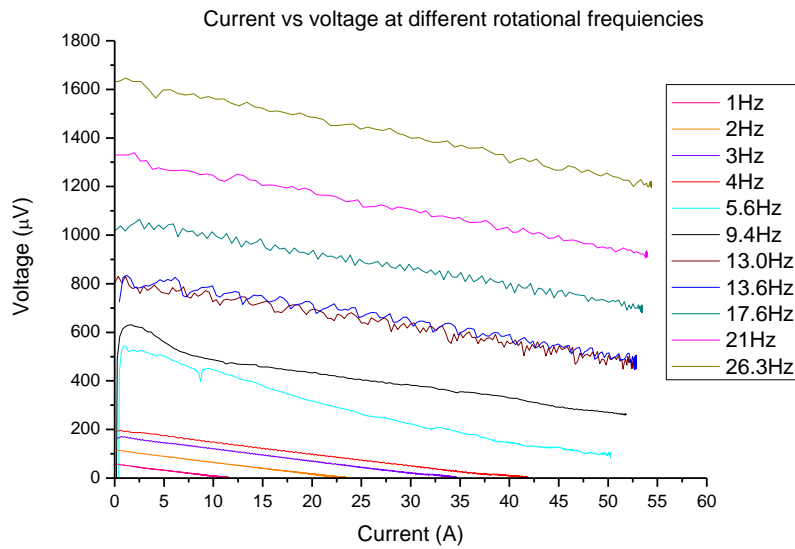


Figure 9-16 - Current vs voltage for different rotational frequencies

There is an asymmetric relationship in ramping up the field and ramping down. This can be realised in the equation below.

Equation 9-4

$$V = 2IR + d\Phi / dt = dLI / dt$$

During the ramping up stage the voltage across the coil is limited by dLI/dt . The voltage source comes from the rotation of the flux pump (the changing flux $d\phi/dt$). For ramping down (reverse direction) the dLI/dt term adds to the $d\phi/dt$ term of the flux pump to create a voltage that is larger in magnitude but is dependent on the rotation frequency as seen in Figure 9-16. A model has not been developed yet that relates the mechanical rotation of the flux pump to the field production. This is a complex system that is new and no current literature relating to a model exists. Thus it needs further investigation to identify all the parameters involved and what effect they have. A mathematical model can then be developed and a transfer function derived. This will be done in later work and for the moment manual tuning of the PID controller is used to achieve a satisfactory level of control. The control stage at this point is more about

establishing a base to work from. It will identify if the current hardware is working correctly or if it needs to be developed further for any new variables that may arise.

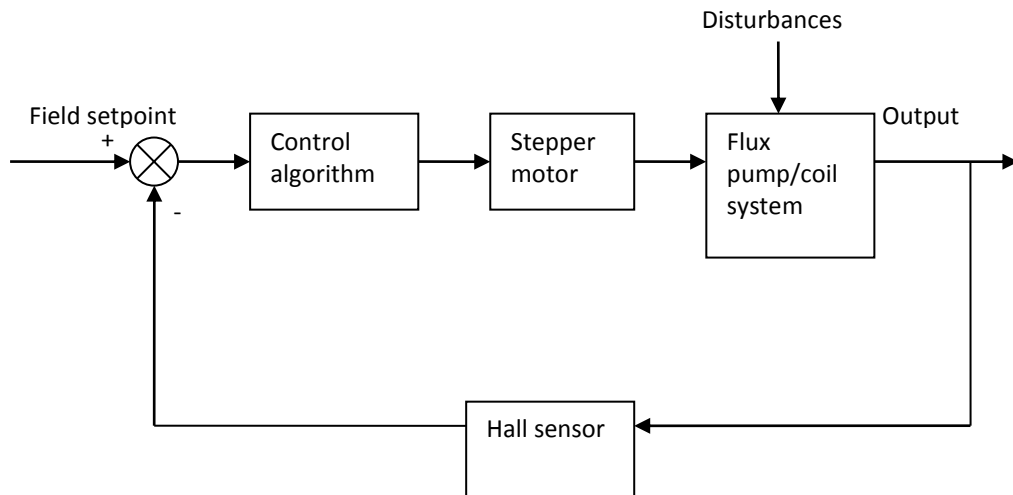


Figure 9-17 - Feedback control loop for the FP

The feedback loop shown in Figure 9-17 is set out as follows. The hall sensor value, being the process value (PV) is subtracted from the desired field, the set point (SP). This is inputted into the control algorithm. The output of this is the manipulated variable (MV) which is sent to the stepper motor controller which acts accordingly. The output of the stepper motor affects the field in the coil as well as reacting with additional disturbances, which could include but are not limited to temperature variation and signal noise. The control algorithm will manipulate the MV so that the error remains as close as possible to zero.

9.7.1 Control algorithm

Due to the limitations of Picbasic Pro (PBP) currently using 16 bit variables, the full 22 bits of the ADC could not be used in one variable. So to save on code space and have a relatively simple control system it was decided to use the 16 most significant bits of the ADC for the PV. The 22 bit value from the ADC was an offset value of the field so the positive and negative field of 1T could fit in the 22 bit variable. The PV used 0 - 32767 (-1000 mT - 0 mT) as the negative field and 32768 - 65535 (0 mT - 1000 mT) as the positive field. This is a two's complement representation. In the traditional sense of two's complement, the lower 8 bits are denoted as positive integers and the upper 8 bits as negative. The notation used for the field is opposite, because it was more convenient for signal processing. This is purely at the human interface level. The PIC microcontroller uses a two's complement arithmetic so adding different signed integers together will be automatically taken care of.

The basic pseudo code for the PID algorithm is shown below. For the full listing see Appendix 12.3.4.

PID:

```
Error = SetPoint - Actual
P = Error * Kp
I = I + (Error * Ki)
D = (Error - previousError) * Kd
Frequency = P + I + D
previousError = Error
Wait
```

Goto PID

There is additional code used to turn on the integral only when the error gets below a threshold. This is to prevent integral wind up when the initial error is large. The proportional term K_p is dynamic, it increases depending on the error until it reaches a threshold value, then it will stay fixed. This is to ensure that it does not exceed the value 32767 and be perceived as a negative number, as this would cause the output to be in the wrong direction.

The process for tuning the PID algorithm was done as follows. Only the P term was used in the beginning. This was to see what sort of response was obtained when varied.

Various P terms were used. Making the P value very large caused the set point to be approached faster however if it was too large it would overshoot and a positive offset was created. If the P value was too small the opposite would occur and there would be a negative offset between the PV and the set point.

PI control was implemented to increase the rise time as the PV got close to the set point. This meant that the P value could be reduced, which in turn creates less of a change around the set point for a given error. The integral term was not used until an error of 100 was present (0.45 % of the set point).

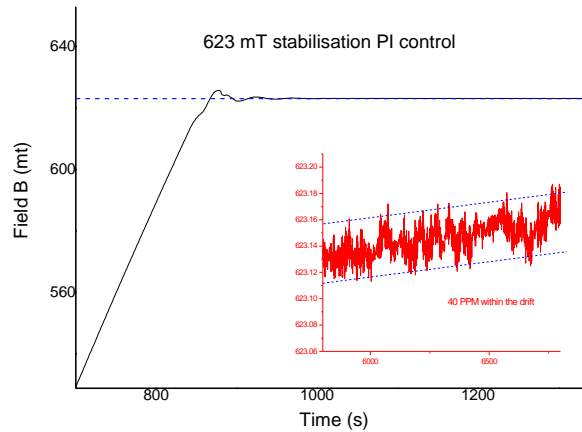


Figure 9-18 - PI control stability plot

Figure 9-18 shows the PI control stability plot. The black line plot is the PV (magnetic field). The range on the y scale has been set between 500 mT to 650 mT, so the convergence to the set point can be seen. The blue line is the set point which is set at 623.12 mT. The red plot is a scaled version of the PV with the time scale of 5800 s to 6800s. The dashed blue lines are upper and lower limits for the field change. Looking at the black plot it can be seen that there is minimal over shoot and the PV converges to the set point within 100 s. However looking at the red plot in the region where the field appears to be stable, it can be seen that there is a drift. Within the blue lines which denotes the drift, it can be seen that the field stability is within 40 PPM.

Due to the asymmetric relationship of the field when ramping, an overshoot should be avoided as much as possible, as the changing direction of the motor will have the effect of increasing the rate of the field change significantly as mentioned earlier in Equation 9-4. So it was decided to reduce the P action, as well as I and introduce D action. This will decrease the over shoot. The increased settling time is not critical at this stage as the intention for the FP is not to have continually changing fields, rather a stabilised field for a long period of time.

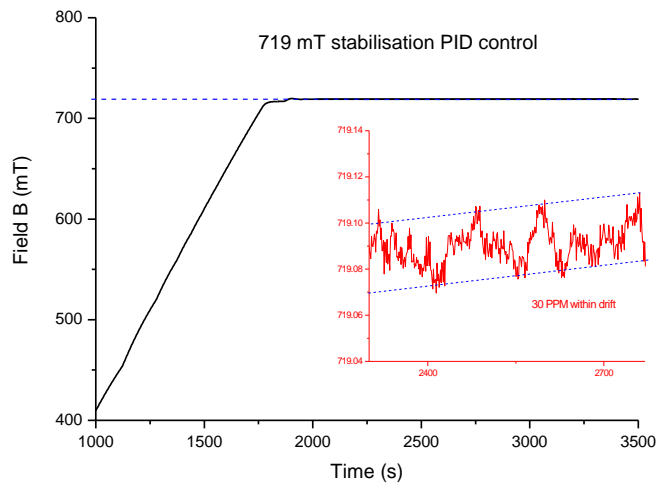


Figure 9-19 - PID control stability plot

Figure 9-19 is set out in the same way as Figure 9-18 except the set point has been changed to 719.08 mT. Looking at the black plot it can be seen that there appears to be minimal overshoot and the field converges to the set point in a similar time as the PI control. The red insert shows that the deviation in the drift is 30 PPM which is the limit of the resolution of the sensing module. Thus it is not possible to obtain a higher stability in the drift with using a 16 bit variable and it needs to be extended to accommodate the full 22 bits of the ADC. In addition this result is approaching the level of the sensor precision as well, so investigation into a higher precision sensor will be necessary in future research.

10 Discussion and Conclusion

An HTS flux pump (FP) was successfully implemented into a HTS-110 commercial magnet. The total static heat load of the system was seen to be no larger than 700 mW. When the FP was energised to a field of 750 mT, which equated to a current of 68 A in the circuit, the total heat load was 1.2 W. If the conventional method of current lead feed throughs were to be used on the same system, a heat load purely due to the ohmic heating of the current leads of 5.12 W would be seen. This would put the temperature of the coil at 77 K, compared to a temperature of 57K using a FP. The larger temperature would decrease the total current in the circuit by over a factor of 3.5, thus significantly reducing the field size from the coil. The significant reduction in heat load due to having the FP embedded in the cryogenic environment, maximises the benefits of operating at high temperature. Furthermore the produced field of 750 mT was stabilised to within 30 PPM, which is within reach to the 1 PPM NMR standard. This standard is currently the highest field stability one has to measure against. However, for most applications the demonstrated level of stability is more than required. Overall the FP system completely removes the need for an external PS to supply a constant current to the SC coil. The superfluous power supply reduces overall space and the expense for such a high stability unit.

The design of the flux pump system incorporated mechanical, cryogenic, electrical and software aspects. All of these elements needed to be worked on concurrently in order to achieve a functional system in an efficient manner.

A mechanical design was produced using the CAD package Solidworks. Focus was designing for a cryogenic environment. This included minimising heat load in some areas and maximising it in others. Both of which had a high importance, as did designing with contraction coefficients in mind. Compression and tension of various parts with respect to such coefficients were considered. Traditional mechanical principles were applied to minimise the effect of fatigue, stresses and strains. Experiments were carried out to validate assumptions and calculations. A final FEM analysis was carried out on the FP design to validate the calculations and design methods with respect to the static heat load and temperature. The FP was found to have a total static heat load of 500 mW according to the FEM analysis. Combined with an estimation of heat load acting on the FP due to radiation, this result is in excellent agreement with the measured value of 600 mW. The heat load, although relatively low, could be further reduced by connecting the suspension mounts of the FP to the cold head. The validity and benefits of this can be investigated in future work.

The finalised design was fabricated. This included a variety of machining operations and fabrication mediums. Various parts were outsourced to external companies. Where possible, standard parts were incorporated into the design to reduce cost and save time. The design for this work is purely a prototype, so minimising the cost as much as possible was not the top priority. However, once the FP is designed for a specific magnet and will become a product, an emphasis on designing it for manufacture will need to be done. This will mean designing the product so it can be fabricated and built efficiently in terms of cost and time.

With the assembled system a maximum field size of 860 mT was reached for a short period of time with the current configuration. The limitation was due to the quality of the superconducting wire, which was driven into the resistive state by the FP. The Stirling cryo cooler used could not provide enough cooling power to absorb the heat produced from the operation of the FP and dissipation in the coil at field of 860 mT. Therefore a temperature rise of each component occurred and limited the field strength.

An attempt at manual control at 750 mT revealed, that at a constant rotation speed the field would not come to a steady state level and it would drift over time. This was believed to be due to varying temperatures in the FP and coils, thus changing the characteristics of the system. Further investigation is to be carried out in identifying how various parts in the system affect field stability when subject to a temperature variation. This will lead to a better understanding and characterisation of the FP method.

A control system was needed to stabilise a field that was input by a user. This involved using the field size as a feedback signal to adjust the rotation of the FP rotor accordingly. A full system was successfully designed and implemented. This task included the selection of sensory equipment, hardware modules to energise such sensors and hardware modules to obtain and manipulate the signals from the sensors. Furthermore various human interaction hardware was necessary, that allowed for a visual interpretation of the system as well as the input of system variables. The hardware modules were interfaced into a central microcontroller where signals could be processed accordingly. The design phase involved iterative designs of hardware on vero board followed by a final fabrication on a series of PCBs. The completed and tested hardware was then utilised in a higher level by implementing software on the microcontroller. A PID algorithm was encapsulated in the micro controller along with other software modules to display information on a LCD and allow user interaction. The end product was a system where the user could input a field size and the control system would act accordingly and generate the desired field. The achieved stability of 30 PPM at a magnetic field of 719 mT with the developed system has reached the upper boundaries of the resolution of the sensory equipment. Future work will see the FP being implemented into a NMR system with the

required NMR sensory equipment at ones disposal and further experiments carried out into characterising the FP.

The proposed research task set by HTS-110 was carried out at IRL. The research outcome is very positive. The work in successfully implementing a FP into a purely conduction cooled HTS commercial magnet is seen to be a world first. It has identified that the FP is a viable current source that has a lot of potential for future research. IRL already applied for the patent of the FP developed by this research. The outcome of this research is significant and will further the reality of such a device being used in a commercial NMR system and other SC magnet technologies.

11 References

- AMS-02. "The Superconducting magnet." *AMS02 The alpha magnetic spectrometer Experiment*. n.d. <http://www.ams02.org/what-is-ams/tecnology/magnet/scmagnet/> (03 November 2010) (accessed November 10, 2010).
- Brown, Ward. "Brushless DC Motor Control Made Easy." *Microchip*. 2002. <http://ww1.microchip.com/downloads/en/AppNotes/00857a.pdf> (accessed October 30, 2011).
- Christian, Hoffmann, Rowan Walsh, Eva Karrer-Mueller, and Donald Pooke. "Design parameters for an HTS flux pump." *Physics Procedia 2011, yet to be published*, n.d.
- Ekin, Jack. "Temperature measurement and control." In *Experimental techniques for low-temperature measurements*, by Jack Ekin, 186-192. Oxford University Press, 2006.
- Ekin, Jack W. *Experimental techniques for low-temperature measurements*. Oxford University Press, 2006.
- FTDI. "Schematics and footprints." *FTDI*. n.d. Internet: <http://www.ftdichip.com/Support/Documents/Schematics.htm> (accessed August 2, 2011).
- Hoffman, Christian, Donald Pooke, and David Caplin. "Flux pump for HTS magnets." *IEEE Transactions on Applied Superconductivity*, Vol. 21, 2011: 1628-1631.
- Hoffmann, Christian, interview by Walsh Rowan. *Personal communication* (November 2010).
- Instruments, National. "Measuring Temperature with RTDs- A tutorial. Application note 046." *National Instruments*. November 1996. <http://newton.ex.ac.uk/teaching/CDHW/Sensors/an046.pdf> (accessed August 16, 2011).
- "Introduction to Stepper Motors." *Mechatronics*. n.d. http://mechatronics.mech.northwestern.edu/design_ref/actuators/stepper_intro.html (accessed October 2010, 2011).
- Kitchin, C, and L Counts. "A designers guide to instrumentation amplifiers, 3rd edition." *Analog*. September 2006 . http://www.analog.com/static/imported-files/design_handbooks/5812756674312778737Complete_In_Amp.pdf (accessed August 17, 2011).
- Microchip. "Precision temperature-sensing with RTD circuits, AN687." *Microchip*. n.d. <http://ww1.microchip.com/downloads/en/AppNotes/00687c.pdf> (accessed August 16, 2011).
- Nave, R. *Type I superconductors and type II superconductors*. 2010. <http://hyperphysics.phy-astr.gsu.edu/hbase/hframe.html> (accessed November 5, 2010).
- NMB. "BLDC Motor – Brushless DC Motor Introduction." *NMB*. 12 June 2010. <http://www.nmbtc.com/brushless-dc->

motors/engineering/brushless_dc_motors_engineering.html (accessed October 30, 2011).

Rohlf, James William. *Modern Physics from $\alpha\alpha$ to Z0*. Wiley, 1994.

Solarbotics. 10 July 2003. <http://www.solarbotics.net/library/pdflib/pdf/motorbas.pdf> (accessed October 30, 2010).

Stutz, Michael. "Brushless DC motor." *All about circuits*. 19 February 2000.

http://www.allaboutcircuits.com/vol_2/chpt_13/6.html (accessed October 30, 2010).

"Thermal Design." *National*. n.d.

<http://www.national.com/AU/design/courses/122/cla04/04cla04.htm> (accessed August 29, 2011).

Tinkham, Micheal. *Introduction to superconductivity*. Dover books on physics, 2004.

Van Sciver, S. "Cryogenics Engineering short course." Wellington, 4 November 2010.

Young, W C, R G Budynas, and R J Roark. *Formulas for stress and strain, Edition 7*. New York: McGraw-Hill, 1975.

12.3 Embedded software

12.3.1 LCDOUT

```
*****
'* Name : LCDOut.BAS *
'* Author : [Rowan Walsh] *
'* Notice : Copyright (c) 2010 *
'* : All Rights Reserved *
'* Date : 25/11/2010 *
'* Version : 1.0 *
'* Notes : *
'* : *
*****

'Include "bs1defs.bas"
Include "bs2defs.bas"
OSCCON = %01111100
DEFINE OSC

Define LCD_DREG PORTB 'Set LCD data port
Define LCD_DBIT 0 'Set starting data bit
Define LCD_RSREG PORTD ' Set LCD Register Select port
DEFINE LCD_RSBIT 6 'Set LCD Register Select bit
define LCD_EREG PORTD 'Set LCD Enable Port
define LCD_EBIT 7 'Set LCD Enable bit
Define LCD_BITS 4 'Set LCD Bus size (4 or 8 Bits)
Define LCD_LINES 4 'Set number of lines on LCD
DEFINE LCD_COMMANDUS 1500 'Set command delay in us
DEFINE LCD_DATUS 44 'Set data delay time in us

,

'All ports as outputs
PORTD = %00000000
PORTB = %00000000
PORTC = %00000000
TRISD = %00000000
TRISB = %00000000
TRISC = %00000000

LATB = 1
LATD = 1
INTCON2.7 = 0 'Switch pull ups on

PAuse 200

mainloop:
    LCDOUT $FE,1
    PAUSE 500 'wait for LCD to start

    LCDOUT $FE,$80,"Hello" 'Clear dsplay and show hello
    lcdout $FE,$C0,"World" 'Move to second line and show world

    Pause 2000 ' Wait .5 second
```

```
Goto mainloop      ' Do it forever
End
```

12.3.2 SPIHall code

```
*****
'* Name   : SPIhall.BAS                *
'* Author : [Rowan Walsh]              *
'* Notice : Copyright (c) 2011        *
'*       : All Rights Reserved         *
'* Date   : 8/07/2011                 *
'* Version : 1.0                      *
'* Notes  :                            *
'*       :                              *
*****
```

```
Include "bs2defs.bas"
OSCCON = %01111111
DEFINE OSC 8
```

```
' Define LCD registers and bits
Define LCD_DREG PORTD 'Set LCD data port
Define LCD_DBIT 0 'Set starting data bit
Define LCD_RSREG PORTD ' Set LCD Register Select port
DEFINE LCD_RSBIT 6 'Set LCD Register Select bit
define LCD_EREG PORTD 'Set LCD Enable Port
define LCD_EBIT 7 'Set LCD Enable bit
Define LCD_BITS 4 'Set LCD Bus size (4 or 8 Bits)
Define LCD_LINES 4 'Set number of lines on LCD
DEFINE LCD_COMMANDUS 1500 'Set command delay in us
DEFINE LCD_DATUS 44 'Set data delay time in us
```

```
'Timer 2 Set up
T2CON = %00000100 ' post scale 16, prescale 1 freq =125 kHz
```

```
SSPCON1 = %00110010
SSPSTAT = %01000000
```

```
INTCON.6=1 'Turn on nesscessary interupts
INTCON.7=1
PIE1.3=1
TRISD = %00000000
TRISB = %111110000
TRISC.3 = 0
TRISF = %11111001
TRISG = %00000000
PORTD = %00000000
```

```
SSPEN VAR SSPCON1.5 ' SSP Enable bit
CKP VAR SSPCON1.4 ' Clock Polarity Select
SMP VAR SSPSTAT.7 ' Data input sample phase
CKE VAR SSPSTAT.6 ' Clock Edge Select bit
SSPIF VAR PIR1.3 ' SPI interrupt flag
CS var PORTG.2 ' Chip select 1
CS1 var PORTF.2 ' Chip select
```

```
CS2 var PORTG.1 ' Chip select
clk var PORTG.1
```

```
DataWord VAR WORD
Offset VAR WORD
Divi var Word
Conver var word
Conver2 var word
Remainder var word
i VAR BYTE ' loop counter
a VAR byte[3] ' Holds 6 characters read from slave
Decimal var byte
h var byte
polarity var bit
conv var word[2]
temp var word[2]
Perc var word
b var word
c var word
A32bitVar var word[2]
Dummy var word
```

Asm

```
PutMulResult?D macro Din
    MOVE?BB Din, R2
    MOVE?BB Din + 1, R2 + 1
    MOVE?BB Din + 2, R0
    MOVE?BB Din + 3, R0 + 1
    RST?RP
endm
EndAsm
```

ASM

```
GetMulResult macro Dword
    MOVE?WW R2, Dword ; Low Word
    MOVE?WW R0, Dword + 2 ; High Word
endm
endasm
```

```
Pause 500 ' Wait for LCD to start up

SSPEN = 1 ' enable SPI pins
CKP = 1 ' clock idle high
CKE = 0 ' transmit on idle to active transition
SSPIF = 0 ' clear buffer full status
SMP = 0 ' sample in middle of data
LCDOUT $FE,1
high cs
high cs1
high cs2
polarity = 0
```

```

mainloop:
For h = 1 to 100
  GoSub getdata ' initiate conversion and receive data
  Gosub converter
  if h mod 5 = 0 then
    gosub LCDUpdate2 '
  endif
  Pause 50
next
GoTo mainloop ' do it forever

getdata:
  low cs2
  pause 120

  For i = 0 to 2 ' loop for 3 characters
    SSPBUF = 0 ' write to SSPBUF to start clock
    gosub letclear
    a[i] = SSPBUF ' store received character in array
  Next i ' get next character
  high CS2
  Return

letclear:
  IF SSPSTAT.0 = 0 Then letclear ' wait for SPI Buffer full status
  pauseus 50
  SSPSTAT.0 = 0 ' reset flag
  Return

Converter:
  conv[0] = a[1]
  conv[0] = (conv[0] << 8) + a[2] '(a[1] >> 1) 'shift first byte by 8 bits, add next 8 bits
  conv[1] = a[0]
@ PutMulResult?D _conv ; Load PBP internal vars - Max= 2,147,483,648
  b = div32 992 ' Divide by 992 (same as * 0.001008)
@ MOVE?WW R2, _Remainder
  Remainder = Remainder * 10000
  Remainder = div32 992
  if b >= 1057 then
    b = b - 1057 ' conversion equation X*0.001008 - 1057
    polarity = 1 'Flag used to identify field polarity
  else
    b = b - 1057 ' conversion equation X*0.001008 - 1057
    b = 65535 - b + 1
    polarity = 0
  endif
  return

LCDUpdate2:
  LCDOUT $FE, 1, #a[0]
  LCDout $FE, $C0, #a[1]

```

```

LCDout $FE, $94, #a[2]
if polarity = 1 then
    LCDout $FE, $D4, #b, ".", dec4 remainder, " mT"
else
    LCDout $FE, $D4, "-", #b, ".", dec4 remainder, " mT"
endif
Return

```

End

12.3.3 SPI-eprom code

```

*****
'* Name   : SPIeprom.pbp           *
'* Author : Rowan Walsh           *
'* Notice : Copyright (c) 2011    *
'*       : All Rights Reserved    *
'* Date   : 6/07/2011            *
'* Version : 1.0                  *
'* Notes  :                        *
'*       :                          *
*****

```

Include "bs2defs.bas"

DEFINE OSC 8

```

' Define LCD registers and bits
Define LCD_DREG PORTD 'Set LCD data port
Define LCD_DBIT 0 'Set starting data bit
Define LCD_RSREG PORTD ' Set LCD Register Select port
DEFINE LCD_RSBIT 6 'Set LCD Register Select bit
define LCD_EREG PORTD 'Set LCD Enable Port
define LCD_EBIT 7 'Set LCD Enable bit
Define LCD_BITS 4 'Set LCD Bus size (4 or 8 Bits)
Define LCD_LINES 4 'Set number of lines on LCD
DEFINE LCD_COMMANDUS 1500 'Set command delay in us
DEFINE LCD_DATUS 44 'Set data delay time in us

```

T2CON = %00000100 ' post scale 16, prescale 1 freq =125 kHz

```

SSPCON1 = %00110001
SSPSTAT = %00000000
ADCON0.0=0

```

```

TRISD = %00000000
TRISB = %11111000
TRISC.3 = 0
TRISC.4 = 1
TRISC.5 = 0
TRISF = %00000000
TRISG = %00000000

```

PORTF = %00000000

PORTD = %00000000

```
SSPEN VAR SSPCON1.5 ' SSP Enable bit
CKP VAR SSPCON1.4 ' Clock Polarity Select
SMP VAR SSPSTAT.7 ' Data input sample phase
CKE VAR SSPSTAT.6 ' Clock Edge Select bit
BF Var SSPSTAT.0 'Buffer full status bit
'SSPIF VAR PIR1.3 ' SPI interrupt flag
CS var PORTG.2 ' Chip select
CS1 var PORTF.2 ' Chip select 2
CS2 var PORTG.1 ' Chip select 3
WP var PORTG.4 ' Wirte protect
Hold var PORTG.3 ' Hold data transmission

Out Var byte 'temp variable to store value used for SSPBUF
rxData Var Byte 'temp varibale to store value from SSPBUF
Status1 var byte
DataWord VAR WORD
Offset VAR WORD
Divi var Word
Conver var word
Conver2 var word
DataTable1 CON EXT
DataTable2 CON EXT
DataTable3 CON EXT

i VAR BYTE ' loop counter
j var byte
adrs var byte
value var byte
a VAR BYTE[3] ' Holds 6 characters read from slave
temp var word
Perc var word
b var word
c var word

Pause 100 ' Wait for LCD to start up

' TRISC = 0 ' set PORTC I/O
SSPEN = 1 ' enable SPI pins
CKP = 1 ' clock idle high
CKE = 0 ' transmit on idle to active transition
'SSPIF = 0 ' clear buffer full status
SMP = 0 ' sample in middle of data

cs = 1 'disable SPI 1
cs2 = 1 'disable SPI 2
'low CS1 'Enable SPI 2
WP = 1 'Allow writing to EEPROM
hold = 1 'Dont suspend transmission

low portf.7
high portf.6

LCDOUT $FE,1
LCDOUT $FE,1, "starting"
```

pause 200

mainloop:

gосub writedata

GoTo mainloop ' do it forever

WriteData:

```
'Send the write enable sequence (WREN)
CS1 = 0      ' Enable serial EEPROM
out = 6      ' load write enable sequence
gосub Outputdata
CS1 = 1      ' Disable serial EEPROM
'Send the write status register sequence (WRSR)
CS1 = 0      ' Enable serial EEPROM
out = 1      ' load write status
gосub Outputdata
out= 0
gосub outputdata
CS1 = 1      ' Disable serial EEPROM
;Wait the required 5mS for the write cycle timer Twc
pause 5
;Send the write enable sequence (WREN)
CS1 = 0      ' Enable serial EEPROM
out = 6      ' load WREN sequence
gосub Outputdata
CS1 = 1      ' Disable serial EEPROM
;Send the read status register sequence (RDSR)
CS1 = 0      ' Enable serial EEPROM
out = 5      ' load RDSR sequence
gосub Outputdata
CS1 = 1      ' Disable serial EEPROM
;Send the write sequence (WRITE)
CS1 = 0      ' Enable serial EEPROM
out = 2      ' load write sequence
gосub Outputdata
out = 0      'Load high adress byte
gосub outputData
'
Out = 55     'Load address location (low byte)
gосub outputData
Out = 29     'Load actual storage variable
gосub outputData
CS1 = 1      ' Disable serial EEPROM
;Perform data polling (RDSR bit 0)
'For i = 0 to 16 'allow time to set WIP to true
'next
gосub polling

;Send read sequence (READ), read address 0x55
Cs1=0
out = 3      'load read sequence
gосub outputdata
out = 0      'load high adress part
```

```

gosub outputdata
out = 55      'load low adress part
gosub outputdata
out = 0       'call output to read 1 byte
gosub outputdata
cs1=1
gosub lcdUpdate2
;Send the write enable sequence (WREN)
CS1 = 0      ' Enable serial EEPROM
out = 6      ' load WREN sequence
gosub Outputdata
CS1 = 1      ' Disable serial EEPROM
;Send the read status register sequence (RDSR)
CS1 = 0      ' Enable serial EEPROM
out = 5      ' load RDSR sequence
gosub Outputdata
out = 0      'call output to read 1 byte
gosub outputData
CS1 = 1
;Send the write disable sequence (WRDI)
CS1 = 0      ' Enable serial EEPROM
out = 4      ' load WRDI sequence
gosub Outputdata
CS1 = 1
;Send the read status register sequence (RDSR)
CS1 = 0      ' Enable serial EEPROM
out = 5      ' load RDSR sequence
gosub Outputdata
out = 0
gosub outputdata
cs1=1

```

Return

OutputData:

```

SSPBUF = out  'Write value to SSPBUF register
Gosub letclear
rxData = SSPBUF  'Write value of SSPBUF register to rxData varaible
Return

```

Polling:

```

Cs1 = 0
gosub outputData
out = 0
gosub outputData
cs1 = 1
status1 = rxData
IF rxData > 0 Then Polling ' wait for SPI Buffer full status

```

```

CS1 = 1
LCDOUT $FE, 1, "found"
pause 10

```

Return

getdata:

```

    low cs1
    pause 30
    SSPBUF = 5
    gosub letclear
    'CS1 = 1
    'CS1 = 0
    SSPBUF = 1
    gosub letclear
    For i = 0 to 2 ' loop for 3 characters
        'SSPBUF = 0 ' write to SSPBUF to start clock

        a[i] = SSPBUF ' store received character in array
        gosub letclear

    Next i ' get next character

    high CS1

Return

letclear:
IF SSPSTAT.0 = 0 Then letclear ' wait for SPI Buffer full status
pauseus 25
SSPSTAT.0 = 0 ' reset flag
Return

LCDUpdate2:
    LCDOUT $FE, 1, #rxData
    LCDout $FE, $C0, #Status1
    'LCDout $FE, $94, #a[1]
    pause 50
    Return

End

```

12.3.4 Control code

```

*****
'* Name   : Control-v2.1.BAS                *
'* Author : Rowan Walsh                      *
'* Notice : Copyright (c) 2011 Industrial research Ltd *
'*       : All Rights Reserved                *
'* Date   : 29/08/2011                       *
'* Version : 1.0                             *
'* Notes  :                                  *
'*       :                                    *
*****

Include "bs2defs.bas"

OSCCON = %01110111 '8 MHz clock source
OSCCON2 = %01000010
DEFINE OSC 16

```

```

' Define LCD registers and bits
Define LCD_DREG PORTD      'Set LCD data port
Define LCD_DBIT 0          'Set starting data bit
Define LCD_RSREG PORTH     'Set LCD Register Select port
DEFINE LCD_RSBIT 1         'Set LCD Register Select bit
define LCD_EREG PORTE     'Set LCD Enable Port
define LCD_EBIT 2          'Set LCD Enable bit
Define LCD_BITS 4          'Set LCD Bus size (4 or 8 Bits)
Define LCD_LINES 4         'Set number of lines on LCD
DEFINE LCD_COMMANDUS 1500 'Set command delay in us
DEFINE LCD_DATUS 44        'Set data delay time in us

;PWM defines
DEFINE CCP4_REG PORTG      'Hpwm 1 pin port
DEFINE CCP4_BIT 3          'Hpwm 1 pin bit
DEFINE HPWM1_TIMER 2       'Hpwm 1 timer 2 select

;ADC defines
DEFINE ADC_BITS 12         'ADC set at 10 bits
DEFINE ADC_CLOCK 5         ' Set clock source to Frc/32
DEFINE ADC_SAMPLEUS 10     'set the number of microseconds the program waits between
setting the ADC channel and taking a reading

PIR1 = $00                ' clear interrupt flags

SSP1CON1 = %00110010      'Enable SPI1, high level for clock idle state, Fosc/64
SSP1STAT = %01000000      'Input data sample in middle, Transmit occurs from active to idle
clock state

ANCON2 = %00000000

INTCON = %11010000        'Turn on all unmasked, Peripheral, INTOIE
INTCON2 = %11111000       'Interrupt on rising edges
INTCON3 = %00111000       'Enable external interrupts 3, 2, 1
PIE1 = %00001000         'Enable SSP1E
'PIE2 = %00100000         'Enable SSP2E

ADCON1 = %11110000        'internal VREF+ 4.096V
ADCON2 = %10010101        'right justified, 4 TAD, FOSC/16

RCSTA2.7 = 0
TXSTA2.5 = 0
CM3CON.7 = 0

T2CON = %00000100        'Timer2 is on, prescaler = 0
CCP4CON = %01111100      ' Set CCP4 to PWM
CCPTMRS1 = %00000000     'CCP4 is based on TMR1/TMR2

SSPEN VAR SSP1CON1.5     ' SSP Enable bit
CKP VAR SSP1CON1.4       ' Clock Polarity Select
SMP VAR SSP1STAT.7       ' Data input sample phase
CKE VAR SSP1STAT.6       ' Clock Edge Select bit
SSPIF VAR PIR1.3         ' SPI interrupt flag
CSH var PORTF.7          ' Chip select Hall sensor

```

```

CS0  var PORTF.6  ' Chip select Temp 1
CS1  var PORTF.5  ' Chip select Temp 2
CS2  var PORTF.4  ' Chip select Temp 3
CS3  var PORTF.3  ' Chip select EEPROM

INT0 var INTCON.1  'External Interupt 0
INT1 var INTCON3.0 'External Interupt 1
INT2 Var INTCON3.1 'External Interupt 2
INT3 Var INTCON3.2 'External Interupt 3

TRISA = %11000011
TRISB = %00001111
TRISC = %10010011
TRISD = %00000000
TRISE = %00000000
TRISF = %00000000
TRISG = %00000000
TRISH = %00000000
TRISJ = %00000000

DataWord  VAR WORD
Offset    VAR WORD
Divi      var Word
Conver    var word
Conver2   var word
Remainder var word
Remainder2 var word
b         var word
bb        var word
bLCD      var word
c         var word
Perc      var word
Dummy     var word
temp      var word[2]
A32bitVar var word[2]
conv      var word[2]  ' Holds 6 characters read from slave

j var byte
ac var word
Decimal var byte
a VAR byte[3]
polarity var bit

convH var conv(1)
convL var conv(0)

AdcVar    VAR WORD 'variable for ADC value
Frequency var Word 'PWM frequency
Divide    var word
speed     var WORD 'Actual speed (Hz)
Duty      VAR Byte 'PWM Duty cycle
Dir       Var PortG.2
oldDir    var bit
newDir    var bit
Enab      var Porth.3
RST       var PortG.1

```

```

SLP    var PortH.2
Out    var PortJ.1
RW     var portH.0
Freq   var bit
Sett   Var Bit
sr     var word
sr2    var word
sr3    var word
h      var byte
polSetP var bit
SetP   var word
SetPLCD Var Word
Error  var word
Actual var word
Kp     var word
Ki     Var Word
Kd     Var word
Kpbase var word
Integral var word
IntThresh var word
P      var word
I      var word
D      Var word

Direction var word
oldFreq  Var word
diff     var word
prevError var word

```

```

low Dir
low Enab
high RST
high SLP
low RW

```

```

freq = 1
sett = 0
duty = 250 ' Set duty cycle to 50%
Frequency = 0

```

Asm

```

PutMulResult?D macro Din
    MOVE?BB Din, R2
    MOVE?BB Din + 1, R2 + 1
    MOVE?BB Din + 2, R0
    MOVE?BB Din + 3, R0 + 1
    RST?RP
endm
EndAsm

```

ASM

```

GetMulResult macro Dword
    MOVE?WW R2, Dword ; Low Word
    MOVE?WW R0, Dword + 2 ; High Word
endm

```

endasm

```
Pause 200      ' Wait for LCD to start up

SSPEN = 1     ' enable SPI pins
CKP = 1       ' clock idle high
CKE = 0       ' transmit on idle to active transition
SSPIF = 0     ' clear buffer full status
SMP = 0       ' sample in middle of data
                LCDOUT $FE,1
                LCDOUT $FE,1, "Bottle Inc"
```

```
high CSH
high CS0
high CS1
high CS2
high CS3
polarity = 0
```

```
Kpbase = 100
Ki = 1
kd = 2
IntThresh = 90
Integral = 0
Setp = 62500
```

```
on interrupt goto inthand
```

```
mainloop:
```

```
for h = 1 to 90
  GoSub getdata      ' initiate conversion and receive data
  Gosub converter
  if sett = 0 then
    ADCIN 0, adcVar
    pause 10
    if adcvar < 615 then
      Frequency = adcVar * 8 'change resolution for 0 - 1.5Hz range
    else
      Frequency = AdcVar * 8 'Scale for speed range, 0 - 10Hz ouput speed
    endif
    if adcVar <= 75 then
      HPwm 4,0,0
      high enab
      if freq = 1 then
        HIGH dIR
      ELSE
        LOW dIR
      ENDIF
```

```

Else
  low enab

  HPwm 4,Duty,frequency

endif
else

  Gosub AutoPID
endif

if h mod 3 = 0 then
  gosub LCDupdate
endif

toggle Out
next
GoTo mainloop ' do it forever

AutoPID:
oldDir = Dir
oldFreq = Frequency
Actual = bb
Error = Setp - Actual 'Calculate current Error
Kp = Kpbase min (32767/ABS(Error)) ' limit Kp to max of 32767/Error
if (abs(Error) < IntThresh) then 'Prevent integral windup
  I = I + (Error * KI) 'accumulate the error integral
else
  I = 0 ' Zero if out of range
endif
P = Error * Kp 'Proportional value
D = (Error-PrevError) * Kd 'derivative value
Frequency = P + I + D 'Sum terms for ouptut frequency
if frequency.15 = 1 then 'check polarity of frequency
  newdir = 1
else
  newdir = 0
endif
Frequency = ABS(Frequency)
Frequency = Frequency min 32000 'Limit speed
If (abs(oldFreq - Frequency) >= 600) or (oldDir <> newDir) then
  gosub Accel
endif
Frequency = Frequency max 980 ' lower limit speed
If Frequency <= 980 then
  HPWM 4, Duty, 0
else
  HPwm 4,Duty,frequency
endif
prevError = Error
Return

getdata:
  low CSH

```

```

pause 80

For j = 0 to 2 ' loop for 3 characters
  SSP1BUF = 0 ' write to SSPBUF to start clock
  gosub letclear
  a[j] = SSP1BUF ' store received character in array
Next j ' get next character
  high CSH
Return

letclear:
  IF SSP1STAT.0 = 0 Then letclear ' wait for SPI Buffer full status
  pauseus 25
  SSP1STAT.0 = 0 ' reset flag
Return

Converter:
  conv[0] = a[1]
  conv[0] = (conv[0] << 8) + a[2] '(a[1] >> 1) ' shift first byte by 8 bits, add next 8 bits
  conv[1] = a[0]
@ PutMulResult?D _conv ; Load PBP internal vars - Max= 2,147,483,648
'b = div32 992 ' Divide by 992 (same as * 0.001008)
Diasble 'So interrupt does not overwitre data
b = div32 32
bb = b ' 16bit variable for microcontroller to use
b = b * 100 'variable for human interface
b = div32 3857
Remainder = R2 * 1000
Remainder = div32 3857
if b >= 850 then
  b = b - 850
  polarity = 1 'Flag used to identify field polarity
else
  polarity = 0
endif
ENABLE
Return

LCDUpdate:
  Divde = 10000

  'Determine actual speed
  speed = frequency / Divde
  sr = Frequency // Divde
  sr = sr * 1000
  sr = div32 Divde

  lcdout $FE, 1
  LCDout $FE, $80 + 1, "Freq= ", #Frequency, " Hz", #abs(Error)

  If dir = 1 then
    LCDOut $FE, $C0 +1, "Speed= ", "+", #speed, ".", dec3 sr, " Hz"
  Else
    LCDOut $FE, $C0 +1, "Speed= ", "-", #speed, ".", dec3 sr, " Hz"
  endif

  If sett = 1 then

```

```

        LCDout $FE, $94 + 1, "SP= ", #SetP, " mT"
    else
        LCDout $FE, $94 + 1, "Manual mode", #bb
    endif

    if polarity = 0 then
        LCDout $FE, $D4 + 1, "Field= ", "-", #b, ".", dec3 Remainder, " mT"
    else
        LCDout $FE, $D4 + 1, "Field= ", "+", #b, ".", dec3 Remainder, " mT" "" , #abs(Error)
    endif

Pause 10      ' Delay for time to read the display

Return

Accel:
    diff = abs(Frequency - oldFreq)      'Difference in speed
    if oldDir <> newDir then              ' If new speed is - then ramp down first

        for ac = oldFreq to 0 step - 200

            HPwm 4,Duty,ac
            pause 10
        next

        toggle Dir
        pause 10

        for ac = 0 to Frequency step 200          'ramp up to new speed

            HPwm 4,Duty,ac
            pause 10
        next

    else
        for ac = 0 to diff step 200

            Frequency = oldFreq + ac
            Frequency = frequency min 32000
            Frequency = frequency max 980
            HPwm 4,Duty,Frequency
            pause 10
        next
    endif
return

DISABLE
    inthand:      'Interut handler routines
    if INTO = 1 then
        toggle freq
        pause 5
        INTO = 0
    endif
    if INT1 = 1 then

```

```
Toggle Setp
  pause 5
  INT1 = 0
ENDIF

if INT2 = 1 then
  Setp = Setp + 100
  INT2 = 0
  pause 5
endif

if INT3 = 1 then
  Setp = Setp - 100
  INT3 = 0
Endif

RESUME
ENABLE
```

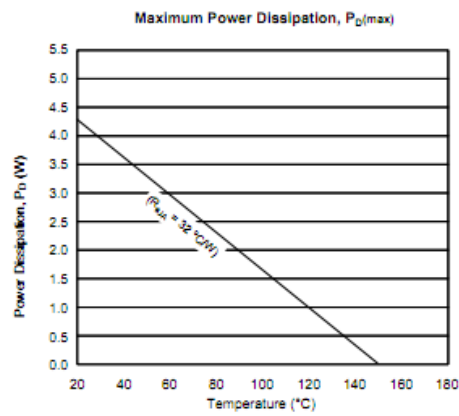
12.4 Data sheets

Data sheets that are bigger than two pages will only have the cover paper of the data sheet included in this section and the title will be marked with an astrix (*). For the full data sheet, it can be either accessed from the URL stated or from the accompanying CD.

THERMAL CHARACTERISTICS may require derating at maximum conditions

Characteristic	Symbol	Test Conditions*	Value	Units
Package Thermal Resistance	$R_{\theta JA}$	Package ET; 4-layer PCB, based on JEDEC standard	32	°C/W

*In still air. Additional thermal information available on Allegro Web site.



Allegro Microsystems, Inc.
115 Northeast Cutoff, Box 15038
Worcester, Massachusetts 01615-0038 (508) 853-6000
www.allegromicro.com

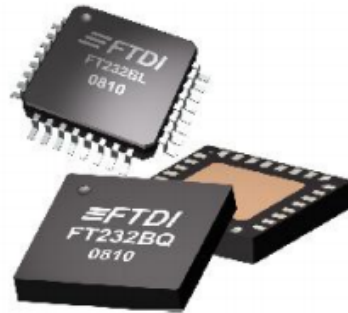
12.4.3 FT232BL USB UART IC *

http://www.ftdichip.com/Support/Documents/DataSheets/ICs/DS_FT232BL_BQ.pdf



Document No.: FT_000329
FT232BL/BQ USB UART IC Datasheet Version 2.1
Clearance No.: FTDI# 171

Future Technology Devices International Ltd. FT232BL/BQ USB UART IC



The FT232B is a USB to serial UART interface with the following advanced features:

- Single Chip USB to Asynchronous Serial Data Transfer
- Full Handshaking & Modem Interface Signals
- UART I/F Supports 7 / 8 Bit Data, 1 / 2 Stop Bits and Odd/Even/Mark/Space/No Parity
- Data rate 300 => 3M Baud (TTL)
- Data rate 300 => 1M Baud (RS232)
- Data rate 300 => 3M Baud (RS422/RS485)
- 384 Byte Receive Buffer / 128 Byte Transmit Buffer for high data throughput
- Adjustable RX buffer timeout
- Fully Assisted Hardware or X-On / X-Off Handshaking In-built support for event characters and line break condition
- Auto Transmit Buffer control for RS485
- Support for USB Suspend / Resume through SLEEP# and RI# pins
- 4.35V to 5.25V single supply operation
- Support for high power USB Bus powered devices through PWREN# pin
- Integrated level converter on UART and control signals for interfacing to 5V and 3.3V logic
- Integrated 3.3V regulator for USB IO
- Integrated Power-On-Reset circuit
- Integrated 6MHz - 48Mhz clock multiplier PLL
- UHCI / OHCI / EHCI host controller compatible
- USB 1.1 and USB 2.0 compatible
- USB VID, PID, Serial Number and Product Description strings in external EEPROM
- EEPROM programmable on-board via USB
- Available as a compact lead free RoHS compliant 32-LD LQFP package (FT232BL) or 32-LD QFN package (FT232BQ).

Neither the whole nor any part of the information contained in, or the product described in this manual, may be adapted or reproduced in any material or electronic form without the prior written consent of the copyright holder. This product and its documentation are supplied on an as-is basis and no warranty as to their suitability for any particular purpose is either made or implied. Future Technology Devices International Ltd will not accept any claim for damages howsoever arising as a result of use or failure of this product. Your statutory rights are not affected. This product or any variant of it is not intended for use in any medical appliance, device or system in which the failure of the product might reasonably be expected to result in personal injury. This document provides preliminary information that may be subject to change without notice. No freedom to use patents or other intellectual property rights is implied by the publication of this document. Future Technology Devices International Ltd, Unit 1, 2 Seaward Place, Centurion Business Park, Glasgow G41 1HH United Kingdom. Scotland Registered Company Number: SC136640

12.4.4 Arepoc HHP_NP 768 Hall probe

ELECTRICAL SPECIFICATIONS OF THE HALL PROBE

HIGH LINEARITY HALL PROBE FOR ROOM AND CRYOGENIC TEMPERATURES

TYPE:	HHP-NP	PRODUCT NUMBER:	768
-------	---------------	-----------------	------------

PARAMETER	UNIT	300 K	77 K	4.2 K
Nominal control current, I_n	mA	20	20	20
Maximum control current	mA	22	30	30
Sensitivity at I_n	mV/T	180.9		
Offset voltage at I_n	μ V	< 30	< 180	
Input resistance	Ω	6.5	5.8	
Output resistance	Ω	23	20	
Linearity error up to 1 T	%	< 0.2		
Change of sensitivity due to reversing of the magnetic field	%	< 1		

Active area dimensions [mm]: 0.5 x 0.1

Overall dimensions [mm]: 5 x 7 x 1

COLOR CODE:

Control current leads: green, black

Hall leads: orange, red

AREPOC s.r.o., Iljušinova 4, 851 01 Bratislava, SLOVAKIA

FAX: +421 2 6382 4613 E-mail: kopera@arepoc.sk

<http://www.arepoc.sk>

12.4.5 AD620 instrumentation amplifier *

<http://docs-asia.electrocomponents.com/webdocs/077f/0900766b8077fed8.pdf>



Low Cost, Low Power Instrumentation Amplifier

AD620

FEATURES

EASY TO USE

Gain Set with One External Resistor
(Gain Range 1 to 1000)

Wide Power Supply Range (± 2.3 V to ± 18 V)
Higher Performance than Three Op Amp IA Designs
Available in 8-Lead DIP and SOIC Packaging
Low Power, 1.3 mA max Supply Current

EXCELLENT DC PERFORMANCE ("B GRADE")

50 μ V max, Input Offset Voltage
0.6 μ V/ $^{\circ}$ C max, Input Offset Drift
1.0 nA max, Input Bias Current
100 dB min Common-Mode Rejection Ratio ($G = 10$)

LOW NOISE

9 nV/ $\sqrt{\text{Hz}}$, @ 1 kHz, Input Voltage Noise
0.28 μ V p-p Noise (0.1 Hz to 10 Hz)

EXCELLENT AC SPECIFICATIONS

120 kHz Bandwidth ($G = 100$)
15 μ s Settling Time to 0.01%

APPLICATIONS

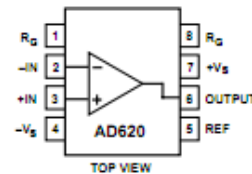
Weigh Scales
ECG and Medical Instrumentation
Transducer Interface
Data Acquisition Systems
Industrial Process Controls
Battery Powered and Portable Equipment

PRODUCT DESCRIPTION

The AD620 is a low cost, high accuracy instrumentation amplifier that requires only one external resistor to set gains of 1 to

CONNECTION DIAGRAM

8-Lead Plastic Mini-DIP (N), Cerdip (Q)
and SOIC (R) Packages



1000. Furthermore, the AD620 features 8-lead SOIC and DIP packaging that is smaller than discrete designs, and offers lower power (only 1.3 mA max supply current), making it a good fit for battery powered, portable (or remote) applications.

The AD620, with its high accuracy of 40 ppm maximum nonlinearity, low offset voltage of 50 μ V max and offset drift of 0.6 μ V/ $^{\circ}$ C max, is ideal for use in precision data acquisition systems, such as weigh scales and transducer interfaces. Furthermore, the low noise, low input bias current, and low power of the AD620 make it well suited for medical applications such as ECG and noninvasive blood pressure monitors.

The low input bias current of 1.0 nA max is made possible with the use of SuperBeta processing in the input stage. The AD620 works well as a preamplifier due to its low input voltage noise of 9 nV/ $\sqrt{\text{Hz}}$ at 1 kHz, 0.28 μ V p-p in the 0.1 Hz to 10 Hz band, 0.1 pA/ $\sqrt{\text{Hz}}$ input current noise. Also, the AD620 is well suited for multiplexed applications with its settling time of 15 μ s to 0.01% and its cost is low enough to enable designs with one in-amp per channel.

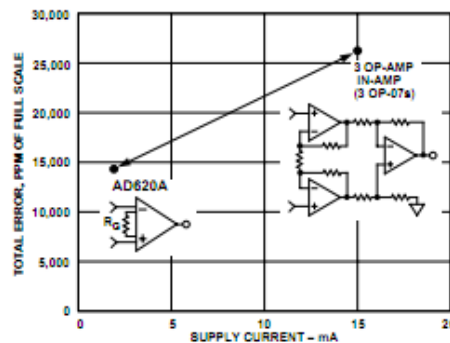


Figure 1. Three Op Amp IA Designs vs. AD620

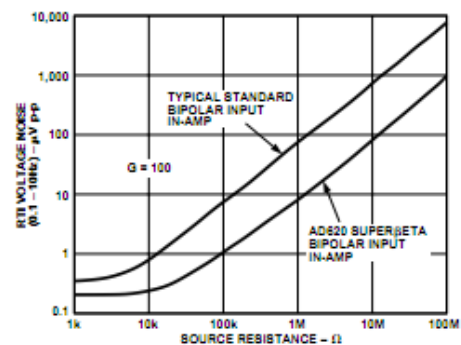


Figure 2. Total Voltage Noise vs. Source Resistance

REV. E

Information furnished by Analog Devices is believed to be accurate and reliable. However, no responsibility is assumed by Analog Devices for its use, nor for any infringements of patents or other rights of third parties which may result from its use. No license is granted by implication or otherwise under any patent or patent rights of Analog Devices.

One Technology Way, P.O. Box 9106, Norwood, MA 02062-9106, U.S.A.
Tel: 781/329-4700 World Wide Web Site: <http://www.analog.com>
Fax: 781/326-8703 © Analog Devices, Inc., 1999

12.4.6 AD623 instrumentation amplifier *

<http://docs-asia.electrocomponents.com/webdocs/0ddf/0900766b80ddf94b.pdf>



Single Supply, Rail-to-Rail, Low Cost Instrumentation Amplifier

AD623

FEATURES

Easy to Use
 Higher Performance than Discrete Design
 Single and Dual Supply Operation
 Rail-to-Rail Output Swing
 Input Voltage Range Extends 150 mV Below Ground (Single Supply)
 Low Power, 575 μ A Max Supply Current
 Gain Set with One External Resistor
 Gain Range 1 (No Resistor) to 1,000

HIGH ACCURACY DC PERFORMANCE

0.1% Gain Accuracy ($G = 1$)
 0.35% Gain Accuracy ($G > 1$)
 25 ppm Gain Drift ($G = 1$)
 200 μ V Max Input Offset Voltage (AD623A)
 2 μ V/ $^{\circ}$ C Max Input Offset Drift (AD623A)
 100 μ V Max Input Offset Voltage (AD623B)
 1 μ V/ $^{\circ}$ C Max Input Offset Drift (AD623B)
 25 nA Max Input Bias Current

NOISE

35 nV/ $\sqrt{\text{Hz}}$ RTI Noise @ 1 kHz ($G = 1$)

EXCELLENT AC SPECIFICATIONS

90 dB Min CMRR ($G = 10$); 84 dB Min CMRR ($G = 5$)
 (@ 60 Hz, 1K Source Imbalance)
 800 kHz Bandwidth ($G = 1$)
 20 μ s Settling Time to 0.01% ($G = 10$)

APPLICATIONS

Low Power Medical Instrumentation
 Transducer Interface
 Thermocouple Amplifier
 Industrial Process Controls
 Difference Amplifier
 Low Power Data Acquisition

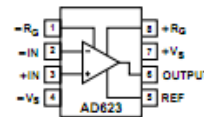
PRODUCT DESCRIPTION

The AD623 is an integrated single supply instrumentation amplifier that delivers rail-to-rail output swing on a single supply (+3 V to +12 V supplies). The AD623 offers superior user flexibility by allowing single gain set resistor programming, and conforming to the 8-lead industry standard pinout configuration. With no external resistor, the AD623 is configured for unity gain ($G = 1$) and with an external resistor, the AD623 can be programmed for gains up to 1,000.

The AD623 holds errors to a minimum by providing superior AC CMRR that increases with increasing gain. Line noise, as well as line harmonics, will be rejected since the CMRR remains constant up to 200 Hz. The AD623 has a wide input

CONNECTION DIAGRAM

8-Lead Plastic DIP (N),
 SOIC (R) and μ SOIC (RM) Packages



common-mode range and can amplify signals that have a common-mode voltage 150 mV below ground. Although the design of the AD623 has been optimized to operate from a single supply, the AD623 still provides superior performance when operated from a dual voltage supply (± 2.5 V to ± 6.0 V).

Low power consumption (1.5 mW at 3 V), wide supply voltage range, and rail-to-rail output swing make the AD623 ideal for battery powered applications. The rail-to-rail output stage maximizes the dynamic range when operating from low supply voltages. The AD623 replaces discrete instrumentation amplifier designs and offers superior linearity, temperature stability and reliability in a minimum of space. Until the AD623, this level of instrumentation amplifier performance has not been achieved.

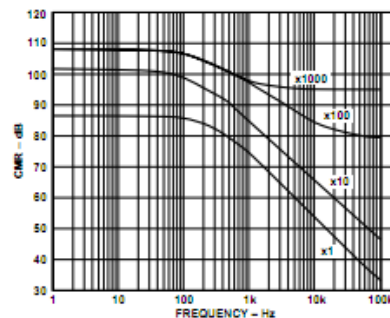


Figure 1. CMRR vs. Frequency, +5 V_S , 0 V_S

REV. C

Information furnished by Analog Devices is believed to be accurate and reliable. However, no responsibility is assumed by Analog Devices for its use, nor for any infringements of patents or other rights of third parties which may result from its use. No license is granted by implication or otherwise under any patent or patent rights of Analog Devices.

One Technology Way, P.O. Box 9108, Norwood, MA 02062-9108, U.S.A.
 Tel: 781/329-4700 World Wide Web Site: <http://www.analog.com>
 Fax: 781/326-8703 © Analog Devices, Inc., 1999

12.4.7 MCP3550 single - channel 22 - bit delta - sigma ADC *

<http://docs-asia.electrocomponents.com/webdocs/0d2a/0900766b80d2a9fe.pdf>



MCP3550/1/3

Low-Power, Single-Channel 22-Bit Delta-Sigma ADCs

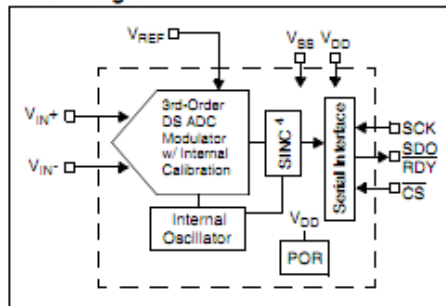
Features

- 22-bit ADC in Small 8-pin MSOP Package with Automatic Internal Offset and Gain Calibration
- Low-Output Noise of $2.5 \mu\text{V}_{\text{RMS}}$ with Effective Resolution of 21.9 bits (MCP3550/1)
- $3 \mu\text{V}$ Typical Offset Error
- 2 ppm Typical Full-Scale Error
- 6 ppm Maximum INL Error
- Total Unadjusted Error Less Than 10 ppm
- No Digital Filter Settling Time, Single-Command Conversions through 3-wire SPI Interface
- Ultra-Low Conversion Current (MCP3550/1):
 - $100 \mu\text{A}$ typical ($V_{\text{DD}} = 2.7\text{V}$)
 - $120 \mu\text{A}$ typical ($V_{\text{DD}} = 5.0\text{V}$)
- Differential Input with V_{SS} to V_{DD} Common Mode Range
- 2.7V to 5.5V Single-Supply Operation
- Extended Temperature Range:
 - -40°C to $+125^{\circ}\text{C}$

Applications

- Weigh Scales
- Direct Temperature Measurement
- 6-digit DVMs
- Instrumentation
- Data Acquisition
- Strain Gauge Measurement

Block Diagram



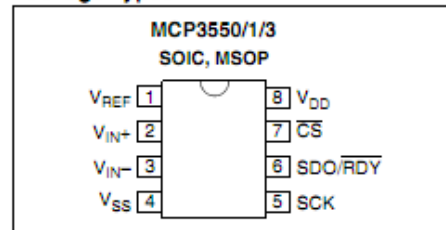
Description

The Microchip Technology Inc. MCP3550/1/3 devices are 2.7V to 5.5V low-power, 22-bit Delta-Sigma Analog-to-Digital Converters (ADCs). The devices offer output noise as low as $2.5 \mu\text{V}_{\text{RMS}}$ with a total unadjusted error of 10 ppm. The family exhibits 6 ppm Integral Non-Linearity (INL) error, $3 \mu\text{V}$ offset error and less than 2 ppm full-scale error. The MCP3550/1/3 devices provide high accuracy and low noise performance for applications where sensor measurements (such as pressure, temperature and humidity) are performed. With the internal oscillator and high oversampling rate, minimal external components are required for high-accuracy applications.

This product line has fully differential analog inputs, making it compatible with a wide variety of sensor, industrial control or process control applications.

The MCP3550/1/3 devices operate from -40°C to $+125^{\circ}\text{C}$ and are available in the space-saving 8-pin MSOP and SOIC packages.

Package Types:



Device Selection Table

Part Number	Sample Rate	Effective Resolution	50/60 Hz Rejection
MCP3550-50	12.5 sps	21.9 bits	50 Hz
MCP3550-60	15 sps	21.9 bits	60 Hz
MCP3551	13.75 sps	21.9 bits	50/60 Hz (simultaneous)
MCP3553	60 sps	20.6 bits	N/A

12.4.8 25LC1024 1 Mbit SPI Bus Serial EEPROM *

<http://docs-asia.electrocomponents.com/webdocs/0b04/0900766b80b04b70.pdf>



25LC1024

1 Mbit SPI Bus Serial EEPROM

Device Selection Table

Part Number	Vcc Range	Page Size	Temp. Ranges	Packages
25LC1024	2.5-5.5V	256 Byte	I, E	P, SM, MF

Features:

- 20 MHz max. Clock Speed
- Byte and Page-level Write Operations:
 - 256 byte page
 - 6 ms max. write cycle time
 - No page or sector erase required
- Low-Power CMOS Technology:
 - Max. Write current: 5 mA at 5.5V, 20 MHz
 - Read current: 7 mA at 5.5V, 20 MHz
 - Standby current: 1µA at 2.5V (Deep power-down)
- Electronic Signature for Device ID
- Self-Timed Erase and Write Cycles:
 - Page Erase (6 ms max.)
 - Sector Erase (10 ms max.)
 - Chip Erase (10 ms max.)
- Sector Write Protection (32K byte/sector):
 - Protect none, 1/4, 1/2 or all of array
- Built-In Write Protection:
 - Power-on/off data protection circuitry
 - Write enable latch
 - Write-protect pin
- High Reliability:
 - Endurance: 1M erase/write cycles
 - Data Retention: >200 years
 - ESD Protection: >4000V
- Temperature Ranges Supported:
 - Industrial (I): -40°C to +85°C
 - Automotive (E): -40°C to +125°C
- Pb-free and RoHS Compliant

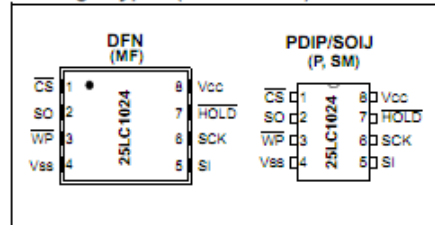
Description:

The Microchip Technology Inc. 25LC1024 is a 1024 Kbit serial EEPROM memory with byte-level and page-level serial EEPROM functions. It also features Page, Sector and Chip erase functions typically associated with Flash-based products. These functions are not required for byte or page write operations. The memory is accessed via a simple Serial Peripheral Interface (SPI) compatible serial bus. The bus signals required are a clock input (SCK) plus separate data in (SI) and data out (SO) lines. Access to the device is controlled by a Chip Select (CS) input.

Communication to the device can be paused via the hold pin (HOLD). While the device is paused, transitions on its inputs will be ignored, with the exception of Chip Select, allowing the host to service higher priority interrupts.

The 25LC1024 is available in standard packages including 8-lead PDIP and SOIJ, and advanced 8-lead DFN package. All devices are Pb-free.

Package Types (not to scale)



Pin Function Table

Name	Function
CS	Chip Select Input
SO	Serial Data Output
WP	Write-Protect
Vss	Ground
SI	Serial Data Input
SCK	Serial Clock Input
HOLD	Hold Input
Vcc	Supply Voltage

12.4.9 M542 Economical microstepping driver *

http://www.oceancontrols.com.au/datasheet/lea/smc003_M542_manual.pdf

User's Manual
For
M542

Economical Microstepping Driver

Version 1.0

©2000 All Rights Reserved

Attention: Please read this manual carefully before using the driver!



Leadshine Technology Co., Ltd.

F/3, Block 2, Nanyou Tianan Industry Park, Nanshan Dist, Shenzhen, China

PH. (86)755-26434369 FAX (86)755-26402718

Web site: www.leadshine.com E-Mail: sales@leadshine.com

12.4.10 1.8° size 42mm high torque hybrid stepping motor

MOT-120 FL42STH38-1684B Stepper Motor Specifications

1.8° Size 42mm High Torque Hybrid Stepping Motor

● General Specification for High Torque Hybrid Stepping Motor

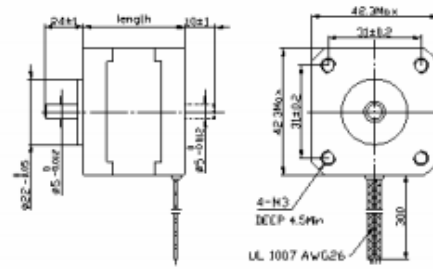
Item	Specifications
Step Angle	1.8
Step Angle Accuracy	± 5% (full step, no load)
Resistance Accuracy	± 10%
Inductance Accuracy	± 20%
Temperature Rise	80°C Max. (rated current, 2 phase on)
Ambient Temperature	-20°C~+50°C
Insulation Resistance	100M Ω Min., 500VDC
Dielectric Strength	500VAC for one minute
Shaft Radial Play	0.02Max. (450 g-load)
Shaft Axial Play	0.08Max. (450 g-load)
Max. radial force	28N (20mm from the flange)
Max. axial force	10N



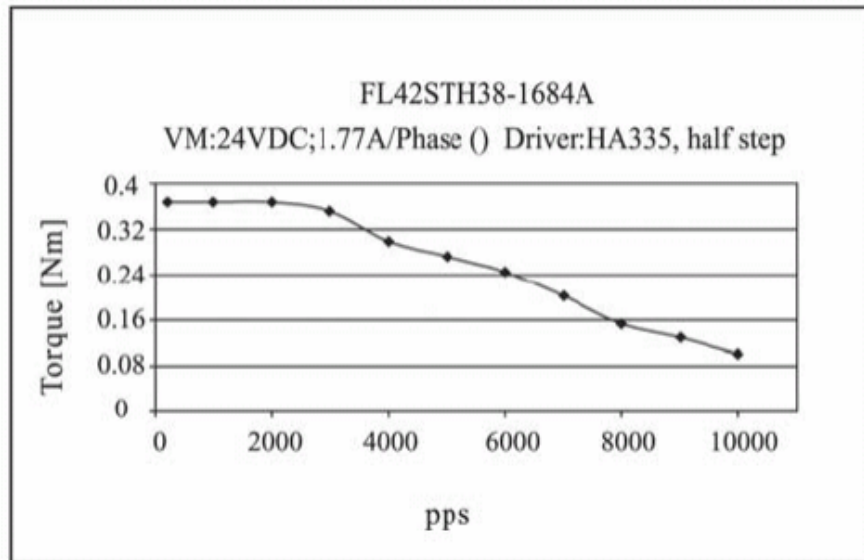
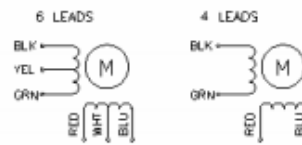
● Size 42mm High Torque Hybrid Stepping Motor Specifications

Model No.		Rated Voltage	Current /Phase	Resistance /Phase	Inductance /Phase	Holding Torque	# of Leads	Rotor Inertia	Weight	Detent Torque	Length
Single Shaft	Double Shaft	V	A	Ω	mH	Kg-cm		g-cm ²	kg	g-cm	mm
FL42STH25-0404A	FL42STH25-0404B	9.6	0.4	24	36	1.7	4	20	0.15	75	25
FL42STH33-0956A	FL42STH33-0956B	4	0.95	4.2	2.5	1.6	6	35	0.22	120	34
FL42STH33-0406A	FL42STH33-0406B	9.6	0.4	24	15	1.6	6				
FL42STH33-0316A	FL42STH33-0316B	12	0.31	38.5	21	1.6	6				
FL42STH33-1334A	FL42STH33-1334B	2.8	1.33	2.1	2.5	2.2	4				
FL42STH38-1206A	FL42STH38-1206B	4	1.2	3.3	3.2	2.6	6	54	0.28	150	40
FL42STH38-0906A	FL42STH38-0906B	6	0.8	7.5	6.7	2.6	6				
FL42STH38-0406A	FL42STH38-0406B	12	0.4	30	30	2.6	6				
FL42STH38-1684A	FL42STH38-1684B	2.8	1.68	1.65	3.2	3.6	4				
FL42STH47-1206A	FL42STH47-1206B	4	1.2	3.3	2.8	3.17	6	68	0.35	200	48
FL42STH47-0906A	FL42STH47-0906B	6	0.8	7.5	6.3	3.17	6				
FL42STH47-0406A	FL42STH47-0406B	12	0.4	30	25	3.17	6				
FL42STH47-1684A	FL42STH47-1684B	2.8	1.68	1.65	2.8	4.4	4				
FL42STH60-1206A	FL42STH60-1206B	7.2	1.2	6	7	6.5	6	102	0.5	280	60

Dimension



Wiring Diagram



12.4.11 Display tech LCD module *

<http://docs-asia.electrocomponents.com/webdocs/06dd/0900766b806dda1c.pdf>

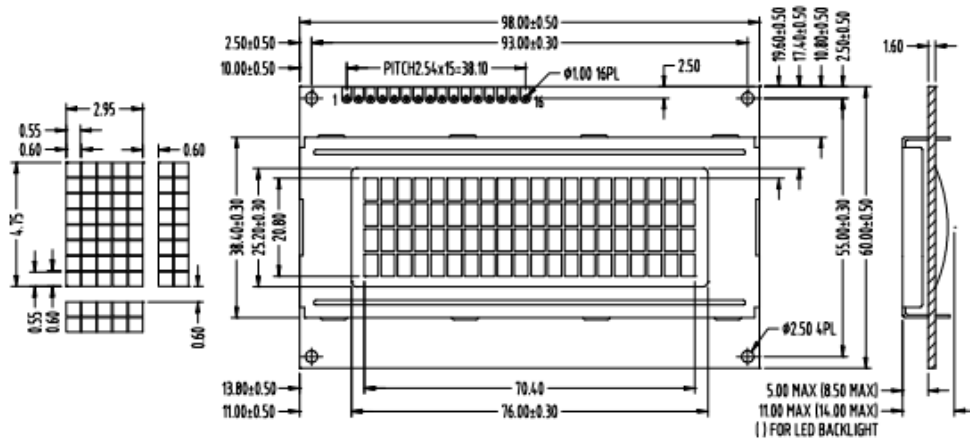
Displaytech Ltd

LCD MODULE 204A SERIES Version : 1.2 P 2 of 17

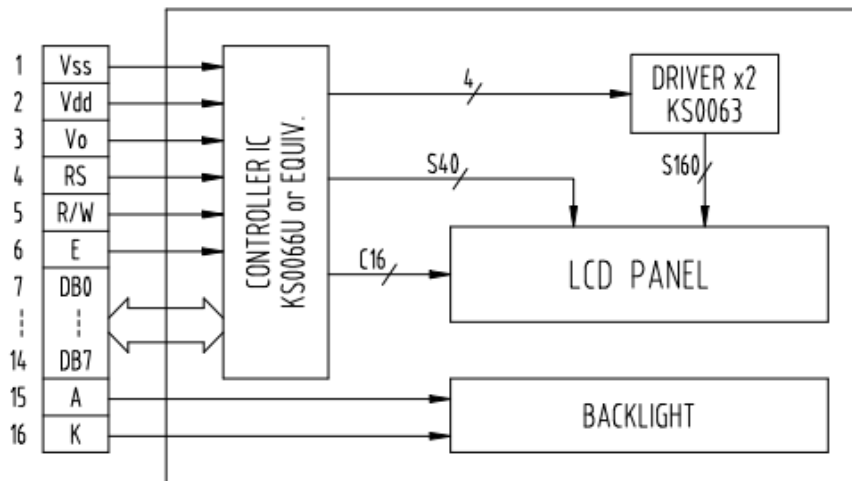
■ PHYSICAL DATA

Item	Contents	Unit
LCD type	TN / STN / FSTN	---
LCD duty	1/16	---
LCD bias	1/5	---
Viewing direction	6 / 12	o'clock
Module size (W×H×T)	98 × 60 × 11.0 MAX (14.0 MAX W/LED BACKLIGHT)	mm
Viewing area (W×H)	76 × 25.2	mm
Number of characters (characters×lines)	20 × 4	---
Character matrix (W×H)	5 × 8	dots
Character size (W×H)	2.95 × 4.75	mm
Dot size (W×H)	0.55 × 0.55	mm
Dot pitch (W×H)	0.60 × 0.60	mm

■ EXTERNAL DIMENSIONS



■ BLOCK DIAGRAM



12.4.12 PIC18F87K90 microcontroller *

<http://docs-asia.electrocomponents.com/webdocs/0eab/0900766b80eabced.pdf>



PIC18F87K90 Family Data Sheet

64/80-Pin, High-Performance
Microcontrollers with LCD Driver and
nanoWatt XLP Technology